Abstract

The symmetry of the superfluid A-phase of He^3 has previously been suggested to describe the unconventional superconducting state of Sr_2RuO_4 which would make this material a chiral p-wave superconductor. In this thesis we discuss tools, results and techniques useful in the theoretical description of superconductors with this symmetry.

In Paper I we use field-integral techniques to investigate the effects of spin-orbit coupling on the coefficients of the phenomenological Ginzburg-Landau theory of chiral p-wave superconductors. We find that these coefficients have a non-linear anisotropic dependence on the spin-orbit coupling strength and direction in spin-space. This dependence necessitates two independent phenomenological parameters for the mixed gradient terms and the mixed component terms respectively, even in the weak-field limit when written using dimensionless variables.

In Paper II we use large-scale Monte-Carlo simulations to investigate the vortex-matter of a superconducting system that can be modelled by a Ginzburg-Landau theory with chiral p-wave symmetry such as the one investigated in Paper I, but now in the limit of vanishing spin-orbit coupling. We find that a square vortex lattice consisting of single-quanta vortices is stable at high temperatures close to $T_c(B)$. The single-quanta vortices merge into double-quantum vortices at lower temperature which together then stabilizes a triangular vortex lattice.

In Paper III we investigate a Z_2 Ising transition resulting from spontaneously broken time-reversal symmetry in the neutral sector of chiral p-wave symmetric superconductors subjected to zero external field.

We find that this transition is irrevocably tied to the superconducting transition for all realistic values of the phenomenological parameters in our model.

Preface

This thesis is submitted in partial satisfaction of the requirements of the degree Philosophiae Doctor (PhD) at the Norwegian University of Science and Technology, in Trondheim Norway.

The work that this thesis presents started in September 2015 and ended in early spring 2021 at the Center for Quantum Spintronics (QuSpin), NTNU. During this time, one year of accumulated time was dedicated to teaching duties at the Department of Physics, and half a year was devoted to completion of courses (30 ECTS) as pr. the requirements of the degree. The research was supervised by Prof. Asle Sudbø as main supervisor, and Prof. Jacob Linder as co-supervisor.

Computation-time was granted at the Vilje and Fram supercomputers through the UNINETT $\int$igma2 e-infrastructure. The code was written in the Julia programming language. The figures and plots were produced by the use of Julia and Inkscape. The thesis was written in LaTeX based on a template by J. A. Ouassou available under CC BY 4.0 license, that was heavily modified.

Fredrik Nicolai Krohg
Oslo, March 2021

Acknowledgements

First I would like to thank my supervisor Prof. Asle Sudbø for his willingness to take on a PhD student that had little in regards to previous knowledge of condensed matter systems, for providing me with a steady stream of insights and ideas for interesting research topics and for his long patience with my own slow and sometimes meandering progress towards publishable results.

I would like to thank the rest of the people in our research group who I have come to know along the way; Troels Arnfred Bojesen who I met for the first time during my visit to the March Meeting in New Orleans in 2017, who shared my fascination for Japan and whom have been of invaluable assistance in understanding and troubleshooting the intricacies of Monte-Carlo algorithms and techniques. Stephan Rex, who apart from inspiring me to start running, helped me in times when I was stuck on mathematical technicalities and proved an excellent travelling companion. Peder Notto Galteland, who helped ease my introduction into the social circles of the theory-section as it stood back in 2015. Henning Goa Hugdal, whose gentle demeanor and generosity made him always approachable and provided a soothing presence in times of need. Even Thingstad, whose vast depth of knowledge in all things physics I both benefited from, and which inspired me greatly, who was an amazing partner in our task of inspiring the younger generation, and whose friendship I hold dearly. Håvard Homleid Haugen who has been an excellent collaborator with a keen eye for programming, and intuitive understanding, with whom I've had

numerous very stimulating discussions about physics and in general. Jonas Blomberg Ghini, whose outlook on life seems so much like my own and who I regret not getting to know sooner. And lastly, Eirik Erlandsen whose brilliant and vigorous gregariousness has been a source of tremendous amounts of laughter and joy.

In the department of physics at NTNU there are many others who deserve recognition and praise for their role in creating a friendly and interesting social environment. To mention everyone by name in such a long PhD as I have had would prove excessive and frankly a boring read. Therefore I will not attempt to make an exhaustive list but mention only a select few.

Of these, first I want to extend a thank you to all the post-docs and doctoral students who were already there in the "theory corridor" and in the (old) lunchroom when I started my PhD. You were all role models and people I respected greatly. People such as Sol, Alireza and Roberto. André, with whom I shared an interest in sci-fi. Eirik, whom I already knew from our masters program, Eirik Torbjørn Bakken who gave me a connection to the experimentalists at NTNU and Manu Lineares with whom I shared an office. During my stay at the March Meeting I travelled with Dag-Vidar who proved splendid and stimulating company. When I started my PhD it was my honor to start at the same time as the other doctoral students Sverre, Therese, Jabir, and Vetle. You have perhaps shaped my stay most of all and deserve special thanks for all our shared memories of running, climbing, conversations, painting and music. In this connection I also want to mention Marina, who we almost counted as a theorist for all her gifts of company during our lunch-breaks and outside of work.

The next generation of students included Martin and Øyvind. Two brilliant people: Martin with his many cat-stories and perceptive humor, and Øyvind with his thoughtfulness and warm smile. Also, I have to mention of-course Jeroen and his student Arnau who I feel have been there almost from the beginning. Jeroen who contributed greatly to forming a sense of community among the doctoral students of what has become QuSpin, lifting the intelligence-level in all conversations he joined and making me aware of resources of learning I had previously missed. Arnau, who I came to know better gradually as the years passed as having a great sense of humor and taste, and impor-

tantly: a willingness to join me for Beatz! Another co-conspirator in that endeavour has been Akash, a man I learned a great deal from not only about physics and its thinly veiled politics but also in areas of life, philosophy and sociology, one who has been integral in the culture of QuSpin and who it's been an absolute pleasure knowing.

I want to give a big thanks to Frode, my other office-mate and good friend whose many discussion on physical fitness have been inspiring and educational. I want to thank my good friends Matthias and Maximillian for many intelligent conversations over good food and drink, and foraging expeditions into the forests of Trondheim.

In the last generation of QuSpin students I would be remiss not to mention Atousa, Lina, Marion, Payel, Jonas and Longfei who have provided laughter, good company and engaging conversations, and whom I hope will have a nice and productive future in QuSpin in spite of the limitations that the pandemic enforces.

My fantastic family deserve recognition above everyone as the ones who have shown me unwavering support and love all through my life and this journey in spite of our long-standing geographical separation and my own need for seclusion when I immerse myself in my studies. To my mom and dad. To know that your door always is open should I fall, allows me the courage to continue walking. To my two brothers who endured the consequences of all my uncertainties, thank you for always letting our unity overshadow our differences. To my last sibling who in many ways reminds me much of myself, thank you for all your warm hugs and for showing me your strength. To my paternal grandfather and late grandmother who from an early age helped encourage my interest in science and maternal grandmother whose wisdom and love supersedes even Her long age.

A special thanks to David for providing much needed office-space and shelter during this time of corona. A huge thank you to my girlfriend, who perhaps more than anyone has had a front row seat in all the ups and downs in this long journey. I am so so grateful for all you have taught me, healed me and all the love you have given and continue to give.

Finally a big thank you to myself for staying the course and never yielding no matter how insurmountable the challenges have seemed.

List of papers

Paper I:
Fredrik Nicolai Krohg and Asle Sudbø
Derivation of Ginzburg-Landau free energy density containing mixed gradient terms of a $p + ip$ superconductor with spin-orbit coupling
Physical Review B **98**, 014510 (2018) [1]

Paper II:
Fredrik Nicolai Krohg, Egor Babaev, Håvard Homleid Haugen and Asle Sudbø
Thermal fluctuations and vortex lattice structures in chiral p-wave superconductors: robustness of double-quanta vortices
arXiv:2007.09161 (2020) [2]

Paper III:
Håvard Homleid Haugen, Egor Babaev, Fredrik Nicolai Krohg and Asle Sudbø
Zero field phase transitions in a chiral two-component superconductor
pre-print

Contents

Chapter 1

Introduction

Research into superconductors holds a vital key in the development of technologies that can reduce global emissions of greenhouse gasses and thus prevent large economic as well as human losses due to the effects of the climate crisis. In IPCC's special report, they state that in order to have no or limited overshoot in global temperature from the goal of 1.5 °C, the global net anthropogenic emissions of CO_2 need to decline by 45% compared to such emission levels in 2010, and this has to happen by 2030. The emission levels must then continue to decline, reaching net zero around 2050 [3]. In order for the member nations of the Paris Agreement to meet this goal, the NDC Synthesis report [4] highlights the need for further increase in the nations' contributions compared to those that are currently declared. Measures mentioned by member nations for mitigating the release of greenhouse gasses include renewable energy generation, electrification of the transport sector and more efficient electrical grids. Because of the non-traditional properties of superconductors, such materials could potentially be of great benefit in further strengthening such mitigation strategies.

In aircraft travel, designs for hybrid electric aircraft such as NASA's N3-X are underway. Analysis shows that fully utilizing high temperature superconductors in the propulsion system could provide as much as 3.5 times higher power-to-weight ratio than previous designs due to superconductors' high current-densities [5].

In Norway there has recently been a debate about the development of wind turbine parks close to population centers and in vulnerable natural habitats. Moving the wind power production from land to sea solves some of the debated issues but needs effective turbines. Including high temperature superconductors into the design of such offshore wind-turbines is beneficial for much the same reasons as for aircraft design: the high power-density makes for a compact, lightweight and efficient construction [6, 7].

Other examples of future applications of superconductors include their use in more efficient power grids [8, 9], sustaining the high magnetic fields needed for nuclear fusion [10, 11] and for the operation of a particle collider more powerful than the LHC [12], faster, more efficient electronics for digital logic and memory devices and more robust quantum computers [13].

Superconductors also currently have numerous important applications. In the Chūō Shinkansen magnetic levitation line, which is currently under construction, the interaction between superconducting coils in the train and copper coils on both sides of the track provides levitation and guidance of the train at high speeds [14]. Superconductors are essential for generating the high strength magnetic fields needed in MRI imaging. They are also used in other medical settings such as measurements of the electrical currents in the heart (magnetocardiography), in measuring the concentration of iron stored in the liver (biomagnetic liver susceptometry) and cancer treatments through their role in particle accelerators [15].

All of this is the product of fundamental research into the electronic properties of metals and other materials that has shown that for some of them, at a critical temperature T_c, the electrical resistivity of the material suddenly vanishes and any external magnetic field is expelled. These are the two main properties that we associate with the phase of superconductivity. Zero resistivity means that electricity can travel through the material without losing any energy, in contrast to a normal conductor where energy is usually lost through heat. The expulsion of magnetic fields is called the Meissner effect and is in a sense the more fundamental of the two properties. On a microscopic level it is due to electrons forming paired states that share certain features in such a way that different pairs can behave as one. Because a macroscopic

number of states share these features, the quantum mechanical nature of such states which is usually only significant for tiny particles, becomes apparent through these non-classical macroscopically measurable effects.

1.1 A brief history of superconductivity

Superconductivity was first discovered in mercury at $T_c \approx -268.99\,^{\circ}\mathrm{C}$ by Heike Kamerlingh Onnes in the Netherlands in 1911 [16]. The Meissner effect was then discovered in 1933 by W. Meissner and R. Ochsenfeld [17]. These discoveries happened without any previous theoretical prediction or explanation. Theoretical description was then gradually developed, first by a simple thermodynamic two-fluid model of electron densities by Garter and Casimir and then in 1935 by the phenomenological theory of the electromagnetic properties by H. and F. London [18]. WWII came and went and then a significant improvement on the London-model was published by V. L. Ginzburg and L. D. Landau in 1950 [19], which built on Landau's previous description [20] of a second order phase-transition by an order-parameter quantity. Based on this theory, Abrikosov introduced the concept of a type-II superconductor in 1952, which has negative surface energy and a mixed phase at non-zero magnetic field [21].

An attempt at a microscopic theory was given by Frölich in 1950 based on electron-phonon interaction [22]. Even though the perturbation theory he derived failed to predict important superconducting properties such as the Meissner effect, his Hamiltonian later became well known as a fruitful starting point for the application of field theoretic methods. In 1953 Pippard introduced a second length scale, the coherence length ξ, through a non-local modification of the London-model [23]. This length scale was a measure of the width of the interface between normal and superconducting regions. Although not a theory of superconductivity itself, Landau's Fermi-liquid theory which came in 1956 would prove crucial in the development of a microscopic theory and describes the electronic properties of many metals that at lower temperature become superconducting [24]. A complete microscopic theory of superconductivity was published by J. Bardeen, L. N. Cooper, and J. R. Schrieffer in 1957 [25, 26]. The BCS-theory was based on the idea that Fermi-liquid quasiparticles with opposite momentum

could form an attractive interaction through an intermediate interaction with a phonon. This would then lead to the formation of pairs that could form a condensate, and which implied an energy gap Δ between the energies of paired electrons and energies of normal quasiparticle states in the Fermi-sea. This year Abrikosov also published his prediction of the existence of a lattice of vortices in the mixed state of type-II superconductors [27].

A separate form of a microscopic theory appeared in 1958 by N. N. Bogoliubov in a series of papers [28–30]. This methodology of solving the Frölich Hamiltonian was presented in a book [31] by P. G. de Gennes and has since become known as the Bogoliubov-de Gennes or BdG equations.

The diagrammatic methods developed for high-energy physics was first applied by Gor'kov to the problem of superconductivity in 1958 when he calculated Green's functions based on the ideas of BCS-theory that reproduced its results [32]. He then in 1959 used these methods to prove that the Ginzburg-Landau theory follows from the BCS theory in the limit $T \to T_c$ [33]. The application of field theoretic methods was extensively developed by the work of Nambu, published in 1960, where he introduced the Nambu-spinor for calculating the Gor'kov Green's functions. A perturbation theory for these Green's functions were calculated by Éliashberg in the same year following a similar approach as Nambu, which later become known as the Éliashberg theory [34].

The understanding of the effects of impurities got an important contribution in 1959 by what is known as Anderson's theorem [35]. It says that any instability of the Fermi-surface that does not lift the Kramer degeneracy of time-reversed paired quasi-particles do not affect the mean-field transition temperature [36]. The idea of an energy gap in the excitation spectrum, which was integral to the BCS theory, was given strong experimental backing by the tunneling experiments of I. Giæver in 1960 [37]. Such experiments were given a theoretical understanding by B. D. Josephson in 1962, through what is now known as the Josephson effect [38].

From the framework of the Gor'kov Green's functions, a set of transport equations were derived for type-II superconductors in 1968 by

Eilenberger [39]. These equations were further simplified for the case of a dirty superconductor by Usadel in 1970 [40].

From the perspective of our work, the discovery of a new phase in He^3 by Osheroff et al. in 1972 was of particular importance. Although a superfluid and not a superconducting phase, the A-phase of this system has an unconventional anisotropic pairing symmetry which was famously described by Leggett in his 1975 review article [41]. This is the same symmetry that we have considered in our work.

Superconductivity was found in the first heavy-fermion system $CeCu_2Si_2$ in 1979 by Steglich et al. [42]. The heavy-fermion superconductors are systems where the superconducting state consists of quasiparticles that are fermions with large effective masses and where the superconducting order is of an unconventional character. For a review see Ref. [43].

The first high-T_c superconductor was discovered in the form of $La_{2-x}Ba_xCuO_4$ by Bednorz and Müller in 1986 [44]. This was followed up one year later by the discovery of $YBa_2Cu_3O_{7-x}$ by M. K. Wu et al. [45]. These discoveries ushered in an era of superconductivity research dominated by cuprates — ceramic compounds consisting of metal oxides between planes of CuO_2. These are truly unconventional superconductors in that their pairing symmetry is demonstrably non-isotropic. It was in 1987 proposed by V. J. Emery that antiferromagnetic spin-fluctuations could cause such an anisotropic pairing [46]. This theory of the cuperate superconductive mechanism was then extensively studied by P. Monthoux, D. Pines and D. J. Scalapino [47–49], among many others in the early 90s, however a consensus on its validity is yet to be reached due to its seeming inconsistency with normal state properties of the materials [50]. Through a group-theoretical approach, a vast array of unconventional symmetries and their Ginzburg-Landau theories and physical properties were enumerated by Sigrist and Ueda in 1991 [51]. By which of these symmetries the superconducting state of cuprates could be described was in the early 90s a topic of much discussion, however due in part to strong evidence from phase-sensitive SQUID measurements of YBCO by Wollmann et al. in 1993 [52], it was by 2000 firmly established as a $d_{x^2-y^2}$ symmetry [53].

In 1994, superconductivity was discovered in the perovskite structure of Sr_2RuO_4 by Y. Maeno et al. [54]. This proved that copper was

not a necessary ingredient for superconductivity in layered perovskite crystal structures and would be the starting point of a still-standing debate about its pairing symmetry which served as the immediate backdrop to our own research.

One of the phenomena that needs a theoretical explanation for a full understanding of superconductivity in the cuperate family of high-T_c superconductors is the pseudogap phase. Above the transition temperature, but below a characteristic temperature T^* there is a hitherto undiscovered phase in such compounds where the electronic density of states near the Fermi-surface continues to be suppressed by an energy gap Δ_{PG}. This phase was named the pseudogap phase by Ding et al. in 1996 [55], and its origin continues to be a hotly debated topic.

2008 marked the beginning of the "iron age" of superconductivity research by the discovery of the first iron-based superconductor La$[O_{1-x}F_x]$FeAs by Y. Kamihara et al. [56]. The materials in this family of superconductors, called iron-pnictides, feature high T_c and several other exotic properties including nematic order [57]. For a review see Ref. [58].

Lastly one could argue that we now have entered a "hydrogen age", as an increasing number of hydrogen-rich compounds are approaching room-temperature superconductivity when they are placed under insane pressures [59, 60]. It could also be argued that we are currently in a "topological age" as topological edge states in superconductors constitute a field under intense study [61] that potentially have far-reaching consequences through their immediate application to quantum computing. Others again, would surely argue that we are in a "graphene age" as novel forms of superconductivity have been observed in twisted layers of graphene [62]. Which age we are in, I suspect, depends on what field the researcher you are asking works on, and a clear answer will have to be postponed until seen through the coarse-grained eyes of history.

1.2 About this work

In the last section we saw how the research into the phenomena of superconductivity has blossomed into a myriad of different directions and sub-fields. Through all this research, an implicit motivation has been the search of one day finding a theory or a specific system of a

material that is superconducting at room temperature. This has become a goal, similar to how the alchemists searched for the philosopher's stone, that we still have not quite reached, but whose continued pursuit itself has borne numerous fruits.

As for this thesis, we have focused on a branch of unconventional superconductivity that pertains to the description of phases with $k_x \pm ik_y$ chiral p-wave pairing symmetry. The p in p-wave implies that the pairing states internal angular momentum has $l = 1$, i.e. it has a 1st order (linear) dependence on its internal angular momentum.[1] As we mentioned, this is the same kind of state that describes the real world system of the He^3 superfluid A-phase. In that context it is often referred to as the ABM-state after Anderson Brinkman and Morel who first described this pairing state in the context of the BCS-theory [63] in 1961, and then demonstrated how this state was stable in the A-phase of He^3 in 1973 [64]. It was for a long time thought that the unconventional superconducting phase of the perovskite compound Sr_2RuO_4 had such a pairing symmetry, with one of the chief reasons being that it clearly features spontaneously broken time-reversal symmetry. This formed in part the motivation for much of our work.

The determination of pairing symmetries is an important step in understanding what type of superconductivity is in a system because it leads to distinct experimental consequences. Roughly speaking one can think of the pairing symmetry as determining the $\boldsymbol{k}$ dependence of the gap function

$$\Delta(\boldsymbol{k}) = \sum_m \eta_m b_m(\boldsymbol{k}), \tag{1.1}$$

where $b_m(\boldsymbol{k})$ are basis functions that depend on the point group symmetry of the system and $\boldsymbol{k}$ determines a point on the Brillouin zone. Depending on these basis functions then, $\Delta(\boldsymbol{k})$ could have points or lines in the Brillouin zone where it vanishes, so-called point- or line-nodes. The existence of such nodes implies distinct signatures such as quadratic low temperature-dependence of the specific heat. Other examples of experimental signatures of unconventional symmetry include temperature-independent Knight-shift, magnetic field depen-

1. The letter-convention stands for "principal" and comes historically from the study of atomic emission spectra that result when electrons jump between different orbitals.

dent Kerr-angle rotation and unconventional symmetry of lattices of magnetic vortices. For an introduction to superconductors with unconventional pairing symmetries we highly recommend the lecture notes by Sigrist in Ref. [65] and [66].

Importantly, one may derive the form of the Ginzburg-Landau theory of the superconductor based solely on the pairing-symmetry as was done by Sigrist and Ueda for a large number of different symmetries in 1991 [51]. The Ginzburg-Landau theory is a phenomenological theory, meaning that it explains the effective phenomenon observable in superconductors without necessarily knowing all the microscopic details. As such, any correct microscopic theory should then reduce to the phenomenological Ginzburg-Landau theory in the limit of $T \to T_c$. As we mentioned, Gor'kov first did this for a conventional s-wave superconductor in 1959 through a Green's function approach [33]. One fruitful starting point for such a microscopic theory is the Hubbard-Hamiltonian

$$\hat{H} = \sum_{ijss'} H_{ij;ss'} \hat{c}^{\dagger}_{is} \hat{c}_{js'} + \mathcal{O}(\hat{c}^4), \tag{1.2}$$

which itself can be viewed as an effective theory of the underlying many-body quantum mechanics. In a Hubbard-theory, electrons can occupy sites in an atomic crystal lattice and hop from one site to another. Any long-range interaction such as the Coulomb interaction is then written in terms of how electrons at different sites interact through nearest neighbor terms, next-nearest neighbor terms, etc. In Chapter 3 we will describe some of the tools useful in deriving an effective Ginzburg-Landau theory from such a microscopic starting point. We then in Chapter 4 present the group-theory needed for deriving the requirements on such a microscopic theory, for this to result in a sought-after pairing-symmetry.

In the last chapter of Chapter 7, we present some tools useful when investigating magnetic vortices and vortex-lattices in chiral p-wave superconductors.

As was said by Leggett in his Nobel lecture, there are very few things that can be proved rigorously in condensed matter physics, by which he referred to analytic arguments [67]. To get around this difficulty, we have used Monte-Carlo techniques that relies on the power of computers to simulate physical consequences of a theoretical Ginzburg-

Landau model. Such techniques have a long history in our group of being successfully able to simulate superconductive systems. For a few examples, see [68–72]. Although similar techniques have been used for centuries, their modern form was first developed in the context of nuclear research in the Manhattan project. After the researchers had become familiar with the Monte Carlo casino in Monaco, they named it after the casino because of the technique's reliance on random or pseudo-random numbers to calculate multidimensional integrals [73].

In our use of Monte-Carlo techniques, which we present in Chapter 6, they are used to calculate thermal averages of statistical-mechanical observables. The rough procedure is that first, the theory under investigation is discretized to a corresponding lattice model as described in Chapter 5, such that the probability of any configuration of fields on this numerical lattice can be computed. The theory then implies a probability distribution for how likely certain field-configurations are to materialize in a real system. Then, from a predetermined starting configuration, small changes are made incrementally to the numerical configuration in such a way as to yield numerous statistical samples of field configurations that follow the theoretical probability distribution after a sufficient number of incremental changes have been done. These samples of field configurations finally are used to calculate statistical averages, which corresponds to taking thermal averages in statistical mechanics of the observables we are interested in.

We begin this thesis in Chapter 2 with a brief review of some relevant aspects of statistical mechanics that should refresh what is meant by thermal averages of observables, how these are tied to probability distributions of system configurations, and a brief introduction to Landau and Ginzburg-Landau theory as it pertains to phase transitions.

Chapter 2

Statistical Mechanics

In statistical mechanics we attempt to describe an ensemble of particles that may be interacting to extract not precise information about what each and every particle is doing, but statistical information about what most of the particles are doing. One can imagine this process as zooming out from a detailed view of individual entities and viewing the resulting collection through squinted eyes. This amounts to treating the collection in a course-grained manner. Through such eyes, only the most significant behavior is perceptible such that it can be understood and described in a simplified way.

2.1 Canonical ensemble and the partition function

Most of the business of statistical mechanics is about calculating what is known as the partition- function. Once this function is known, all the heavy lifting is done since most important statistical quantities can be extracted from it following already established systematic steps. To calculate the partition function is theoretically very simple: we sum the quantity $e^{-\beta E_i}$ over all the possible states of the system. Every state is a particular configuration of things in the system, and since all things in the system have a certain energy, the energy of a system state is given by the sum of all these things' individual energy, plus any energy given by interactions between them. If we label each state of the system with the index i, then we can denote the energy of each

state E_i. The definition of the partition function Z in the canonical ensemble can then be written

$$Z = \sum_i e^{-\beta E_i}, \tag{2.1}$$

where $\beta = 1/(k_\mathrm{B}T)$ and k_B is the Boltzmann constant,[1] given that the number of different possible states is countable.

As we can see, the essential ingredients needed to calculate the partition function is one: to be able to enumerate all possible states i of the system, and two: to be able to calculate their corresponding energies E_i. Since we have used the summation sign $\sum_i$ in Eq. (2.1), we have assumed that there exists a countable number of different states. However, if there is one thing in the system that can change in a continuous fashion, which we would measure using the set of real numbers $\mathbb{R}$ and some unit, then the number of states is infinite and uncountable. In this case we sum over the different numbers of states by simply integrating over the things that are continuous, and the unit of the partition function becomes the product of the units of the continuous variables (things) unless we normalize by some constant dimensionful quantity. In most cases, it is the position $\boldsymbol{r}$ and momentum $\boldsymbol{p}$ of particles in the system that are continuous, hence the definition of the partition function becomes[2]

$$Z \sim \sum_i \int \mathrm{d}^3 r \int \mathrm{d}^3 p \, e^{-\beta E_i(\boldsymbol{r},\boldsymbol{p})}. \tag{2.2}$$

The canonical partition function is directly related to the Helmholtz free energy F (often only referred to as the free energy) of the system through a simple exponential

$$Z = e^{-\beta F}. \tag{2.3}$$

Because of the exponentials inherent in the definition of Z, calculating realistic values often results in excessively high numbers. This is one

1. In SI units, the value of the Boltzmann constant is given by $k_\mathrm{B} \approx 1.380\,649 \times 10^{-23}\,\mathrm{JK}^{-1}$
2. The reason why there is a $\sim$ sign in Eq. (2.2) is that technically there is a factor of Planck's constant h in the denominator for each $\mathrm{d}r\,\mathrm{d}p$ in the integral measure since this makes the partition function dimensionless and thus consistent with the definition in terms of countable number of states in Eq. (2.1).

of the reasons why it is more useful to work with F, rather than Z itself, since inverting Eq. (2.3) $F = -\ln(Z)/\beta$, reducing the value of Z through a logarithm.

2.2 Calculating observables

An observable in statistical mechanics is a quantity that we can both calculate from the statistical theory, and (at least in principle) go out and measure in the real world. In quantum mechanics, observables are restricted to operators that have real expectation-values, as opposed to the complex values the theory usually deals with. This is to enforce the connection between observables and measurements, which we intuitively understand to always be reducible to a series of real values, i.e. points on a line.

We are interested in statistical information on observables of systems consisting of several quantum mechanical particles. To get this information we need some kind of probability distribution of the different states of the system. We are imagining that we for each such state (indexed by j) can calculate a real number for the thing (observable) we are interested in measuring. Let's call this observable O. Then O is a statistical variable which takes a particular value o_j in the state j of the system. Since the state is quantum mechanical, it is usually denoted by a Dirac bracket $|j\rangle$. A real observable O corresponds to a Hermitian operator $\hat{O}$ in quantum mechanics whose expectation value we can then write as $o_j = \langle j|\hat{O}|j\rangle$.

If we now let P_j be the probability distribution, i.e. the probability that the system exists in state j, then we know from probability theory that the expectation value of O is

$$\langle O\rangle = \sum_j o_j P_j. \tag{2.4}$$

The probability distribution P_j is in the canonical ensemble given by a Maxwell-distribution

$$P_j = e^{-\beta E_j}/Z, \tag{2.5}$$

normalized by the partition function Z. Inserting this we get

$$\langle O\rangle = \sum_j \frac{o_j e^{-\beta E_j}}{Z}. \tag{2.6}$$

The observable of specific heat at constant volume C_v is particularly important in the study of phase transitions since its thermal behavior can be used to classify these transitions into categories. The specific heat is the measure of how much energy must be transferred to the system for its temperature to change by an infinitesimal amount given constant volume of the system. Thus it is defined by the equation $C_v = (\frac{\partial E}{\partial T})_V$. In the canonical ensemble, this quantity is calculated by

$$C_v = k_{\mathrm{B}}\beta^2(\langle E^2\rangle - \langle E\rangle^2) = -k_{\mathrm{B}}\beta^2\Big(2\frac{\partial F}{\partial \beta} + \beta\frac{\partial^2 F}{\partial \beta^2}\Big). \tag{2.7}$$

From this form of the specific heat, we see that it can be interpreted as a measure of the variance or width of the distribution of energies, and also that it is related to the second derivative of the free energy. Any discontinuity in the second derivative of the free energy, thus implies a discontinuity in the specific heat.

2.3 Ginzburg-Landau model

The experimental discovery of superconductivity was a surprise to the scientists at the time. No theoretical model had so far predicted the properties that the experimentalists were measuring. The theoretical models in use at that time predicted a decrease in resistivity as the temperature was lowered, but its sudden disappearance was completely unprecedented and impossible to explain classically in a convincing manner. Therefore, superconductivity seemed to demand a radically different understanding of how electrons moved inside atomic structures.

2.3.1 Landau Model

Before such an understanding had been developed, Ginzburg and Landau took a shortcut and came up with a theory that could describe the phenomenon of superconductivity without knowing its microscopic origin. In other words, they treated superconductivity as a black box and instead of asking what was inside to give the box's output, they used the output to determine a small set of *material parameters* which could then be used to predict how the box would react to a large range of stimuli or conditions. Now, given a large enough number of parameters, you can usually construct a model to fit any set of experimental

observations that you like. The merit of this theory came from use of symmetry arguments to reduce this set into only a few parameters, which still allowed it to describe the observations, while also embedding the theory with great predictive power.

The Ginzburg-Landau (GL) theory of superconductivity is based on Landau's previous work on a theory of general second order phase-transitions.[3] The approach is given by two ideas. The first is simply that the phase transition should be able to be characterized by the appearance of some kind of measurable order that can be described by a function Ψ which we call the *order parameter*. In the liquid-water to ice-transition, it is the position of the molecules that become ordered in a lattice.[4] In the magnetization of a metal it is the individual spins that become ordered along a particular direction.

The second idea is that at the phase transition, it is the appearance of this order that should dominate the behaviour of the system, to the exclusion of all other effects. Thus, the system should be described in terms of the order-parameter, and since this is infinitesimally small close to the transition, the free energy can be expanded in a Maclaurin-series with respect to this parameter as

$$F = F_0 + c_1\Psi + c_2\Psi^2 + c_3\Psi^3 + c_4\Psi^4 + c_5\Psi^5 + \ldots \tag{2.8}$$

The real constants F_0 and c_i constitute the set of material parameters of the theory and this set can then be reduced by any symmetries that we suspect should be inherent in the underlying theory. For example, if Ψ should represent the order parameter of magnetization of a system of Ising-spins, which can point either up or down, then the free energy should be invariant to this global choice, i.e. we need to enforce that the free energy be invariant with respect to the transformation $\Psi \mapsto -\Psi$. Then all the constants c_i for odd i vanish.

In the case of superconductivity, the order parameter Ψ represents the probability amplitude of the collective state of the superfluid of

3. 2nd order phase-transitions are phase transitions of systems whose free energy has a discontinuous second order derivative at the transition point, but is continuous for lower orders. Since the specific heat is given by the second order derivative, then the specific heat is discontinuous in this case.
4. The astute reader might have noticed that this example is a first order phase transition because of the existence of latent heat. Actually first order phase transitions can also be described by a modified Landau theory, however we will here focus on the second order kind.

Cooper-paired electrons such that $|\Psi|$ can be interpreted as the density of such electron pairs. Since Ψ is complex, it has to be combined with its complex conjugate Ψ^* in ways that yield real numbers to produce terms that are valid in the free energy, since F itself should be a real number. Furthermore, the phenomenon of superconductivity is produced as a result of the breaking of $U(1)$ symmetry, so F also needs to be $U(1)$ symmetric, i.e. it has to be invariant under the transformation $\Psi \mapsto e^{i\phi}\Psi$ for $\phi \in \mathbb{R}$. These restrictions result in the free energy

$$F = F_0 - a|\Psi|^2 + b|\Psi|^4, \tag{2.9}$$

when keeping the lowest order terms that produce a phase transition.

Thermodynamic equilibrium is reached at the minimum of free energy. This restricts $b \geq 0$ since negative b yields a free energy with no global minimum.[5] The minimum is then found by the condition

$$\frac{\partial F}{\partial \Psi^*} = (-a + 2b|\Psi|^2)\Psi = 0, \tag{2.10}$$

which yields the possibilities $|\Psi| = 0$ or $|\Psi| = \sqrt{a/2b}$. The first case gives the energy $F = F_0$, while the second gives $F = F_0 - a^2/(4b)$. We see that the second case is energetically favorable, but only exists and is different from the first case when $a > 0$. Furthermore, the second case represents the ordered state, since in this case the order-parameter $|\Psi| \neq 0$, in the conventional Landau theory.[6]

It is the thermodynamic parameter of temperature that traditionally determines whether a system is in one phase or another. Looking at the free energy in Eq. (2.9), the order parameter Ψ is the dynamical variable of the theory while the explicit temperature dependence lies in the material parameters a and b. Denoting the critical temperature where the phase transition happens T_c, the dimensionless parameter $t = (T - T_c)/T_c$ is small close to the critical point which means that

5. If there is no such minimum, then we say that the theory is unbounded or divergent.
6. Actually this only represents when Cooper-pairs are forming and the real onset of superconductivity is determined by the point in parameter-space where the gauge-mass becomes non-zero, which is closely related but not exactly the same as where the density of Cooper-pairs becomes non-zero. The real onset of superconductivity is thus more related to when the phase of the wave-function settles on a value.

it can be used to expand the temperature-dependence of the material parameters such that

$$\begin{aligned} a(T) &= a_0 + a_1 t + ... \\ b(T) &= b_0 + b_1 t + ... \end{aligned} \tag{2.11}$$

Now we argue for what terms to keep in these expansions. Since $a(T)$ should change sign at $t = 0$ based on the discussion of Eq. (2.10), then we only keep odd terms of a. Since we need $b(T) > 0$ for the theory to be thermodynamically stable it seems that b_0 is the important term that needs to be larger than any negative contributions from the other terms. Keeping only lowest order terms, then the expansions reduce to $a(T) = a_1(T - T_c)/T_c$ and $b(T) = b_0$. Since the ordered state is the solution of the theory when $a > 0$ and this ordered state exists at temperatures $T < T_c$ then $a_1 < 0$ and the final temperature dependence of a becomes $a(T) = -|a_1|(T - T_c)/T_c$. From this temperature dependence, it is straightforward to derive critical exponents, the specific heat, etc. See Ref. [74].

2.3.2 Gradient Terms

The simple Landau theory described above is a type of mean field theory in that there is no spatial dependence in the order parameter Ψ, and thus it gives a simplified picture that can only be valid far away from any defects or boundaries. This simple approach can be extended to include spatial variation by allowing terms with gradients of the order parameter in the free energy through a gradient expansion of f in

$$F = \int \mathrm{d}^3 r \; f(\Psi, \nabla\Psi, \nabla^2\Psi, \nabla^3\Psi, ...). \tag{2.12}$$

Keeping only the lowest order in this expansion that is invariant under $U(1)$ symmetry, we get the term $|\nabla\Psi|^2$ added to the free energy F in Eq. (2.9).

Perhaps the single most important phenomenon of superconductivity from a theoretical standpoint is the fact that it expels magnetic fields, hence it is clear that any theory that attempts to explain superconductivity needs to have some way for the superconducting order to interact with magnetic fields. The standard way to achieve this is through the recipe of *minimal coupling*, where the vector potential $\boldsymbol{A}$

times a constant is subtracted from any momentum in the previously neutral theory. Specifically, $\boldsymbol{p} \mapsto \boldsymbol{p} - q/c\boldsymbol{A}$, where q is the charge of the particle and c is the speed of light. Using this trick, then the free energy density becomes

$$f = f_0 - a|\Psi|^2 + b|\Psi|^4 + K|(\nabla + ig\boldsymbol{A})\Psi|^2, \tag{2.13}$$

by letting $g = q/\hbar c$, which is the form of the free energy in the Ginzburg-Landau theory of conventional s-wave superconductivity. The form of the gradient that results from minimal coupling is called the covariant derivative and is defined as

$$D_\mu = \partial_\mu + igA_\mu. \tag{2.14}$$

For unconventional symmetries, the form of the gradient terms can vary substantially from that in Eq. (2.13). Even if the transition can be described by a single component, i.e. a single function Ψ, then an unconventional symmetry could still lead to anisotropies in the gradient terms such that K in Eq. (2.13) becomes directionally dependent. An example is single-component pairing in a tetragonal crystal. The symmetry group of tetragonal crystals is denoted D_{4h} in the Schönflies notation and consists of four-fold rotations in, and mirror symmetry about, the xy-plane. The rotational symmetry makes the gradient isotropic in the plane, but because of the lack of symmetry in the z-direction, the gradient terms in general must take the form

$$K_1 \sum_{\mu=x,y} |(\partial_\mu + igA_\mu)\Psi)|^2 + K_2|\partial_z + igA_z)\Psi|^2. \tag{2.15}$$

Even more complex gradient terms are possible when the order-parameter consists of multiple components, i.e. there are degenerate states that all give significant contributions to the physics at the phase-transition. A particular case of this is when the pairing state is an irreducible representation of the crystal symmetry-group that is multi-dimensional.[7] In this case, instead of a single complex function Ψ describing the order, we need several complex functions η_i.

A chiral p-wave superconductor has a pairing state that belongs to such a two-dimensional irreducible representation. It comes from the

7. For a more detailed explanation of irreducible representations and group theory, see Chapter 4.

Γ_5 irreducible representation of the tetragonal symmetry group D_{4h}. This representation consists of two components η_x and η_y that combine to form the general gradient terms

$$\begin{aligned} &K_1\left[|D_x\eta_x|^2+|D_y\eta_y|^2\right]+K_2\left[|D_x\eta_y|^2+|D_y\eta_x|^2\right] \\ &+K_3\left[(D_x\eta_x)^*(D_y\eta_y)+\text{c.c.}\right]+K_4\left[(D_x\eta_y)^*D_y\eta_x+\text{c.c.}\right] \\ &+K_5\left[|D_z\eta_x|^2+|D_z\eta_y|^2\right]. \end{aligned} \tag{2.16}$$

This is the general expression of the gradient terms in the model we have investigated in our work and can be found in Ref. [51].

Chapter 3

Field Theory Methods

In this chapter we will give a short introduction to the use of Graßmann variables and complex numbers in the calculation of the field-integrals in the partition function. We will also describe how these variables can be used to transform the expression for the action through the Hubbard-Stratonovich (HS) transformation.

A field theoretic expression for the quantum mechanical partition function $\mathcal{Z}$ is obtained by using a coherent state basis. A coherent state is the eigen-state of an annihilation operator; thus, it produces an eigenvalue when operated on by the annihilation operator. Letting $\hat{H}$ be the quantum mechanical Hamiltonian of the system for which we are interested in calculating the partition function, μ be the chemical potential and $\hat{N}$ be the number operator, then the partition function is defined as

$$\mathcal{Z} = \mathrm{Tr}(e^{-\beta(\hat{H}-\mu\hat{N})}). \tag{3.1}$$

Inserting a basis of coherent states $\{|\xi\rangle\}$ when calculating the trace, we obtain a functional integral over the coherent state eigenvalues ξ_α and ξ^*_α by substituting these variables for c_α and $c^\dagger_\alpha$ respectively in the $\hat{H}$- and $\hat{N}$-operators. Here α symbolizes the set of quantum-numbers needed to specify a state. The functional integral then takes the form

$$\mathcal{Z} = \int \mathcal{D}[\xi^*\ \xi] e^{-\int_0^\beta \mathrm{d}\tau \sum_\alpha [\xi^*_\alpha(\partial_\tau - \mu)\xi_\alpha + H(\xi_\alpha, \xi^*_\alpha)]}. \tag{3.2}$$

The integration variable τ is the imaginary time and a τ-dependence is implicit in the notation such that $\xi_\alpha = \xi_\alpha(\tau)$. This path-integral notation is a shorthand for a more involved expression where the imaginary time-dependence of τ is split into a collection of time-indexed coherent state eigenfunctions $\xi_{\alpha,\tau}$, and the integration measure is a product over these indices and the quantum-state indices α. For further detail we refer to Ref. [75] which we will follow for a large part of this chapter.

3.1 Quadratic Fermionic Field Integrals

Because of the anti-commuting property of the fermion annihilation operators, any coherent state has to have eigenvalues that anti-commute as well. This leads to Graßmann numbers being the central variables used in constructing the partition function when it is written in the convenient basis of coherent states.

3.1.1 Graßmann algebras

A Graßmann algebra is constructed on a set of generators $\{\xi_\alpha\}$ such that a specific product of the generators $\xi_{\alpha_1}\xi_{\alpha_2}\cdots\xi_{\alpha_n}$ together with a complex coefficient ϕ constitute a number in the algebra and the generators anti-commute such that $\xi_\alpha\xi_\beta = -\xi_\beta\xi_\alpha$. On such an algebra, differentiation can be defined such that

$$\frac{\mathrm{d}}{\mathrm{d}\xi_{\alpha_m}}\,\phi\,\xi_{\alpha_1}\cdots\xi_{\alpha_n} = (-1)^{m-1}\phi\,\xi_{\alpha_1}\cdots\xi_{\alpha_{m-1}}\xi_{\alpha_{m+1}}\cdots\xi_{\alpha_n}, \tag{3.3}$$

provided that the generator ξ_{α_m} is in the number, and 0 otherwise. The factors of (-1) comes from anti-commuting the generator ξ_{α_m} such that it is next to the differentiation operator. In Graßmann algebra, integration can (perhaps a little non-intuitively) be defined such that it acts in the same way as differentiation, i.e. generators have to be anti-commuted until they are next to the symbolic infinitesimal differential $\mathrm{d}\xi_\alpha$, and then use

$$\int \mathrm{d}\xi\ \xi = 1, \tag{3.4}$$

while

$$\int \mathrm{d}\xi\ 1 = 0. \tag{3.5}$$

If the integral consists of several differentials of generators, then these differentials also have to be anti-commuted such that $\mathrm{d}\xi_1\mathrm{d}\xi_2 = -\mathrm{d}\xi_2\mathrm{d}\xi_1$. On an algebra consisting of $2n$ generators we define conjugation as a map from the first half of the generators $\{\xi_{\alpha_i}\}_{i=1}^n$ to the other half $\{\xi^*_{\alpha_i}\}_{i=1}^n$ and in such a way that when applied to a particular number

$$(\phi\xi_\alpha\xi_\beta)^* = \phi^*\xi^*_\beta\xi^*_\alpha, \tag{3.6}$$

for $\phi \in \mathbb{C}$.

3.1.2 Nambu Spinor

In the Nambu notation, we group spin-dependent Graßmann numbers $\xi_\uparrow$ and $\xi^*_\downarrow$, which correspond to the annihilation- and creation-operators $\hat{c}^\dagger_\uparrow$ and $\hat{c}_\downarrow$, in a vector called a Nambu spinor

$$\boldsymbol{\xi} = \begin{pmatrix} \xi_\uparrow \\ \xi^*_\downarrow \end{pmatrix}. \tag{3.7}$$

A sesquilinear form can then be created with this vector and its adjoint such that

$$\boldsymbol{\xi}^\dagger S\boldsymbol{\xi} = S_{11}\xi^*_\uparrow\xi_\uparrow + S_{22}\xi^*_\downarrow\xi_\downarrow + S_{12}\xi^*_\uparrow\xi^*_\downarrow + S_{21}\xi_\uparrow\xi_\downarrow. \tag{3.8}$$

This allows any action that contains spin-dependent terms of the form of the right-hand side of Eq. (3.8) to be put on sesquilinear form. Assuming this is the case, then the partition function in the field-integral representation takes the form

$$\mathcal{Z} = \int \mathcal{D}[\xi^*\,\xi]\; e^{-\int_0^\beta \mathrm{d}\tau\, \boldsymbol{\xi}^\dagger_\gamma S_{\gamma\delta}\boldsymbol{\xi}_\delta}. \tag{3.9}$$

In this equation, the indices γ and δ are arbitrary collections of quantum numbers needed to specify a state other than spin, for example they could be momentum indices $\gamma = \boldsymbol{k}, \delta = \boldsymbol{k}'$, and summation over these repeated indices is implicitly understood.

Splitting the integral over τ into M imaginary time-slices and expanding the path integral measure into a product of individual integrals over specific quantum numbered and time-sliced Graßmann variables such that

$$\int \mathcal{D}[\xi^*\,\xi] \;\propto\; \lim_{M\to\infty} \int \prod_{\tau=1}^{M} \prod_{\alpha} \mathrm{d}\xi^*_{\alpha,\tau}\mathrm{d}\xi_{\alpha,\tau}, \tag{3.10}$$

the path-integral in Eq. (3.9) can be evaluated by the Gaussian Graßmann integral identity

$$\int \prod_i (\mathrm{d}\xi_i^* \mathrm{d}\xi_i)\; e^{-\xi_i^* S_{ij} \xi_j} = \det S, \tag{3.11}$$

for which a derivation can be found in Ref. [75]. This identity holds for any Hermitian matrix S, even if it is not positive definite. The result is then that the partition function in Eq. (3.9) becomes $\mathcal{Z} = \det S$. To calculate this determinant one has to consider the matrix S as also a matrix with time-slice indices. This is perhaps most easily accomplished using the Matsubara formalism in which the τ dependence is substituted with a dependence on Matsubara frequencies through a Fourier-like transform. More details on this formalism can be found in Section 3.2, but first we consider what to do when a spin-dependent action cannot be written on the form in Eq. (3.8).

3.1.3 Extended Nambu Spinor

From Eq. (3.8) we see that the Nambu spinor sesquilinear product fails to accommodate terms in a Hamiltonian that mix creation and annihilation operators of differing spins, e.g. a term $\propto \hat{c}_\uparrow^\dagger \hat{c}_\downarrow$. In general, a quadratic Hamiltonian can contain any combination of spin-indices of the form $\hat{c}_{s_1}\hat{c}_{s_2}$, $\hat{c}_{s_1}^\dagger \hat{c}_{s_2}$, $\hat{c}_{s_1}\hat{c}_{s_2}^\dagger$ and $\hat{c}_{s_1}^\dagger \hat{c}_{s_2}^\dagger$. This gives in total 16 different combinations, and to accommodate them all we thus need a 4×4 matrix. Exchanging to Graßmann numbers, we define the vector

$$\boldsymbol{\xi}_\gamma = \begin{pmatrix} \xi_{\gamma,\uparrow}^* \\ \xi_{\gamma,\uparrow} \\ \xi_{\gamma,\downarrow}^* \\ \xi_{\gamma,\downarrow} \end{pmatrix}, \tag{3.12}$$

where all quantum numbers except spin is included in the index γ. Writing the elements of this vector $(\boldsymbol{\xi}_\gamma)_i = \tilde{\xi}_{\gamma,i}$ regardless of whether it is a conjugate or not, we can write all quadratic terms of a Hamiltonian on the bilinear form

$$\boldsymbol{\xi}_\gamma^\mathsf{T} S_{\gamma\delta} \boldsymbol{\xi}_\delta = \tilde{\xi}_{\gamma,i} S_{\gamma i;\delta j} \tilde{\xi}_{\delta,j}, \tag{3.13}$$

where $S_{\gamma\delta}$ is a 4×4 antisymmetric[1] matrix, and $S_{\gamma i;\delta j}$ denotes its elements. Let there be n number of different quantum numbers, now including spin. Then there must be $2n$ different Graßmann generators $\tilde{\xi}_{\gamma,i}$. All of these are integrated over in the discrete version of the partition function field integral

$$\mathcal{Z} = \int \mathcal{D}[\xi^* \, \xi] \; e^{-\int_0^\beta \mathrm{d}\tau \, \tilde{\xi}_{\gamma,i} S_{\gamma i;\delta j} \tilde{\xi}_{\delta,j}}. \tag{3.14}$$

Even though this superficially looks like the field integral in Eq. (3.9), we now have a bilinear and not a sesquilinear form, and S is now a $2n \times 2n$ matrix and not an $n \times n$ matrix. This means that we cannot use the integral in Eq. (3.11) to evaluate the integral, but instead have to rely on the more general Gaussian Graßmann integral

$$\int \prod_i (\mathrm{d}\tilde{\xi}_i) \; e^{-\frac{1}{2}\tilde{\xi}_i S_{ij} \tilde{\xi}_j} = \mathrm{Pf}(S), \tag{3.15}$$

which applies for any antisymmetric matrix S. The right-hand side is called the Pfaffian $\mathrm{Pf}(S)$ of the matrix S and is defined for any antisymmetric matrix to be given by

$$\mathrm{Pf}[S] = \frac{1}{2^n n!} \sum_{P \in S_n} (-1)^P S_{P_1 P_2} \cdots S_{P_{n-1} P_n}, \tag{3.16}$$

where P is a permutation in the finite group S_n of all possible permutations of n numbers. This matrix function is related to the determinant by the relation $\mathrm{Pf}(S)^2 = \det(S)$.

1. To see why this matrix can always be said to be antisymmetric lets first simplify the notation and write the bilinear product as $\tilde{\xi}_i S_{ij} \tilde{\xi}_j$. Then the matrix $S = (S + S^\mathsf{T})/2 + (S - S^\mathsf{T})/2$, such that we can write it as a symmetric matrix $\mathcal{S} = (S + S^\mathsf{T})/2$ and an antisymmetric matrix $\mathcal{A} = (S - S^\mathsf{T})/2$. Considering only the symmetric part of the bilinear form we get

$$\tilde{\xi}_i \mathcal{S}_{ij} \tilde{xi}_j = -\tilde{\xi}_j \mathcal{S}_{ij} \tilde{\xi}_i = -\tilde{\xi}_i \mathcal{S}_{ji} \tilde{\xi}_j = -\tilde{\xi}_i \mathcal{S}_{ij} \tilde{\xi}_j.$$

Hence $\tilde{\xi}_i \mathcal{S}_{ij} \tilde{\xi}_j = 0$ and all that remains is the antisymmetric bilinear form.

Applying the integral identity in Eq. (3.15) to the partition function[2] in Eq. (3.14) after applying the proper discretization of the imaginary time, then yields the result

$$\mathcal{Z} = \int \mathcal{D}[\xi^*\,\xi]\; e^{-\int_0^\beta \mathrm{d}\tau\, \tilde{\xi}_{\gamma,i} S_{\gamma i;\delta j} \tilde{\xi}_{\delta,j}} = \sqrt{\det(S)}. \tag{3.17}$$

We have chosen the positive result in $\mathrm{Pf}(S) = \pm\sqrt{\det(S)}$ since the partition function $\mathcal{Z}$ needs to be positive on physical grounds. The matrix S on the right-hand side of Eq. (3.17), which we take the determinant of, is the full matrix one gets after discretizing the imaginary time into slices which is usually done through the Matsubara-frequency formalism.

Now that we know that the partition function is given in terms of the determinant of the action-matrix S, we can use this information to manipulate the definition of $\tilde{\xi}_{\gamma,i}$ so that we can still write the action as a sesquilinear form. In particular, switching the position of $\xi^*_{\gamma,s}$ and $\xi_{\gamma,s}$ for both spins in the transposed vector on the left of the bilinear form $\boldsymbol{\xi}^\mathsf{T}_\gamma S_{\gamma\delta}\boldsymbol{\xi}$, the transposed vector becomes the adjoint vector. This affects the matrix S by switching two pairs of rows. Denoting the matrix where the rows are switched S', we can thus rewrite the bilinear form such that

$$\boldsymbol{\xi}^\mathsf{T}_\gamma S_{\gamma\delta}\boldsymbol{\xi}_\delta = \boldsymbol{\xi}^\dagger_\gamma S'_{\gamma\delta}\boldsymbol{\xi}_\delta. \tag{3.18}$$

Now, the integral over the exponent has not changed since all we have done is simply re-ordering its terms. However, since exchange of rows in a determinant at most produces a minus sign and we do this twice, we get that $\det S = \det S'$, and we can write

$$\mathcal{Z} = \int \mathcal{D}[\xi^*\,\xi]\; e^{-\int_0^\beta \mathrm{d}\tau\, \boldsymbol{\xi}^\dagger_\gamma S'_{\gamma\delta}\boldsymbol{\xi}_\delta} = \sqrt{\det(S')}. \tag{3.19}$$

In this equation, it is important to remember that S' is the row-switched matrix of an antisymmetric matrix S.

2. In relating the discrete version of Eq. (3.15) to (3.14) we have to make sure that the spinor elements $\tilde{\xi}_i$ are defined in terms of ξ_i and ξ^*_i in such a way as to get a correspondence to the sequence of Graßmann generators $\mathrm{d}\xi^*_i\mathrm{d}\xi_i$ in the measure to avoid any sign errors. One solution is to set $\xi^*_i = \tilde{\xi}_{2i-1}$ and $\xi_i = \tilde{\xi}_{2i}$ as we have done in Eq. (3.12). With this definition, then the measure $\int \prod_i \mathrm{d}\xi^*_i\mathrm{d}\xi_i$, which results from the discretized version of the field-integral measure, becomes equal to $\int \prod_{i=1}^{2n} \mathrm{d}\tilde{\xi}_i$ such that Eq. (3.15) can be directly applied.

3.2 Matsubara formalism

The Matsubara formalism[3] is a way of handling the imaginary time τ dependence of the coherent state eigenvalue fields $\xi_\alpha(\tau)$, where α denotes a collection of quantum numbers that are necessary to specify a state, without having to go back to the time-sliced path-integral. It also lets us automatically satisfy the imaginary-time boundary conditions $\xi_\alpha(0) = \zeta\xi_\alpha(\beta)$, where $\zeta = +1$ for bosons and $\zeta = -1$ for fermions. Imagining that τ is a continuous variable as suggested in the path-integral notation, we define two countable infinite sets of new field-variables through the Fourier-transforms

$$\xi_{\alpha,n} = \frac{1}{\sqrt{\beta}} \int_0^\beta \mathrm{d}\tau \, e^{i\omega_n \tau} \xi_\alpha(\tau), \tag{3.20a}$$

$$\xi^*_{\alpha,n} = \frac{1}{\sqrt{\beta}} \int_0^\beta \mathrm{d}\tau \, e^{-i\omega_n \tau} \xi^*_\alpha(\tau). \tag{3.20b}$$

The frequencies ω_n are called Matsubara frequencies and are defined by $\omega_n = (2n+1)\pi/\beta$ with $n \in \mathbb{Z}$ for fermions. For bosons we use instead the notation ν_n where $\nu_n = 2n\pi/\beta$. The inverse relations are given by

$$\xi_\alpha(\tau) = \sum_{n\in\mathbb{Z}} e^{-i\omega_n \tau} \xi_{\alpha,n}, \tag{3.21a}$$

$$\xi^*_\alpha(\tau) = \sum_{n\in\mathbb{Z}} e^{i\omega_n \tau} \xi^*_{\alpha,n}. \tag{3.21b}$$

3.2.1 Matsubara sums

When the Matsubara formalism $\xi_{\alpha,n}$ is used for the field variables in the action of a partition-function field-integral, we will often need to evaluate infinite sums of Matsubara frequencies of the form

$$\sum_n h(if_n), \tag{3.22}$$

where f_n is either a fermionic- or bosonic Matsubara-frequency, to evaluate the field integral. A useful strategy in such evaluations is to

3. Named after the Japanese physicist Matsubara, Takeo.

transform the sum to a complex integral by using reverse residue integration. We consider the complex contour integral along a path $\mathcal{C}$ running counterclockwise around the complex plane infinitesimally close to the imaginary axis as shown in Fig. 3.1. The integrand we consider

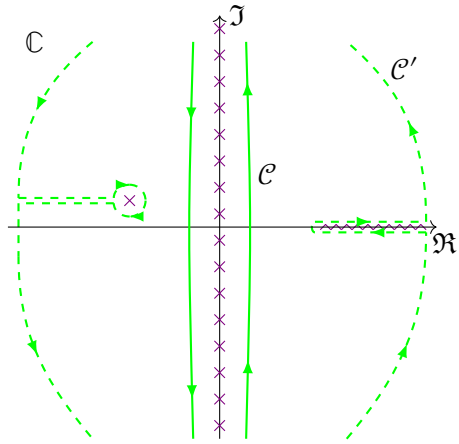

Figure 3.1: Integration contour for the Matsubara sum $\sum_n h(if_n)$. The contour is marked by a solid line and is imagined continuing to $\pm i\infty$. The crosses along the imaginary axis symbolize the simple poles of the Fermi-Dirac distribution-function. A deformed integration contour is shown with dashed lines that is imagined to cross the real axis at $\pm\infty$. This contour then encloses a simple pole on the left and a branch cut on the right belonging to the summand.

is given by the product of the summand and the complex continuation of the Fermi-Dirac- or Bose-Einstein distribution-function

$$n_\zeta(z) = (e^{\beta z} - \zeta)^{-1}, \quad z \in \mathbb{C}, \tag{3.23}$$

depending on whether the Matsubara frequency in the sum is of fermionic ($\zeta = -1$) or bosonic ($\zeta = +1$) nature. This function has simple poles[4] at $z = if_n$ and thus integration around the contour results in a sum of residues of the integrand at these poles such that we get

$$\sum_n h(if_n) = \frac{\zeta\beta}{2\pi i} \oint_{\mathcal{C}} \mathrm{d}z\, h(z) n_\zeta(z), \tag{3.24}$$

4. That the poles are simple, i.e. 1st order, is easily seen by expanding the exponential around if_n to leading order.

given that $h(z)$ does not contain any poles at these points. The contour can now be continuously deformed at will, as long as it does not cross any singularities, which can greatly facilitate the calculation of the integral. The default approach is to see if the integrand vanishes as $|z| \to \infty$, in which case it is usually useful to expand the contour as much as possible as illustrated by the deformed contour $\mathcal{C}'$ in Figure 3.1.

Using the method outlined above, we may calculate the sums

$$\sum_{n\in\mathbb{Z}} \frac{1}{if_n - x} = -\zeta\beta n_\zeta(x), \tag{3.25a}$$

$$\sum_{n\in\mathbb{Z}} \frac{1}{(i\omega_n - x)(i\omega_n - y)} = \frac{\beta}{x-y}\left(\frac{1}{1+e^{\beta x}} - \frac{1}{1+e^{\beta y}}\right), \tag{3.25b}$$

$$\sum_{n\in\mathbb{Z}} \ln[\beta(i\omega_n + x)] = \ln(1+e^{-\beta x}). \tag{3.25c}$$

3.3 Hubbard-Stratonovich transformation

The HS transformation is a transformation in the fields of a theory, where a new complex field is introduced in order to convert a term that is quadratic in an existing field variable, into a linear coupling between the existing- and new field. This is particularly useful when the existing field is Fermionic and thus a Graßmann variable, since it makes it possible to consider low energy excitations of the theory using e.g. a saddle-point approximation. It is however important to point out that the transformation itself is not in any way approximative but is an exact transformation that maintains all information of the original theory.

In technical terms, the HS transformation can be viewed simply as the solution of a complex multivariate integral. Let A have a strictly positive Hermitian part and $\boldsymbol{J}$ be a vector of coefficients that could contain Graßmann- or complex variables. Then

$$e^{\boldsymbol{J}^\dagger A \boldsymbol{J}} = \det A^{-1} \int_{\mathbb{C}} \prod_i \left[\frac{\mathrm{d}z_i^* \mathrm{d}z_i}{2\pi i}\right] e^{-(\boldsymbol{z}^\dagger A^{-1}\boldsymbol{z} + \boldsymbol{z}^\dagger \boldsymbol{J} + \boldsymbol{J}^\dagger \boldsymbol{z})}, \tag{3.26}$$

exchanges a quadratic term in $\boldsymbol{J}$ with an integration over the complex $\boldsymbol{z}$ variables. Since $\boldsymbol{J}$ usually represents some field in a field theory, the new $\boldsymbol{z}$ is called the auxiliary- or conjugate field because of its linear

coupling to $\boldsymbol{J}$. In the less general case that A is a Hermitian matrix, this formula is proved simply by completing the square, then diagonalizing A by a unitary transformation and calculating the resulting integrals by the formula $\int_{\mathbb{C}} \mathrm{d}z^* \mathrm{d}z\, e^{-azz^*} = 2\pi i/a$.

From Eq. (3.26), we see that what we have to do to perform the HS transformation is first to make a choice for what to interpret as part of the matrix A and what to interpret as part of $\boldsymbol{J}$. We then have to check that this definition of A leads to its Hermitian part having only positive eigenvalues. Finally, we need to know an analytical expression for its inverse. It is usually the first step that is the most difficult, since this dictates the low energy excitation a subsequent saddle point approximation or a stationary phase approximation will produce. Typically, we are interested in transforming a Fermionic interaction potential of the form

$$V = \frac{1}{2} \sum_{\alpha\beta\gamma\delta} V_{\alpha\beta\gamma\delta} \xi^*_\alpha \xi^*_\beta \xi_\delta \xi_\gamma, \tag{3.27}$$

where ξ_α are Graßmann variables, which can be sketched in the way of the single-vertex diagram in Figure 3.2. The HS-transformation is

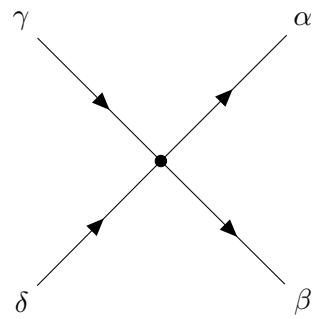

Figure 3.2: Generic two-body interaction.

classified into being done in a specific *channel* depending on which pair of Graßmann variables are considered to be part of $\boldsymbol{J}$ and consequently $\boldsymbol{J}^\dagger$. The direct channel[5] is given by the identification $J_i \sim \xi^*_\alpha \xi_\gamma$, the Cooper channel[6] is defined by the identification $J_i \sim \xi_\delta \xi_\gamma$ while the

5. Also known as the density-density channel.
6. Also known as the particle-particle channel.

exchange channel is given by the identification $J_i \sim \xi^*_\alpha \xi_\delta$. Depending on exactly how $\boldsymbol{J}$ is chosen, the Gaussian integral in Eq. (3.26) might have to be modified. For example, in the case of the direct- and exchange-channel, the exponential argument on the left side will have the form $\boldsymbol{J}^\mathsf{T} A \boldsymbol{J}$, which necessitates the Gaussian integral identity

$$e^{-\frac{1}{2}\boldsymbol{J}^\mathsf{T} A \boldsymbol{J}} = \sqrt{\det A^{-1}} \int_{\mathbb{R}} \prod_i \left[\frac{\mathrm{d}x_i}{\sqrt{2\pi}}\right] e^{-\frac{1}{2}\boldsymbol{x}^\mathsf{T} A^{-1} \boldsymbol{x} - i \boldsymbol{J}^\mathsf{T} \boldsymbol{x}}, \tag{3.28}$$

where the auxiliary field $\boldsymbol{x}$ now is a *real* conjugate field.

3.3.1 Transformation in symmetry channels

In the Cooper-channel of the HS transformation, the complex field $\boldsymbol{z}$ is conjugate to some combination of pairs of annihilation operators $\hat{c}_\delta \hat{c}_\gamma$ (or their corresponding Graßmann variables). The symmetry of the specific combination in turn then determines the symmetry of any low energy field theory obtained through a subsequent stationary phase approximation. By diagonalizing the interaction potential $\hat{V}$ into its different irreducible representations as we will do in Section 4.8, then a HS transformation in a specific symmetry channel is done by identifying $\boldsymbol{J}$ with irreducible representation (IR) basis function combinations of latter operators.

Let's take the case of a BCS theory of superconductivity where the interaction can be written in terms of basis functions $d^{(b),m}_{s_1 s_2}(\boldsymbol{k})$ such that the diagonalized interaction takes the form

$$\hat{V} = \sum d^{(b),m}_{s_1 s_2}(\boldsymbol{k})^* v_{(b)} d^{(b),m}_{s'_1 s'_2}(\boldsymbol{k}') c^\dagger_{\frac{\boldsymbol{q}}{2}+\boldsymbol{k}\, s_1} c^\dagger_{\frac{\boldsymbol{q}}{2}-\boldsymbol{k}\, s_2} c_{\frac{\boldsymbol{q}}{2}-\boldsymbol{k}' s'_2} c_{\frac{\boldsymbol{q}}{2}+\boldsymbol{k}' s'_1}, \tag{3.29}$$

where $\sum$ indicates the sum over the indices, $\boldsymbol{k}, \boldsymbol{k}', \boldsymbol{q}, s_1, s_2, s'_1, s'_2, b$ and m. Here b specifies the irreducible representation while m enumerates the representation basis .[7] Identifying

$$\hat{J}^{(b_m)}_{\boldsymbol{q}} = \sum_{\boldsymbol{k} s_1 s_2} d^{(b),m}_{s_1 s_2}(\boldsymbol{k}) \hat{c}_{\frac{\boldsymbol{q}}{2}-\boldsymbol{k}, s_1} \hat{c}_{\frac{\boldsymbol{q}}{2}+\boldsymbol{k}, s_2}, \tag{3.30}$$

the interaction potential is simply written

$$\hat{V} = \sum_{\boldsymbol{q}, b, m} \hat{J}^{(b_m)\,\dagger}_{\boldsymbol{q}} v^{(b)} \hat{J}^{(b_m)}_{\boldsymbol{q}}. \tag{3.31}$$

7. For an exposition on the basics of irreducible representations in superconductivity theory see Chapter 4.

In the path-integral representation of the partition function, the annihilation operators become Graßmann variables which we denote by writing J instead of $\hat{J}$, such that the contribution from the interaction potential results in the exponential

$$\mathcal{Z}_I = e^{-\int_0^\beta \mathrm{d}\tau \sum_{\boldsymbol{q},b,m} J_{\boldsymbol{q}}^{(b_m)\dagger} v^{(b)} J_{\boldsymbol{q}}^{(b_m)}}. \tag{3.32}$$

Now it is straightforward to use the HS formula

$$e^{\int_0^\beta \mathrm{d}\tau \sum_{ij} J_i^* A_{ij} J_j} = \int \mathcal{D}[\eta_i^* \eta_i] e^{-\int_0^\beta \mathrm{d}\tau \left(\eta_i^* A_{ij}^{-1} \eta_j + J_i^* \eta_i + J_i \eta_i^*\right)}, \tag{3.33}$$

which is a path integral version of Eq. (3.26), to transform each pair of irreducible representation basis vectors to individual conjugate fields. In the notation of Eq. (3.33) implicit summation over repeated indices is used and each index i is a collection $i = (b, m, \boldsymbol{q})$ of indices. Comparing Eq. (3.33) and (3.32) we gather that

$$A_{ij} = A_{b,m,\boldsymbol{q};b',m',\boldsymbol{q}'} = -\delta_{\boldsymbol{q}\boldsymbol{q}'} \delta_{mm'} \delta_{bb'} v^{(b)}, \tag{3.34}$$

which is trivially Hermitian and positive definite provided $v^{(b)} < 0$. In this case we say that the irreducible representation b is an attractive channel. A is in this case also trivially invertible with $A_{ij}^{-1} = -\delta_{ij}/v^{(b)}$. Writing out all the indices, we finally arrive at the HS transformation of the interaction potential in individually attractive symmetry channels

$$\mathcal{Z}_I = \int \mathcal{D}[\eta_{\boldsymbol{q}}^{(b_m)*} \eta_{\boldsymbol{q}}^{(b_m)}] e^{\int_0^\beta \mathrm{d}\tau \sum_{\boldsymbol{q}bm} \left[\frac{|\eta_{\boldsymbol{q}}^{(b_m)}|}{v^{(b)}} - \left(J_{\boldsymbol{q}}^{(b_m)*} \eta_{\boldsymbol{q}}^{(b_m)} + J_{\boldsymbol{q}}^{(b_m)} \eta_{\boldsymbol{q}}^{(b_m)}\right)\right]}, \tag{3.35}$$

where

$$J_{\boldsymbol{q}}^{(b_m)} = \sum_{\boldsymbol{k}\, s_1 s_2} d_{s_1 s_2}^{(b),m}(\boldsymbol{k}) \xi_{\frac{\boldsymbol{q}}{2}-\boldsymbol{k},s_1} \xi_{\frac{\boldsymbol{q}}{2}+\boldsymbol{k},s_2} \tag{3.36}$$

in terms of Graßmann variables ξ. We note that this derivation does not assume either odd or even basis functions for the irreducible representations and thus works just as well for either.

3.4 Field theory approximations

3.4.1 Stationary phase and the one loop expansion

Let Z be the partition function

$$Z(l) = \int \mathcal{D}[\eta_\alpha^* \, \eta_\alpha] \; e^{-lS(\eta_\alpha^*, \eta_\alpha)}, \tag{3.37}$$

given in terms of bosonic fields $\eta_\alpha^*, \eta_\alpha$ and where l is some large parameter $l \gg 1$. In what is called the stationary phase approximation[8] of a bosonic field integral, we create an expansion of the free energy around the field configuration $\{\eta_\alpha^c\}$ where the action S is stationary and a minimum. This configuration is the main contribution to the integral in Eq. (3.37) since it provides the maximum of the exponent and determines the leading order asymptotic behavior as $l \to \infty$. It also corresponds in a sense to a classical solution and gives in the case of the Feynman path-integral for the evolution operator of a single particle in an external potential, the classical Euler-Lagrange equations. The configuration is found in the path-integral notation by varying the fields in the action such that

$$\frac{\delta S}{\delta \eta_\alpha} = 0 \quad \wedge \quad \frac{\delta S}{\delta \eta_\alpha^*} = 0. \tag{3.38}$$

As an example, the Hubbard-model with a conventional negative-U Hubbard-potential $U \sum_{\boldsymbol{r}_i} \hat{n}_{\boldsymbol{r}_i,\uparrow} \hat{n}_{\boldsymbol{r}_i,\downarrow}$, can be expressed as a bosonic field integral through a HS transformation. The stationary field configuration $\{\eta_q^c(\tau)\}$ is in this case given by a imaginary-time- and spatially-independent field-configuration η^c. Assuming such a solution, the action reduces to

$$S(\eta^{c\,*}, \eta^c) = \frac{\beta N}{U} |\eta^c|^2 - \sum_{\boldsymbol{q}} \ln \left[\left(1 + e^{\beta E_{\boldsymbol{q}}}\right) \left(1 + e^{-\beta E_{\boldsymbol{q}}}\right) \right], \tag{3.39}$$

where $E_{\boldsymbol{q}} = \sqrt{(\epsilon(\boldsymbol{q}) - \mu)^2 + |\eta^c|^2}$, N is the number of hopping sites, $\epsilon(\boldsymbol{q})$ is the Fourier transformed kinetic hopping energy, μ is the chemical potential, and U is the repulsive Hubbard interaction strength. The

8. The name is misleading in the case of the many-particle partition function since we do not have a strict phase in the exponent but in general a complex function because $\eta_\alpha \in \mathbb{C}$. Technically it is the method of steepest descent for the case of an exponent with stationary points that is used in this case.

stationary action condition in Eq. (3.38) then yields the equation

$$|\eta^c|\Big(\frac{1}{U}-\frac{1}{N}\sum_{\boldsymbol{q}}\frac{1}{2E_{\boldsymbol{q}}}\tanh\frac{\beta E_{\boldsymbol{q}}}{2}\Big)=0, \tag{3.40}$$

which has two solutions: one given by $\eta^c = 0$, and one given by setting the terms in the parenthesis equal to 0. The last non-trivial solution is a form of the BCS solution and represents the order-parameter in an s-wave superconductor. Because of the parameter β, this solution will be temperature dependent and disappears at some critical temperature at which the two solutions for η_c converge.

The stationary phase expansion is then the expansion resulting from expanding the action around the stationary solution. Setting $\tilde{\eta}_\alpha = \sqrt{l}(\eta_\alpha - \eta^c_\alpha)$ we get in general the expansion

$$\begin{aligned}S(\tilde{\eta}_\alpha,\tilde{\eta}^*_\alpha) &= S_c+\frac{1}{l}\Bigg[\frac{1}{2!}\frac{\delta^2 S}{\delta\eta_\alpha\delta\eta_\beta}\Big|_{\eta_c}\tilde{\eta}_\alpha\tilde{\eta}_\beta \\ &\quad+\frac{1}{2!}\frac{\delta^2 S}{\delta\eta^*_\alpha\delta\eta^*_\beta}\Big|_{\eta_c}\tilde{\eta}^*_\alpha\tilde{\eta}^*_\beta+\frac{\delta^2 S}{\delta\eta_\alpha\delta\eta^*_\beta}\Big|_{\eta_c}\tilde{\eta}_\alpha\tilde{\eta}^*_\beta\Bigg]+\mathcal{O}\Big(\frac{1}{l\sqrt{l}}\Big) \\ &= \sum_{n_1+n_2\geq 2}\frac{1}{n_1!n_2!}\frac{\delta^{n_1+n_2}S}{\delta\tilde{\eta}_\alpha^{n_1}\delta\tilde{\eta}_\beta^{*\,n_2}}\tilde{\eta}_\alpha^{n_1}\tilde{\eta}_\beta^{*\,n_2}\Big|_{\eta_c}\frac{1}{l^{(n_1+n_2)/2}}.\end{aligned} \tag{3.41}$$

We have used implicit summation over repeated indices and on the last line we have assumed that new indices should be introduced and summed for each n_1 and n_2. This is simply the multivariate Taylor expansion around η_c where we have treated η and η^* as independent variables.

A simpler expansion can be found when the bosonic fields correspond to order parameters in a system close to a phase transition. In this case we can assume the fields η_α to be small in general such that S simply can be expanded about 0. If the system is fermionic, then the bosonic field integral of the order-parameters will have resulted from a HS transformation, in which case we will have a contribution to the integral of the form

$$\sqrt{\det G^{-1}(\eta_\alpha,\eta^*_\alpha)}=e^{\frac{1}{2}\operatorname{Tr}\ln G^{-1}}, \tag{3.42}$$

where G^{-1} is the result of the integration of a quadratic fermionic action and will in general depend on the auxiliary bosonic fields η_α and

η^*_α in a non-linear way. Then the matrix G^{-1} can be decomposed in a matrix G_0^{-1} that results purely from fermionic integration, and a matrix ϕ that is dependent on the auxiliary fields η_α and importantly vanishes as $\eta_\alpha \to 0$, such that $G^{-1} = G_0^{-1} + \phi$. When the system is close to the phase transition such that the auxiliary fields are small, then this allows for the expansion of the logarithm in Eq. (3.42) such that

$$\begin{aligned} \frac{1}{2}\operatorname{Tr}\ln(G_0^{-1}+\phi) &= \frac{1}{2}\Big(\operatorname{Tr}\ln G_0^{-1} + \operatorname{Tr}\ln(1+G_0\phi)\Big) \\ &= \frac{1}{2}\Big(\operatorname{Tr}\ln G_0^{-1} - \sum_{n=1}^{\infty}\frac{\operatorname{Tr}(-G_0\phi)^n}{n}\Big). \end{aligned} \tag{3.43}$$

This is known as the one-loop expansion since in terms of perturbation theory, G_0 is the fermionic propagator such that the sum in the last line of Eq. (3.43) corresponds to a series of propagators and interactions that are connected in a closed loop by the trace.

3.4.2 Gradient expansion

The gradient expansion rests on the assumption that the fields are sufficiently smooth, such that progressively higher order derivatives with respect to the field parameters are progressively smaller, i.e. we assume

$$l_\alpha^n|\partial_\alpha^n\eta_\alpha| \gg l_\alpha^{n+1}|\partial_\alpha^{n+1}\eta_\alpha|, \tag{3.44}$$

where l_α is some appropriate length scale such as to make $l_\alpha\partial_\alpha$ dimensionless. In practice this usually means that given a momentum-dependent action density, $S(\eta^*_{\boldsymbol{q},\alpha}, \eta_{\boldsymbol{q},\alpha}; \boldsymbol{q})$, we assume q_i small compared to the lattice spacing[9] a_i. Then we expand the explicit $\boldsymbol{q}$ dependence in the action density in the small parameters $a_i q_i$ as a Maclaurin series. In the following notation, we will assume the length parameter a^i is present in the notation q^i where appropriate. The momentum dependence of the fields themselves should not be expanded, as our goal is to have terms of the form $(q^i)^n(\tilde{\eta}_{\boldsymbol{q},\alpha})^m$. If we then let partial momentum-derivatives only act on the explicit momentum-dependence in S, and neglecting the field dependence in the notation

9. This could be the spacing between hopping sites, i.e. stationary ions in an electron model.

for S, the expanded action can be written as the series

$$S(\boldsymbol{q}) = S(0) + \frac{\partial S}{\partial q^i}(0)\, q^i + \frac{1}{2!}\frac{\partial^2 S}{\partial q^i \partial q^j}(0)\, q^i q^j + \mathcal{O}(q^3). \tag{3.45}$$

Usually, the linear term cancels by symmetry of the underlying lattice. In general, it is smart to here check for terms that cancel by considering any internal momentum sums that may be included in the coefficients.

Terms with products between fields $\eta_{\boldsymbol{q},\alpha}$ and q^i lead to gradients of the spatially dependent fields $\eta_{\boldsymbol{R},\alpha}$, which is why the expansion in Eq. (3.45) can be called a gradient expansion. The spatially dependent fields are defined as the coefficients in the inverse Fourier transform

$$\eta_{\boldsymbol{q},\alpha} = \frac{1}{\sqrt{N}} \sum_{\boldsymbol{R}} e^{i\boldsymbol{q}\cdot\boldsymbol{R}} \eta_\alpha(\boldsymbol{R}), \tag{3.46}$$

where N is the number of terms in the sums $\sum_{\boldsymbol{q}}$ and $\sum_{\boldsymbol{R}}$. One way of now obtaining gradients of the spatial fields is to realize that since q^i is small we can set

$$q^i \approx \sin(q^i) = \frac{1}{2i}\left(e^{iq^i} - e^{-iq^i}\right). \tag{3.47}$$

With this identification, all the momentum dependence in $S(\boldsymbol{q})$ exists as phases such that the sum $\sum_{\boldsymbol{q}} S(\boldsymbol{q})$ results in a series of Kronecker-delta functions which we evaluate by the $\sum_{\boldsymbol{R}}$ sums coming from the inverse Fourier transforms in Eq. (3.46). Grouping terms of displaced spatial fields, we can identify derivatives, such that

$$\eta_\alpha(\boldsymbol{R} + a\hat{e}_i) - \eta_\alpha(\boldsymbol{R}) \approx a\frac{\partial}{\partial R^i}\eta_\alpha(\boldsymbol{R}). \tag{3.48}$$

These identifications are justified by going to the continuum limit where $a \to 0$.

As an example, consider the sum

$$S = \sum_{\boldsymbol{q}} K_{\alpha\beta\, ij} q^i q^j \eta^*_{\boldsymbol{q},\alpha} \eta_{\boldsymbol{q},\beta}, \tag{3.49}$$

where there is an implicit summation over repeated indices i, j, α and β. Fourier transforming the fields according to Eq. (3.46) and writing

q^i as $\sin q^i$, we can group terms such that

$$\begin{aligned} S = \frac{1}{N}\sum_{\boldsymbol{R}_1\boldsymbol{R}_2} K_{\alpha\beta ij}\eta_\alpha(\boldsymbol{R}_1)^*\eta_\beta(\boldsymbol{R}_2)\frac{1}{4}\sum_{\boldsymbol{q}}\Big[e^{i\boldsymbol{q}\cdot(\boldsymbol{R}_2-\boldsymbol{R}_1+a\hat{e}_i-a\hat{e}_j)} \\ +e^{i\boldsymbol{q}\cdot(\boldsymbol{R}_2-\boldsymbol{R}_1+a\hat{e}_j-a\hat{e}_i)} - e^{i\boldsymbol{q}\cdot(\boldsymbol{R}_2-\boldsymbol{R}_1+a\hat{e}_i+a\hat{e}_j)} - e^{i\boldsymbol{q}\cdot(\boldsymbol{R}_2-\boldsymbol{R}_1-a\hat{e}_i-a\hat{e}_j)}\Big] \\ = \sum_{\boldsymbol{R}} K_{\alpha\beta ij}a^2\frac{\partial}{\partial R_i}\eta_\alpha(\boldsymbol{R})^*\frac{\partial}{\partial R_j}\eta_\beta(\boldsymbol{R}). \end{aligned} \tag{3.50}$$

A more conventional way of converting to gradients, is to use integration by parts. Then the product rule of partial derivatives is used to obtain

$$q^j\eta_\alpha(\boldsymbol{R})e^{i\boldsymbol{q}\cdot\boldsymbol{R}} = i\frac{\partial\eta_\alpha}{\partial R^i}e^{i\boldsymbol{q}\cdot\boldsymbol{R}} - i\frac{\partial}{\partial R^i}\Big[\eta_\alpha(\boldsymbol{R})e^{i\boldsymbol{q}\cdot\boldsymbol{R}}\Big]. \tag{3.51}$$

Summing on both sides and arguing that the boundary term vanishes because $\eta_\alpha(\boldsymbol{R}) \to 0$ as $R^i \to \infty$, then

$$\sum_{\boldsymbol{R}} q^j\eta_\alpha(\boldsymbol{R})e^{i\boldsymbol{q}\cdot\boldsymbol{R}} = i\sum_{\boldsymbol{R}} e^{i\boldsymbol{q}\cdot\boldsymbol{R}}\nabla_i\eta_\alpha(\boldsymbol{R}). \tag{3.52}$$

Chapter 4

Group Theory

In this chapter we will introduce some basic group-theoretic framework to clarify the meaning of how a free energy can "belong" to an irreducible representation, and to show how group-theory can be applied to quantum-mechanical concepts such as operators and states.

A few words about notation. We will use the semicolon ';' in equations as notation for the words '*such that*', e.g., when defining sets. A colon with a trailing space ': ' is used when defining maps where the symbol representing the mapping itself should be on the left, while the sets being related or how the elements of the sets are related, is on the right of the colon. The colon ':' is also used as a shortcut for the words '*applied through its representation to*' for when group elements are applied to vectors, where the correct representation to use for this application should be implicitly understood.

The material in this section is based on the material covered in Refs. [76] and [75], specified for the use in quantum mechanical theories of unconventional superconducting states.

4.1 Irreducible representations

To know what an irreducible representation (IR) is, let's start with what we mean by a *reducible* representation.

Def. 4.1. *A matrix representation is* ***reducible*** *if there exists a non-trivial invariant subspace of the vector space of the representation.*

The intuition is then that the vector space of the representation is reducible if a "smaller" representation is contained within it. Since there is a smaller vector space within the vector space of the original representation, and this vector space is invariant, it is possible to define another representation on this smaller vector space, i.e., *reduce* the original representation. We have now used the word "invariant" a couple of times, so let's define what it means more precisely.

Def. 4.2. *Let $D(g)$ be a representation of the group G on the vector space V such that $D(g) : V \to V$. Then a subspace $U \subseteq V$ is **invariant** if*

$$\forall g \in G \quad u \in U \implies D(g)u \in U. \tag{4.1}$$

In other words: a vector space is invariant if it is not possible for any vector in it to escape using the representation[1] of any group element. All representations applied to any vector in the invariant subspace must necessarily land in that same subspace from which it started.

4.2 BCS Hilbert Space

We define the BCS Hilbert space as the Hilbert space upon which BCS-type potentials operate. Specifically, this is a reduced form of the two-particle fermionic product Hilbert space $\mathcal{H}_2 = \mathcal{H} \otimes \mathcal{H}$ where $\mathcal{H} = \text{span}\{|\boldsymbol{k}, s\rangle\}$ and we only consider states that have opposite momentum. Thus, this Hilbert space is given by

$$\mathcal{B} = \text{span}\{|\boldsymbol{k}, s_1\rangle|-\boldsymbol{k}, s_2\rangle\}, \tag{4.2}$$

and the identity operator in this space can be written

$$\hat{\mathbb{1}} = \sum_{\boldsymbol{k}\, s_1 s_2} |\boldsymbol{k}, s_1\rangle|-\boldsymbol{k}, s_2\rangle\langle-\boldsymbol{k}, s_2|\langle\boldsymbol{k}, s_1|. \tag{4.3}$$

Acting on the arbitrary vector $|v\rangle \in \mathcal{B}$ with this identity operator, we find that in terms of this basis, the vector can be written

$$|v\rangle = \sum_{\boldsymbol{k}\, s_1 s_2} v_{s_1 s_2}(\boldsymbol{k})|\boldsymbol{k}, s_1\rangle|-\boldsymbol{k}, s_2\rangle, \tag{4.4}$$

1. In this language we use the word *representation* both to mean *linear transformation* that corrresponds to a group element on a vector space, and the *set* of all such linear transformations together with the vector space.

where

$$v_{s_1 s_2}(\boldsymbol{k}) = \langle -\boldsymbol{k}, s_2 | \langle \boldsymbol{k}, s_1 \mid v \rangle. \tag{4.5}$$

The indices s_1 and s_2 can take on only two values each, namely $s_1, s_2 \in \{\uparrow, \downarrow\}$. In total, there are thus 4 different realizations of the pairs $s_1 s_2$, e.g., $s_1 s_2 = \uparrow\uparrow$, for $v_{s_1 s_2}(\boldsymbol{k})$. Putting these different realizations of $v_{s_1 s_2}(\boldsymbol{k})$ as elements in a 2×2 matrix, we get

$$v_{s_1 s_2}(\boldsymbol{k}) = \begin{pmatrix} v_{\uparrow\uparrow}(\boldsymbol{k}) & v_{\uparrow\downarrow}(\boldsymbol{k}) \\ v_{\downarrow\uparrow}(\boldsymbol{k}) & v_{\downarrow\downarrow}(\boldsymbol{k}) \end{pmatrix}. \tag{4.6}$$

Any 2×2 matrix can be written in the conventional basis of the 4 Pauli matrices $\sigma^0 = \mathbb{1}_{2\times 2}$, σ^x, σ^y, and σ^z. This means that we *could* write the matrix in Eq. (4.6)

$$v_{s_1 s_2}(\boldsymbol{k}) = v^0_{\boldsymbol{k}} \sigma^0_{s_1 s_2} + v^i_{\boldsymbol{k}} \sigma^i_{s_1 s_2}. \tag{4.7}$$

It is, however, conventional to factor out a Pauli matrix $i\sigma^y$ to the right in the expansion, since this results in nice transformation properties of the coefficients as we shall see. With the spin-indices expanded in this basis, it is conventional to let the function of $\boldsymbol{k}$ that is in front of σ^0 be called $\psi_{\boldsymbol{k}}$. The three others are conventionally denoted $d_{\boldsymbol{k},i}$ which are components of what we call the $\boldsymbol{d}$-vector.[2] Expanded in this conventional basis, then, $v_{s_1 s_2}(\boldsymbol{k})$ takes the form

$$v_{s_1 s_2}(\boldsymbol{k}) = (\psi_{\boldsymbol{k}} \sigma^0_{s_1 s'} + d_{\boldsymbol{k},i} \sigma^i_{s_1 s'}) i\sigma^y_{s' s_2}, \tag{4.8}$$

and finally, the state $|v\rangle$ can be written

$$|v\rangle = \sum_{\boldsymbol{k}\, s_1 s_2} [(\psi_{\boldsymbol{k}} \sigma^0 + \boldsymbol{d}_{\boldsymbol{k}} \cdot \boldsymbol{\sigma}) i\sigma^y]_{s_1 s_2} |\boldsymbol{k}, s_1\rangle |-\boldsymbol{k}, s_2\rangle. \tag{4.9}$$

Going one step back and writing out the different combinations of $s_1 s_2$ in $v_{s_1 s_2}(\boldsymbol{k})$ as a matrix like we did in Eq. (4.6), but now multiplying out the Pauli matrices in Eq. (4.8), we get

$$\begin{pmatrix} v_{\uparrow\uparrow}(\boldsymbol{k}) & v_{\uparrow\downarrow}(\boldsymbol{k}) \\ v_{\downarrow\uparrow}(\boldsymbol{k}) & v_{\downarrow\downarrow}(\boldsymbol{k}) \end{pmatrix} = \begin{pmatrix} -d_{\boldsymbol{k},x} + i d_{\boldsymbol{k},y} & \psi_{\boldsymbol{k}} + d_{\boldsymbol{k},z} \\ -\psi_{\boldsymbol{k}} + d_{\boldsymbol{k},z} & d_{\boldsymbol{k},x} + i d_{\boldsymbol{k},y} \end{pmatrix}. \tag{4.10}$$

2. Note that a state in $\mathcal{B}$ that is described by a $\boldsymbol{d}$-vector does not necessarily mean that it has d-wave symmetry, which is a symmetry of its $\boldsymbol{k}$-space argument. Rather, it tells us that the state is a spin-triplet state.

This set of linear relations is easily inverted, which yields

$$\psi_{\boldsymbol{k}} = \frac{1}{2}(v_{\uparrow\downarrow}(\boldsymbol{k}) - v_{\downarrow\uparrow}(\boldsymbol{k})) \tag{4.11}$$

$$d_{\boldsymbol{k},x} = \frac{1}{2}(v_{\downarrow\downarrow}(\boldsymbol{k}) - v_{\uparrow\uparrow}(\boldsymbol{k})) \tag{4.12}$$

$$d_{\boldsymbol{k},y} = -\frac{i}{2}(v_{\uparrow\uparrow}(\boldsymbol{k}) + v_{\downarrow\downarrow}(\boldsymbol{k})) \tag{4.13}$$

$$d_{\boldsymbol{k},z} = \frac{1}{2}(v_{\uparrow\downarrow}(\boldsymbol{k}) + v_{\downarrow\uparrow}(\boldsymbol{k})). \tag{4.14}$$

Since the space $\mathcal{B}$ is fermionic, we have the symmetry[3]

$$|\boldsymbol{k}, s_1\rangle|-\boldsymbol{k}, s_2\rangle = -|-\boldsymbol{k}, s_2\rangle|\boldsymbol{k}, s_1\rangle. \tag{4.15}$$

Using this symmetry transformation on the basis vectors in the expansion of $|v\rangle$ in Eq. (4.4), then renaming indices and finally equating coefficients term by term, we see that for the coefficients of $|v\rangle$, this symmetry takes the form

$$v_{s_1 s_2}(\boldsymbol{k}) = -v_{s_2 s_1}(-\boldsymbol{k}). \tag{4.16}$$

4.3 Application of group elements

When we are talking about applying some symmetry transformation to a state, this is synonymous with applying a group element to a vector. Even more specifically, the 'applying' part means that we have some natural representation of the group on the vector space of the states, and we are using the linear transformation of the representation of the group element to act on the state vector. In this thesis, we will use the notation $g : |\psi\rangle$ to refer to this procedure.

Let g be an arbitrary group element in the symmetry group G and D be a representation of G on the d-dimensional vector space V. Let V have a basis $\{\boldsymbol{b}_i\}_{i=1}^{d}$. The application of a group element to a basis vector is then defined as

$$g : \boldsymbol{b}_i = \sum_j \boldsymbol{b}_j D_{ji}(g), \tag{4.17}$$

3. We are here assuming that the state is even in (time) frequency. It is also possible to have superconducting states that are odd in frequency [77], however we will not treat that possibility here.

where $D_{ji}(g)$ are the matrix elements of the linear transformation $D(g)$. The application of a group element to any vector in V is then calculated by expanding the vector in the basis and applying the representation D to each basis vector separately as a linear transformation:

$$g : \boldsymbol{v} = \sum_i v_i g : \boldsymbol{b}_i. \tag{4.18}$$

4.3.1 Active vector transformation

By the definition in Eq. (4.17), the transformation of $g :$ is viewed in a passive perspective since it is the basis vectors that change. It is often useful, and sometimes more intuitive, to consider the application of g to a vector $\boldsymbol{v}$ in the basis $\{\boldsymbol{b}_i\}$ as an application not on the vectors themselves, but on the expansion coefficients v_i of $\boldsymbol{v}$ in the basis. Given the transformation of the basis vectors in Eq. (4.17), we insert this into the transformation of $\boldsymbol{v}$ in Eq. (4.18), which yields

$$g : \boldsymbol{v} = \sum_i v_i \sum_j \boldsymbol{b}_j D_{ji}(g) = \sum_i v_i' \boldsymbol{b}_i, \tag{4.19}$$

where we have defined the transformed coefficients

$$v_i' = \sum_j D_{ij}(g) v_j. \tag{4.20}$$

From this calculation, we see that we can consider the application of g as a transformation of the coefficients of the vector as

$$g : v_i = \sum_j D_{ij}(g) v_j. \tag{4.21}$$

Since, in this case, the basis vectors are left invariant and static, the vector $\boldsymbol{v}$ can be viewed as being actively transformed in a fixed coordinate-system. Thus, the transformation $g : \boldsymbol{v}$ is, when viewed in this perspective, known as an active transformation. The active- and passive-perspective can be notoriously difficult to differentiate since they are, in the end, mathematically equivalent. Therefore, being consistent with a single perspective can dissuade a lot of confusion.

4.3.2 Representation on product spaces

The product space $V \otimes V$, where V is defined as before, is a vector space with a basis $\{\boldsymbol{b}_i \boldsymbol{b}_j\}_{i,j=1}^{d}$. A derived representation can be constructed from D on this product space called the product representation $D^{(D\times D)}(g)$. This is defined through its application on the basis by

$$g : \boldsymbol{b}_i \boldsymbol{b}_j = \sum_{kl} \boldsymbol{b}_k \boldsymbol{b}_l \left[D^{(D\times D)}(g)\right]_{kl,ij} = \sum_{kl} \boldsymbol{b}_k \boldsymbol{b}_l D_{ki}(g) D_{lj}(g). \tag{4.22}$$

To apply group theory to physical problems, we need to know how the objects we are working with in the physical theory transform under group elements. The most important vector space in quantum mechanics is arguably the Hilbert space where particle states are determined by a momentum- and spin quantum numbers. Each quantum number has its own vector space defined by the basis vectors $|\boldsymbol{k}\rangle$ and $|s\rangle$ in the Dirac notation. The combination of both quantum numbers in the description of a particle state, then gives a state in the product space of these vector spaces. A basis for this space is given by the vectors $|\boldsymbol{k}, s\rangle = |\boldsymbol{k}\rangle|s\rangle$. Given $\boldsymbol{k} \in \mathbb{R}^d$ and $s \in \{\uparrow, \downarrow\}$, these basis vectors transform according to the product representation of the representations on each vector space, given by

$$g : |\boldsymbol{k}', s'\rangle = \sum_{\boldsymbol{k}s} |\boldsymbol{k}, s\rangle D^{(\boldsymbol{k}\times s)}_{\boldsymbol{k}s;\,\boldsymbol{k}'s'} = \sum_{\boldsymbol{k}s} |\boldsymbol{k}, s\rangle D_{g\ ss'} \delta_{\boldsymbol{k}, g\cdot\boldsymbol{k}'}, \tag{4.23}$$

under a group element g. Here $g : \boldsymbol{k}'$ means application of g to the vector $\boldsymbol{k}'$ through the standard representation of g in $\mathbb{R}^d$. $D_{g\ ss'}$ is a representation on the spin-up spin-down vector space given by the matrix

$$D_{g\ ss'} = \sigma^0_{ss'} \cos(\phi/2) - i\hat{\boldsymbol{u}} \cdot \boldsymbol{\sigma}_{ss'} \sin(\phi/2), \tag{4.24}$$

where $\hat{\boldsymbol{u}}$ is the rotation axis unit vector, while ϕ is the angle that defines the proper rotation associated with g. $\boldsymbol{\sigma}$ is the vector notation for the 3 Pauli matrices and $\sigma^0_{ss'} = \delta_{ss'}$ [78, 79].

In the BCS Hilbert space, which we discussed in more detail in Section 4.2, the basis vectors are outer products of the momentum spin basis vectors with opposite momentum: $\{|\boldsymbol{k}, s_1\rangle|-\boldsymbol{k}, s_2\rangle\}$. The product representation on this vector space then transforms the basis vectors

according to

$$g : |\boldsymbol{k}', s_1'\rangle|-\boldsymbol{k}', s_2'\rangle = \sum_{\boldsymbol{k}\, s_1 s_2} |\boldsymbol{k}, s_1\rangle|-\boldsymbol{k}, s_2\rangle D^{(D\times D)}_{\boldsymbol{k}\, s_1 s_2;\, \boldsymbol{k}'\, s_1' s_2'}(g), \tag{4.25}$$

where

$$D^{(D\times D)}_{\boldsymbol{k}\, s_1 s_2;\, \boldsymbol{k}'\, s_1' s_2'}(g) = D_{g\, s_1 s_1'} \delta_{\boldsymbol{k}, g:\boldsymbol{k}'} D_{g\, s_2 s_2'} \delta_{-\boldsymbol{k}, g:-\boldsymbol{k}'}. \tag{4.26}$$

Since group representations on $\boldsymbol{k}$ is a linear transformation, then $\delta_{-\boldsymbol{k}, g:-\boldsymbol{k}'} = \delta_{\boldsymbol{k}, g:\boldsymbol{k}'}$, such that the last Kronecker delta function becomes superfluous.

4.3.3 Representation on ψ-$\boldsymbol{d}$ functions

The coefficients of the basis expansion of a vector in the BCS Hilbert space are typically written in the conventional ψ-$\boldsymbol{d}$ notation of Eq. (4.9). Taking the active view of group transformations, we can say that the expansion coefficients of arbitrary states $|v\rangle$ in the BCS Hilbert space $\mathcal{B}$ transform like the v_i in Eq. (4.21), but where now the representation matrix D is given by the matrix $D^{(D\times D)}_{\boldsymbol{k}\, s_1 s_2;\, \boldsymbol{k}'\, s_1' s_2'}$ above in Eq. (4.26). Written out then, the coefficients transform according to

$$g : v_{s_1 s_2}(\boldsymbol{k}) = \sum_{\boldsymbol{k}'\, s_1' s_2'} D^{(D\times D)}_{\boldsymbol{k}\, s_1 s_2;\, \boldsymbol{k}'\, s_1' s_2'} v_{s_1' s_2'}(\boldsymbol{k}'). \tag{4.27}$$

Let now $|v\rangle$ be a state that is even in space, meaning that its expansion only consists of coefficients $\psi(\boldsymbol{k})$ in the ψ-$\boldsymbol{d}$ notation. Then we see from Eq. (4.10) that $\psi(\boldsymbol{k})$ can be written $\psi(\boldsymbol{k}) = v_{\uparrow\downarrow}(\boldsymbol{k})$. The transformation properties of $\psi(\boldsymbol{k})$ are thus given by

$$\begin{aligned} g : \psi(\boldsymbol{k}) = g : v_{\uparrow\downarrow}(\boldsymbol{k}) &= \sum_{\boldsymbol{k}'\, s_1' s_2'} D^{(D\times D)}_{\boldsymbol{k}\uparrow\downarrow;\, \boldsymbol{k}'\, s_1' s_2'} \psi(\boldsymbol{k}') (i\sigma^y)_{s_1' s_2'} \\ &= \psi(g^{-1} : \boldsymbol{k}) (i\sigma^y)_{\uparrow\downarrow} = \psi(g^{-1} : \boldsymbol{k}). \end{aligned} \tag{4.28}$$

In this calculation we inserted the expression of $D^{(D\times D)}_{\boldsymbol{k}\, s_1 s_2;\, \boldsymbol{k}'\, s_1' s_2'}$ in Eq. (4.26) and used the equation $D_g i\sigma^y D_g^{\mathsf{T}} = i\sigma^y$, where D_g are the spin representation matrices given in Eq. (4.24).

To find the transformation properties of $\boldsymbol{d}_{\boldsymbol{k}}$, the principle is the same as above for $\psi(\boldsymbol{k})$, but the calculations become more involved. We

assume that the spin-momentum basis expansion of a state $|v\rangle$ consists of only odd coefficients so that $v_{s_1 s_2}(\boldsymbol{k}) = \boldsymbol{d}_{\boldsymbol{k}} \cdot (\boldsymbol{\sigma} i\sigma^y)_{s_1 s_2}$. Inserting this into the active transformation of the coefficients of $|v\rangle$ in Eq. (4.27), and also inserting the expression for $D^{(D\times D)}_{\boldsymbol{k}\, s_1 s_2;\, \boldsymbol{k}'\, s_1' s_2'}$ as we did before, yields

$$\begin{aligned} g : v_{s_1 s_2}(\boldsymbol{k}) &= \sum_{\boldsymbol{k}'\, s_1' s_2'} \delta_{\boldsymbol{k}, g:\boldsymbol{k}'} D_{g\, s_1 s_1'} D_{g\, s_2 s_2} \boldsymbol{d}_{\boldsymbol{k}'} \cdot (\boldsymbol{\sigma} i\sigma^y)_{s_1' s_2'} \\ &= \sum_s \left(D_g \boldsymbol{\sigma} \sigma^y D_g^{\mathsf{T}} \sigma^y \right)_{s_1 s} \cdot \boldsymbol{d}_{g^{-1}:\boldsymbol{k}}\, i\sigma^y_{s s_2}. \end{aligned} \tag{4.29}$$

Since a group transformation (aka. the linear transformation given by a group representation) cannot transform a state that was even into being odd, or vice versa, then the resulting state given by the transformed coefficients $g : v_{s_1 s_2}(\boldsymbol{k})$ have to remain odd, and thus they can be expanded in terms of a new $\boldsymbol{d}'$ such that

$$g : v_{s_1 s_2}(\boldsymbol{k}) = \sum_s \boldsymbol{d}'_{g^{-1}:\boldsymbol{k}} \cdot \boldsymbol{\sigma}_{s_1 s} i\sigma^y_{s s_2}. \tag{4.30}$$

Having expanded both sides of the transformed coefficients with a common factor $i\sigma^y$ to the right, we can equate the remaining 2×2 spin matrices which gives an expression for $\boldsymbol{d}'_{g^{-1}:\boldsymbol{k}} \cdot \boldsymbol{\sigma}$ by comparing Eq. (4.29) and Eq. (4.30). Furthermore, using the anti-commutation property $\{\sigma^i, \sigma^j\} = 2\delta_{ij}\sigma^0$ of Pauli matrices, we find that

$$d'_{\boldsymbol{k},i} = \frac{1}{4} \operatorname{Tr}\left(\{\sigma^i, \boldsymbol{d}'_{\boldsymbol{k}} \cdot \boldsymbol{\sigma}\} \right). \tag{4.31}$$

Inserting the expression for $\boldsymbol{d}'_{g^{-1}:\boldsymbol{k}} \cdot \boldsymbol{\sigma}$ in terms of the $SU(2)$ spin-representation matrices D_g, and inserting these matrices full expression, which can be found in Eq. (4.24), yields after some algebra

$$\begin{aligned} d'_{g^{-1}:\boldsymbol{k},i} &= \frac{1}{4} \operatorname{Tr}\left(\{\sigma^i, \boldsymbol{d}_{g^{-1}:\boldsymbol{k}} \cdot D_g \boldsymbol{\sigma} \sigma^y D_v^{\mathsf{T}} \sigma^y\} \right) \\ &= R_{ij}(\hat{\boldsymbol{u}}, \phi) d_{g^{-1}:\boldsymbol{k},j}, \end{aligned} \tag{4.32}$$

where we have defined the matrix

$$\begin{aligned} R_{ij}(\hat{\boldsymbol{u}}, \phi) &= \delta_{ij} \cos\phi + \hat{u}_i \hat{u}_j (1 - \cos\phi) - \epsilon_{ijk} \hat{u}_k \sin\phi \\ &= \begin{pmatrix} \cos\phi + \hat{u}_x^2(1-\cos\phi) & \hat{u}_x\hat{u}_y(1-\cos\phi) - \hat{u}_z \sin\phi & \hat{u}_x\hat{u}_z(1-\cos\phi) + \hat{u}_y \sin\phi \\ \hat{u}_y\hat{u}_x(1-\cos\phi) + \hat{u}_z \sin\phi & \cos\phi + \hat{u}_y^2(1-\cos\phi) & \hat{u}_y\hat{u}_z(1-\cos\phi) - \hat{u}_x \sin\phi \\ \hat{u}_z\hat{u}_x(1-\cos\phi) - \hat{u}_y \sin\phi & \hat{u}_z\hat{u}_y(1-\cos\phi) + \hat{u}_x \sin\phi & \cos\phi + \hat{u}_z^2(1-\cos\phi) \end{pmatrix}. \end{aligned} \tag{4.33}$$

This matrix is in fact the rotation matrix of a vector in $\mathbb{R}^3$ by an angle ϕ about a unit vector $\hat{\boldsymbol{u}}$. Since the coefficients of an odd state $|v\rangle$ are fully determined by the vector $\boldsymbol{d}$, their transformation can be regarded just as a transformation of $\boldsymbol{d}$ itself, which thus takes the form

$$g : d_{\boldsymbol{k},i} = R_{ij}(\hat{\boldsymbol{u}}, \phi) d_{g^{-1}:\boldsymbol{k},j}, \tag{4.34}$$

where $\hat{\boldsymbol{u}}$ and ϕ give the unit vector and angle respectively, of the proper rotation[4] that is associated with g. The conclusion is thus that $\boldsymbol{d}$ transforms as a vector by the proper rotation associated with g.

4.3.4 Representation on ladder operators

The fermionic creation and annihilation operators $c^\dagger_{\boldsymbol{k},s}$ and $c_{\boldsymbol{k},s}$, which we will collectively refer to as $c^{(\dagger)}_{\boldsymbol{k},s}$, are second-quantized operators that act on multi-particle states in a fermionic Fock space [75]. To properly define how a group element g transforms these operators, we should strictly speaking first derive the representation $Q(g)$ of g on N-particle states $|\boldsymbol{k}_1, s_1\rangle \wedge ... \wedge |\boldsymbol{k}_N, s_N\rangle$ for arbitrary N, and then use the relation $g : c^{(\dagger)}_{\boldsymbol{k},s} = Q(g) c^{(\dagger)}_{\boldsymbol{k},s} Q(g)^{-1}$ to derive their transformation properties. However, luckily, a shortcut is possible because the $Q(g)$ representation is connected with how g acts on the single-particle basis $\{|\boldsymbol{k}, s\rangle\}$ through the relationship

$$Q(g) c^{(\dagger)}_{\boldsymbol{k},s} Q(g)^{-1} = c^{(\dagger)}(g : |\boldsymbol{k}, s\rangle). \tag{4.35}$$

In this notation we treat the creation and annihilation operators as respectively linear and antiunitary functions of the states that they create or annihilate. If the matrix-components of the representation of g on the single-particle basis is denoted $D^{(\boldsymbol{k}\times s)}_{\boldsymbol{k}s;\boldsymbol{k}'s'}$, then we thus have the transformation property

$$g : c^{(\dagger)}_{\boldsymbol{k},s} = \sum_{\boldsymbol{k}'s'} c^{(\dagger)}_{\boldsymbol{k}',s'} [D^{(\boldsymbol{k}\times s)}_{\boldsymbol{k}'s';\boldsymbol{k}s}]^{(*)}, \tag{4.36}$$

where the matrix-elements are complex conjugated only if we are transforming an annihilation operator.

4. The *proper rotation* of a group element g is the rotation obtained when writing g as this rotation followed by either the group element of inversion or identity, which can be done in all point-groups.

Given that g is an element of some point-group, such that it can be decomposed into a rotation and a parity inversion, then we may use the representation on $\{|\boldsymbol{k}, s\rangle\}$ given in Eq. (4.23) such that

$$g : c^{(\dagger)}_{\boldsymbol{k},s} = \sum_{s'} c^{(\dagger)}_{g\cdot\boldsymbol{k},s'} D^{(*)}_{g\, s's}, \tag{4.37}$$

where the matrix $D_{g\, ss'}$ is defined in Eq. (4.24). As an example, a simple parity transformation $g = \hat{P}$, then transform the operators according to $\hat{P} : c^{(\dagger)}_{\boldsymbol{k},s} = c^{(\dagger)}_{-\boldsymbol{k},s}$.

We will later need the translation transformation $g = \boldsymbol{R}$ as well. In real space it is defined by $\boldsymbol{R} : |\boldsymbol{r}, s\rangle = |\boldsymbol{r} + \boldsymbol{R}, s\rangle$ and given by the linear transformation $L(\boldsymbol{R}) = e^{i\boldsymbol{R}\cdot\hat{\boldsymbol{p}}/\hbar}$, where $\hat{\boldsymbol{p}}$ is the momentum operator[5] $\hat{\boldsymbol{p}} = \hbar\nabla/i$. It then follows by a Fourier-transformation that the fermionic operators transform according to

$$\boldsymbol{R} : c^{(\dagger)}_{\boldsymbol{k},s} = \left(e^{-i\boldsymbol{R}\cdot\boldsymbol{k}}\right)^{(*)} c^{(\dagger)}_{\boldsymbol{k},s}. \tag{4.38}$$

Finally, we discuss the transformation of time-reversal. This operation is traditionally denoted Θ and consists of flipping the sign of time, which implies flipping the spin and momentum. Time-reversal is special in that it is antiunitary, i.e. it transforms all linear coefficients into their complex conjugates. Because of this, any representation of time-reversal is often factorized into a normal linear part and a complex-conjugation operator $\hat{K}$. From its action on the spin-momentum basis vectors $|\boldsymbol{k}, s\rangle$, time-reversal transforms the fermionic creation and annihilation operators according to

$$\Theta : c^{(\dagger)}_{\boldsymbol{k},s} = \sum_{s'} c^{(\dagger)}_{-\boldsymbol{k},s'} (-i\sigma_y)_{s's}. \tag{4.39}$$

Note that the matrix $-i\sigma_y$ is not complex conjugated for the fermionic annihilation operators because of the antiunitarity of Θ.

4.4 Single-particle Hamiltonian symmetries

Any fermionic single-particle operator can be written in the spin-momentum basis as

$$\hat{H} = \sum_{\boldsymbol{k}\boldsymbol{k}' ss'} H^{ss'}_{\boldsymbol{k}\boldsymbol{k}'} c^{\dagger}_{\boldsymbol{k},s} c_{\boldsymbol{k}'s'}. \tag{4.40}$$

5. The form of the linear transformation $L(\boldsymbol{R})$ follows directly from the multivariate Taylor expansion.

In this section we will apply the common finite symmetry-transformations discussed in the last Section and see how this reduces the degrees of freedom in $\hat{H}$ so that it can be written in a more concise form. To begin, we reduce the notational burden by expanding the spin-matrix elements in separate coefficients in the Pauli-matrix basis just as was done for the BCS Hilbert space vector coefficients $v_{s_1 s_2}(\boldsymbol{k})$ in Eq. (4.7), such that

$$\hat{H} = \sum_{\boldsymbol{k}\boldsymbol{k}' ss'} \left[\xi_{\boldsymbol{k}\boldsymbol{k}'}\sigma^0 + \boldsymbol{\gamma}_{\boldsymbol{k}\boldsymbol{k}'} \cdot \boldsymbol{\sigma}\right]_{ss'} c^\dagger_{\boldsymbol{k},s} c_{\boldsymbol{k}'s'}. \tag{4.41}$$

The transformation of a quantum mechanical operator such as the Hamiltonian, is defined by $g : \hat{H} = Q(g)\hat{H}Q(g)^{-1}$ for some many-body representation $Q(g)$. Inserting the form of $\hat{H}$ in Eq. (4.41) as a single-particle operator in the spin-momentum basis, yields

$$g : \hat{H} = \sum_{\boldsymbol{k}\boldsymbol{k}' ss'} \left[\xi_{\boldsymbol{k}\boldsymbol{k}'}\sigma^0 + \boldsymbol{\gamma}_{\boldsymbol{k}\boldsymbol{k}'} \cdot \boldsymbol{\sigma}\right]_{ss'} (g : c^\dagger_{\boldsymbol{k},s})(g : c_{\boldsymbol{k}'s'}), \tag{4.42}$$

after inserting $Q(g)^{-1}Q(g)$ between the creation and annihilation operator. We can now use the transformation properties of these operators presented in Section 4.3.4 to derive the transformation properties and symmetric form of the Hamiltonian.

For a translation invariant system, we need a translation invariant Hamiltonian. Using the transformation of $c^{(\dagger)}$ in Eq. (4.38) under a translation $\boldsymbol{R}$, we get that the coefficients $\xi_{\boldsymbol{k}\boldsymbol{k}'}$ and $\boldsymbol{\gamma}_{\boldsymbol{k}\boldsymbol{k}'}$ have to satisfy the equation

$$(e^{i\boldsymbol{R}\cdot(\boldsymbol{k}'-\boldsymbol{k})} - 1)\left[\xi_{\boldsymbol{k}\boldsymbol{k}'}\sigma^0 + \boldsymbol{\gamma}_{\boldsymbol{k}\boldsymbol{k}'} \cdot \boldsymbol{\sigma}\right] = 0. \tag{4.43}$$

Since the sigma-matrices are linearly independent and the translation $\boldsymbol{R}$ is arbitrary, it follows that both $\xi_{\boldsymbol{k}\boldsymbol{k}'}$ and $\boldsymbol{\gamma}_{\boldsymbol{k}\boldsymbol{k}'}$ must vanish whenever $\boldsymbol{k} \neq \boldsymbol{k}'$, i.e. these coefficients must be diagonal in $\boldsymbol{k}$. The Hamiltonian can then be written on the reduced form

$$\hat{H} = \sum_{\boldsymbol{k}ss'} \left[\xi_{\boldsymbol{k}}\sigma^0 + \boldsymbol{\gamma}_{\boldsymbol{k}} \cdot \boldsymbol{\sigma}\right]_{ss'} c^\dagger_{\boldsymbol{k},s} c_{\boldsymbol{k},s'}. \tag{4.44}$$

In the vast majority of cases, the system is Hermitian such that the Hamiltonian is self-adjoint and has real eigenvalues. Enforcing the

condition $\hat{H}^\dagger = \hat{H}$ on the translationally invariant Hamiltonian in Eq. (4.44) yields the equation

$$(\xi^*_{\boldsymbol{k}} - \xi_{\boldsymbol{k}})\sigma^0 + (\boldsymbol{\gamma}^*_{\boldsymbol{k}} - \boldsymbol{\gamma}_{\boldsymbol{k}}) \cdot \boldsymbol{\sigma} = 0, \tag{4.45}$$

by using the self-adjoint property of the Pauli-matrices. This implies further, by the linear independence of the sigma-matrices, that the coefficients $\xi_{\boldsymbol{k}}$ and $\boldsymbol{\gamma}_{\boldsymbol{k}}$ are self-conjugate and hence real.

Time-reversal symmetry of the system implies that $\hat{H}$ should be invariant under the transformation Θ, which transforms fermionic ladder-operators according to Eq. (4.39). Applying this transformation to the fermionic ladder-operators in the translationally invariant Hamiltonian of Eq. (4.44), and remembering that $Q(\Theta)$ is an antiunitary operator, we get the transformed Hamiltonian

$$\Theta : \hat{H} = \sum_{\boldsymbol{k}ss'} \left[\xi^*_{-\boldsymbol{k}}\sigma^0 - \boldsymbol{\gamma}^*_{-\boldsymbol{k}} \cdot \boldsymbol{\sigma}\right]_{ss'} c^\dagger_{\boldsymbol{k},s} c_{\boldsymbol{k},s'}. \tag{4.46}$$

For the Hamiltonian to be invariant under time-reversal symmetry, its coefficients thus have to satisfy $\xi_{\boldsymbol{k}} = \xi^*_{-\boldsymbol{k}}$ and $\boldsymbol{\gamma}_{\boldsymbol{k}} = -\boldsymbol{\gamma}^*_{-\boldsymbol{k}}$.

Finally, we look at the transformation of the Hamiltonian under point-group elements g. Using the transformation-property of the fermionic creation and annihilation operators in Eq. (4.37), then the translation-invariant Hamiltonian in Eq. (4.44) transforms according to

$$g : \hat{H} = \sum_{\boldsymbol{k}ss'} \left[\xi_{g^{-1}:\boldsymbol{k}}\sigma^0 + \boldsymbol{\gamma}_{g^{-1}:\boldsymbol{k}} \cdot D_g \boldsymbol{\sigma} D_g^\dagger\right]_{ss'} c^\dagger_{\boldsymbol{k},s} c_{\boldsymbol{k},s'}. \tag{4.47}$$

Using the form of the spin-rotation matrix D_g in Eq. (4.24), we find that

$$\boldsymbol{\gamma}_{g^{-1}:\boldsymbol{k}} \cdot D_g \boldsymbol{\sigma} D_g^\dagger = \boldsymbol{\gamma}'_{g^{-1}:\boldsymbol{k}} \cdot \boldsymbol{\sigma}, \tag{4.48}$$

for the transformed vector

$$\boldsymbol{\gamma}'_{g^{-1}:\boldsymbol{k}} = R(\hat{\boldsymbol{u}}, \phi)\boldsymbol{\gamma}_{g^{-1}:\boldsymbol{k}}, \tag{4.49}$$

where $R(\hat{\boldsymbol{u}}, \phi)$ is the 3×3 matrix representation of the proper-rotation associated with g given in Eq. (4.33). Symmetry of $\hat{H}$ under point-group transformation thus implies the symmetry conditions $\xi_{g:\boldsymbol{k}} = \xi_{\boldsymbol{k}}$ and $R(\hat{\boldsymbol{u}}, \phi)\boldsymbol{\gamma}_{g^{-1}:\boldsymbol{k}} = \boldsymbol{\gamma}_{\boldsymbol{k}}$ on the coefficients of the Hamiltonian.

4.5 Projection Operators

Let us assume that we are in a vector space V that can be divided into possibly several different IRs $D^{(\alpha)}$ of some symmetry group G. Further, let the basis vectors of these IRs be denoted by $\boldsymbol{b}_m^{(\alpha)}$ where m thus counts the number of basis vectors in each IR. Then, an arbitrary vector $\boldsymbol{v} \in V$ can be written in terms of these basis vectors as

$$\boldsymbol{v} = \sum_\alpha \sum_m c_m^{(\alpha)} \boldsymbol{b}_m^{(\alpha)}. \tag{4.50}$$

A projection operator can be used to extract any combination of a constant $c_m^{(\alpha)}$ multiplied by a basis vector $\boldsymbol{b}_n^{(\alpha)}$, where m and n can in general be different. Denoting the projection operator that picks out the mth constant multiplied by the lth basis vector in the IR β of the expansion of $\boldsymbol{v}$: $P_{lm}^{(\beta)}$, then

$$P_{lm}^{(\beta)} \boldsymbol{v} = c_m^{(\beta)} \boldsymbol{b}_l^{(\beta)}. \tag{4.51}$$

This is extremely useful in finding explicit expressions for the basis vectors $\boldsymbol{b}_l^{(\beta)}$ of the IRs. To achieve this, the projection operator is defined as

$$P_{l,m}^{(\beta)} = \frac{d_\beta}{|G|} \sum_{g \in G} D_{lm}^{(\beta)}(g)^* g :, \tag{4.52}$$

where d_β is the dimension of IR β, $D_{lm}^{(\beta)}(g)$ is the lm element of the matrix representation of the group element g and finally we have used the notation $g :$ to denote application on vectors by the relevant representation. An example is the application of g to the basis vectors $\boldsymbol{b}_m^{(\alpha)}$. Since the relevant representation of g in this case is the IR for which $\boldsymbol{b}_m^{(\alpha)}$ is a basis vector, the application becomes

$$g : b_m^{(\alpha)} = \sum_n b_n^{(\alpha)} D_{nm}^{(\alpha)}(g). \tag{4.53}$$

Usually, the full generality of the projection operators $P_{l,m}^{(\beta)}$ isn't needed and it suffices to consider the diagonal projection operators $P_{l,l}^{(\beta)} \equiv P_l^{(\beta)}$ or indeed their sum, in which case the resulting operator can be written only in terms of the IR characters $\chi^{(\alpha)}(g)$ since

$$P^{(\beta)} \equiv \sum_l P_l^{(\beta)} = \frac{d_\beta}{|G|} \sum_{g \in G} \sum_l D_{ll}^{(\beta)}(g)^* g := \frac{d_\beta}{|G|} \sum_{g \in G} \chi^{(\beta)}(g)^* g :. \tag{4.54}$$

4.6 Symmetries of the Square Lattice

The symmetry group of the square lattice is denoted C_{4v} in the Schönflies notation. It contains 8 elements in total:

e: The identity element (do nothing),

C_4: Rotation by 90° in the positive direction (ccw),

C_4^{-1}: Rotation by 90° in the negative direction (cw),

C_4^2: Rotation by 180°,

σ_x: Mirror about the zy-plane,

σ_y: Mirror about the zx-plane,

σ_{d_1}: Mirror about the downwards diagonal plane,[6]

σ_{d_2}: Mirror about the upwards diagonal plane.

This results in the group multiplication table in Table 4.1. We can check that this is correct by performing the group transformations in the top row followed by the one in the left column[7] and seeing that this results in the group transformations where these two intersect. As an example consider the vector $(x, y)^\mathsf{T}$. Transforming the basis by the 90° counterclockwise rotation C_4 we get $(-y, x)^\mathsf{T}$. Then mirroring this result about the yz-plane yields $(y, x)^\mathsf{T}$. We now realize that this is the same as mirroring the original basis about the axis $y = x$, hence $\sigma_x C_4 = \sigma_{d_2}$ as the multiplication table says.

4.6.1 Conjugation classes

The conjugation classes of a group are the sets of group elements that are conjugate to each other, meaning that there exists a group element g such that $gAg^{-1} = B$ between conjugate elements A and B. Since conjugation is an equivalence relation, it subdivides the group elements exactly into conjugation classes. The conjugation classes of the

6. We are assuming the western bias of left-to-right movement here. More precisely it is the plane containing the z axis and the line $y = -x$
7. When combining a group-element g_c from the left column and g_r from the top row, the result should be $g_\mathrm{c} g_\mathrm{r}$.

Table 4.1: Group multiplication table of the group C_{4v}.

	e	C_4	C_4^2	C_4^{-1}	σ_x	σ_y	σ_{d_1}	σ_{d_2}
e	e	C_4	C_4^2	C_4^{-1}	σ_x	σ_y	σ_{d_1}	σ_{d_2}
C_4	C_4	C_4^2	C_4^{-1}	e	σ_{d_1}	σ_{d_2}	σ_y	σ_x
C_4^2	C_4^2	C_4^{-1}	e	C_4	σ_y	σ_x	σ_{d_2}	σ_{d_1}
C_4^{-1}	C_4^{-1}	e	C_4	C_4^2	σ_{d_2}	σ_{d_1}	σ_x	σ_y
σ_x	σ_x	σ_{d_2}	σ_y	σ_{d_1}	e	C_4^2	C_4^{-1}	C_4
σ_y	σ_y	σ_{d_1}	σ_x	σ_{d_2}	C_4^2	e	C_4	C_4^{-1}
σ_{d_1}	σ_{d_1}	σ_x	σ_{d_2}	σ_y	C_4	C_4^{-1}	e	C_4^2
σ_{d_2}	σ_{d_2}	σ_y	σ_{d_1}	σ_x	C_4^{-1}	C_4	C_4^2	e

group C_{4v} are $e = \{e\}$, $2C_4 = \{C_4, C_4^{-1}\}$, $C_4^2 = \{C_4^2\}$, $2\sigma_d = \{\sigma_{d_1}, \sigma_{d_2}\}$ and $2\sigma_v = \{\sigma_x, \sigma_y\}$. The character $\chi^\Gamma(g)$ of a representation Γ is the trace of the representation matrix $D^\Gamma(g)$ of a certain group element g. Since the trace is cyclic, then for conjugate group elements A and B

$$\begin{aligned}\chi^\Gamma(B) &= \mathrm{Tr}\left(D^\Gamma(g)D^\Gamma(A)D^\Gamma(g^{-1})\right)\\ &= \mathrm{Tr}\left(D^\Gamma(g^{-1})D^\Gamma(g)D^\Gamma(A)\right)\\ &= \mathrm{Tr}\left(D^\Gamma(g^{-1}g)D^\Gamma(A)\right) = \chi^\Gamma(A).\end{aligned} \tag{4.55}$$

This means that the representations of all group elements in a certain conjugation class have the same character.

It is useful to list the characters of the different conjugation classes in a table according to the different IRs of a group. This is because the number of conjugation classes of a finite group is the same as the number of IRs of that group. This table is known as the character table of the group. The character table of the group C_{4v} is shown in Table 4.2. This table can be derived without knowing the details of the irreducible representations, but instead using character relations from basic group theory.[8] Because of this, the character table can be of immense help, and is typically the first step in determining the irreducible representations of a group.

8. Many of these relations are derived from the great orthogonality theorem which can be found e.g.in [76].

Table 4.2: Character table of the group C_{4v}.

C_{4v}	e	$2C_4$	C_4^2	$2\sigma_v$	$2\sigma_d$
Γ_1	1	1	1	1	1
Γ_2	1	1	1	-1	-1
Γ_3	1	-1	1	1	-1
Γ_4	1	-1	1	-1	1
Γ_5	2	0	-2	0	0

4.6.2 Irreducible representations

The dimensionality of the IR can be found in Table 4.2 by looking up the first column, i.e. the column giving the character of the conjugation class $\{e\}$. Since the group element e maps to the identity transformation in all representations, then its trace gives the dimension of the representation. From the table, we see that all the IRs are 1-dimensional except for Γ_5 which is 2-dimensional. All the 1-dimensional IR matrices are then completely determined by the character table since they are just given by the characters themselves, e.g. $D^{\Gamma_2}(\sigma_x) = -1$.

To find a 2-dimensional representation of C_{4v}, we can imagine how a normal 2D vector $(x, y)^\mathsf{T} \in \mathbb{R}^2$ behaves under its transformations. We take again the example of a counterclockwise rotation by 90° of the basis which transforms a vector

$$C_4 : \begin{pmatrix} x \\ y \end{pmatrix} = \begin{pmatrix} -y \\ x \end{pmatrix} = \begin{pmatrix} 0 & -1 \\ 1 & 0 \end{pmatrix} \begin{pmatrix} x \\ y \end{pmatrix}. \tag{4.56}$$

Obviously, the matrix

$$D^{(\Gamma_5)}(C_4) = \begin{pmatrix} 0 & -1 \\ 1 & 0 \end{pmatrix}, \tag{4.57}$$

is the representation matrix of a two-dimensional representation of C_4. Continuing in this way for all the group transformations, yields the

matrices

$$D^{(\Gamma_5)}(e) = \begin{pmatrix} 1 & 0 \\ 0 & 1 \end{pmatrix}, \qquad D^{(\Gamma_5)}(C_4) = \begin{pmatrix} 0 & -1 \\ 1 & 0 \end{pmatrix}, \tag{4.58a}$$

$$D^{(\Gamma_5)}(C_4^{-1}) = \begin{pmatrix} 0 & 1 \\ -1 & 0 \end{pmatrix}, \qquad D^{(\Gamma_5)}(C_4^2) = \begin{pmatrix} -1 & 0 \\ 0 & -1 \end{pmatrix}, \tag{4.58b}$$

$$D^{(\Gamma_5)}(\sigma_x) = \begin{pmatrix} -1 & 0 \\ 0 & 1 \end{pmatrix}, \qquad D^{(\Gamma_5)}(\sigma_y) = \begin{pmatrix} 1 & 0 \\ 0 & -1 \end{pmatrix}, \tag{4.58c}$$

$$D^{(\Gamma_5)}(\sigma_{d_1}) = \begin{pmatrix} 0 & -1 \\ -1 & 0 \end{pmatrix}, \quad D^{(\Gamma_5)}(\sigma_{d_2}) = \begin{pmatrix} 0 & 1 \\ 1 & 0 \end{pmatrix}. \tag{4.58d}$$

Taking the trace of these matrices, we see that this representation's characters are the same as the ones for the IR Γ_5 in the character table (Table 4.2). This implies that $\sum_g |\chi^{\Gamma_5}(g)|^2 = |C_{4v}|$, which implies in turn that the representation given by the matrices in Eq. (4.58) is irreducible. Thus, this is indeed the Γ_5 IR as advertised, and we have completed the description of the representation matrices of all the IRs of C_{4v}.

4.6.3 Proper rotations of the odd BCS function d_k

When discussing the representation of general group elements on states in the BCS Hilbert space in Section 4.3.3, we learned from Eq. (4.34) that the coefficient $\boldsymbol{d_k} \in \mathbb{R}^3$ of odd states transforms by a proper rotation $R(\hat{\boldsymbol{u}}, \phi)$. As mentioned before, a proper rotation of a group element g is the rotation obtained when writing g as a rotation followed by an inversion P or the identity transformation. We thus obtain the representation matrices of the 3D-representations of group elements $g \in C_{4v}$ directly from the 3D rotation matrix $R(\hat{\boldsymbol{u}}, \phi)$, by envisioning the combination of a rotation and $C_4^2 = P$ or e that leads to g. Because of this, we denote the representation matrices of this representation $R(g)$. As an example $\sigma_x = C_4^2 R(\hat{\boldsymbol{x}}, \pi)$, such that the representation $R(\sigma_x) = R(\hat{\boldsymbol{x}}, \pi)$. Written out in its full matrix form, this yields the

representation matrices

$$R(C_4) = \begin{pmatrix} 0 & -1 & 0 \\ 1 & 0 & 0 \\ 0 & 0 & 1 \end{pmatrix}, \qquad R(C_4^{-1}) = \begin{pmatrix} 0 & 1 & 0 \\ -1 & 0 & 0 \\ 0 & 0 & 1 \end{pmatrix}, \tag{4.59a}$$

$$R(e) = \begin{pmatrix} 1 & 0 & 0 \\ 0 & 1 & 0 \\ 0 & 0 & 1 \end{pmatrix}, \qquad R(C_4^2) = \begin{pmatrix} -1 & 0 & 0 \\ 0 & -1 & 0 \\ 0 & 0 & 1 \end{pmatrix}, \tag{4.59b}$$

$$R(\sigma_x) = \begin{pmatrix} 1 & 0 & 0 \\ 0 & -1 & 0 \\ 0 & 0 & -1 \end{pmatrix}, \qquad R(\sigma_y) = \begin{pmatrix} -1 & 0 & 0 \\ 0 & 1 & 0 \\ 0 & 0 & -1 \end{pmatrix}, \tag{4.59c}$$

$$R(\sigma_{d_1}) = \begin{pmatrix} 0 & 1 & 0 \\ 1 & 0 & 0 \\ 0 & 0 & -1 \end{pmatrix}, \qquad R(\sigma_{d_2}) = \begin{pmatrix} 0 & -1 & 0 \\ -1 & 0 & 0 \\ 0 & 0 & -1 \end{pmatrix}. \tag{4.59d}$$

4.7 Square Lattice Harmonics

Since $\psi(\boldsymbol{k})$ and $\boldsymbol{d_k}$ are invariant with respect to translation by any reciprocal lattice vector $\boldsymbol{Q}$, $\psi(\boldsymbol{k}+\boldsymbol{Q}) = \psi(\boldsymbol{k})$, they can be expanded in a discrete Fourier transform over the real lattice, such that

$$\psi(\boldsymbol{k}) = \frac{1}{\sqrt{N}} \sum_{\boldsymbol{R}} \psi_{\boldsymbol{R}} \cos \boldsymbol{R} \cdot \boldsymbol{k}, \tag{4.60}$$

and

$$\boldsymbol{d_k} = \frac{1}{\sqrt{N}} \sum_{\boldsymbol{R}} \boldsymbol{d_R} \sin \boldsymbol{R} \cdot \boldsymbol{k}, \tag{4.61}$$

where the exponential of the Fourier transform has been reduced to trigonometric functions by the parity assumed of the functions.

We are interested in the basis vectors $|\Gamma, q, m\rangle$ of the representations of the symmetry group C_{4v} of the $2D$ square lattice. In this ket notation, Γ gives the irreducible representation, m enumerates the basis vectors in case the IR is multi-dimensional, while q gives the version of the IR in case the space of possible $|v\rangle$ permits multiple versions of the same IR. In the active view of group transformations, the question of finding the basis vectors translates to finding the basis-functions of the functions $\psi(\boldsymbol{k})$ and $\boldsymbol{d_k}$ for even and odd bases, respectively. In Section 4.3.3, we saw how these functions transformed under group

transformations. In Section 4.5, we saw how the projection operators could be used to extract individual basis vectors. We will now use these operators on the Fourier expansions of $\psi(\boldsymbol{k})$ and $\boldsymbol{d_k}$ to extract possible basis-functions given the symmetry group of the square lattice.

4.7.1 Even basis-functions

We remember from Eq. (4.28) that the function $\psi(\boldsymbol{k})$ transforms as

$$g : \psi(\boldsymbol{k}) = \psi(g^{-1} : \boldsymbol{k}), \tag{4.62}$$

under a group transformation g. Operating on the Fourier expansion of $\psi(\boldsymbol{k})$ in Eq. (4.60) with the projection operator defined in Eq. (4.52) by an arbitrary IR Γ, yields

$$\begin{aligned} P^{(\Gamma)}_{l,l}\psi(\boldsymbol{k}) = \frac{d_\Gamma}{8\sqrt{N}} \sum_{\boldsymbol{R}} \psi_{\boldsymbol{R}} \Big[&(D^{(\Gamma)}_{ll}(e) + D^{(\Gamma)}_{ll}(C_4^2))\cos(\boldsymbol{R}\cdot\boldsymbol{k}) \\ &+(D^{(\Gamma)}_{ll}(C_4) + D^{(\Gamma)}_{ll}(C_4^{-1}))\cos(R_x k_y - R_y k_x) \\ &+(D^{(\Gamma)}_{ll}(\sigma_x) + D^{(\Gamma)}_{ll}(\sigma_y))\cos(R_x k_x - R_y k_y) \\ &+(D^{(\Gamma)}_{ll}(\sigma_{d_1}) + D^{(\Gamma)}_{ll}(\sigma_{d_2}))\cos(R_x k_y + R_y k_x). \end{aligned} \tag{4.63}$$

Since $\boldsymbol{k} \in \mathbb{R}^2$, we have in this calculation used the natural $2D$ representation given by the matrices in Eq. (4.58) of the group elements in C_{4v} to calculate the expressions $g^{-1} : \boldsymbol{k}$ inside the cosine functions. Inserting the matrix elements of the different IRs of C_{4v} which we discussed in Section 4.6, we get the projected functions

$$\begin{aligned} P^{(\Gamma_1)}_{1,1}\psi(\boldsymbol{k}) &\propto \sum_{\boldsymbol{R}} \psi_{\boldsymbol{R}} [\cos R_x k_x \cos R_y k_y + \cos R_x k_y \cos R_y k_x], \\ P^{(\Gamma_2)}_{1,1}\psi(\boldsymbol{k}) &\propto \sum_{\boldsymbol{R}} \psi_{\boldsymbol{R}} [\sin R_x k_y \sin R_y k_x - \sin R_x k_x \sin R_y k_y], \\ P^{(\Gamma_3)}_{1,1}\psi(\boldsymbol{k}) &\propto \sum_{\boldsymbol{R}} \psi_{\boldsymbol{R}} [\cos R_x k_x \cos R_y k_y - \cos R_x k_y \cos R_y k_x], \\ P^{(\Gamma_4)}_{1,1}\psi(\boldsymbol{k}) &\propto \sum_{\boldsymbol{R}} \psi_{\boldsymbol{R}} [\sin R_x k_x \sin R_y k_y + \sin R_x k_y \sin R_y k_x], \\ P^{(\Gamma_5)}_{1,1}\psi(\boldsymbol{k}) &\propto 0, \\ P^{(\Gamma_5)}_{2,2}\psi(\boldsymbol{k}) &\propto 0. \end{aligned} \tag{4.64}$$

Since the projection operators $P_{ll}^{(\Gamma)}$ projects onto the subspace of vectors belonging to the IR Γ, if we let the different basis-functions of the IRs Γ be denoted $\psi^{(\Gamma),q,m}(\boldsymbol{k})$, then we expect the projection to produce the result

$$P_{l,l}^{(\Gamma)}\psi(\boldsymbol{k}) = \sum_q c_{q,l}\psi^{(\Gamma),q,l}(\boldsymbol{k}), \tag{4.65}$$

by the property of projection operators in Eq. (4.51). Here q again enumerates the version of the basis of Γ possible in the space of different $\psi(\boldsymbol{k})$, and $c_{q,l}$ are the coefficients of $\psi(\boldsymbol{k})$ in the basis of the IR basis-functions. Comparing Eqs. (4.65) and (4.64), we see that different sets of basis vectors can be obtained for the IRs by including different order terms in the $\boldsymbol{R}$-sum, i.e. different lattice neighbour sites. It is also worth noting that the IR Γ_5 does not exist in the space of possible $\psi(\boldsymbol{k})$, since it is an odd representation.

Including on-site, nearest neighbour and next-nearest neighbour sites in the $\boldsymbol{R}$ sum of the projected arbitrary function $\psi(\boldsymbol{k})$ on the Γ_1 subspace in Eq. (4.65), we see that any such function can be constructed from the three basis-functions

$$\psi^{(\Gamma_1),1}(\boldsymbol{k}) = \frac{1}{2\pi}, \tag{4.66a}$$

$$\psi^{(\Gamma_1),2}(\boldsymbol{k}) = \frac{1}{2\pi}(\cos k_x + \cos k_y), \tag{4.66b}$$

$$\psi^{(\Gamma_1),3}(\boldsymbol{k}) = \frac{1}{\pi}\cos k_x \cos k_y. \tag{4.66c}$$

Each of these functions give a complete basis-function set of the Γ_1 IR which can be checked by calculating how they transform under group elements $g \in C_{4v}$. In this case, since this is the trivial Γ_1 representation, the functions are symmetric under all group elements g which produces the character 1 for all conjugation classes (compare with the first row in Table 4.2).

These basis-functions are automatically mutually orthogonal since they belong to different IR version subspaces and their normalization coefficients have been chosen such that they are normal on the 1st Brillouin zone, i.e.

$$\int_{-\pi}^{\pi}\int_{-\pi}^{\pi} \mathrm{d}k_x \mathrm{d}k_y \; \psi^{(\Gamma_1),q}(\boldsymbol{k})^* \psi^{(\Gamma_1),q'}(\boldsymbol{k}) = \delta_{qq'}. \tag{4.67}$$

Inserting up to next-nearest neighbor sites for $\boldsymbol{R}$ in the projected functions under the remaining IRs, we find the orthonormal basis-functions

$$\psi^{(\Gamma_3)}(\boldsymbol{k}) = \frac{1}{2\pi}(\cos k_x - \cos k_y), \tag{4.68a}$$

$$\psi^{(\Gamma_4)}(\boldsymbol{k}) = \frac{1}{\pi}\sin k_x \sin k_y, \tag{4.68b}$$

of the representations Γ_3 and Γ_4, respectively. The Γ_3 basis is found by expansion of $\boldsymbol{R}$ to nearest neighbor, while the one for Γ_4 is found at the next-nearest neighbor. To get a basis vector for the representation Γ_2, we would need to expand beyond the next-nearest neighbor site.

The basis-functions in Eqs. (4.68) and (4.66) are also known as square lattice harmonics. The set of square lattice harmonic functions includes the set of functions found when expanding $\boldsymbol{R}$ to arbitrary sites. As we have seen, they can be grouped and found through consideration of the IRs of the symmetry group of the square lattice. We have so far only considered even-in-$\boldsymbol{k}$ basis-functions. In the next section we will complete our discussion of square lattice harmonics with the inclusion of odd functions.

4.7.2 Odd basis-functions

Any state made from exclusively odd basis-functions, is fully determined by the coefficients $\boldsymbol{d}_{\boldsymbol{k}}$. As we derived in Section 4.3.3, these coefficients transform as[9] $g : \boldsymbol{d}_{\boldsymbol{k}} = R(g)\boldsymbol{d}_{g^{-1}\cdot\boldsymbol{k}}$ under group elements $g \in C_{4v}$, where $R(g)$ are the representation matrices in Eq. (4.59). Otherwise, finding bases for irreducible representations can be done by following the same procedure as that outlined for even functions in the last Section.

As an example, we consider finding a basis for the Γ_5 irreducible representation of the group C_{4v} in the space of odd functions $\boldsymbol{d}_{\boldsymbol{k}}$. Acting on the Fourier expansion of the arbitrary function $\boldsymbol{d}_{\boldsymbol{k}}$ in Eq. (4.61) with the projection operators Eq. (4.52) down on the subspace of the

9. See Eq. (4.34).

IR Γ_5 of the symmetry group C_{4v}, yields the results

$$P^{(\Gamma_5)}_{1,1}\boldsymbol{d}_{\boldsymbol{k}} = \frac{\hat{\boldsymbol{z}}}{\sqrt{N}}\sum_{\boldsymbol{R}} d_{\boldsymbol{R},z}\cos R_x k_x \sin R_y k_y, \tag{4.69a}$$

$$P^{(\Gamma_5)}_{2,2}\boldsymbol{d}_{\boldsymbol{k}} = \frac{\hat{\boldsymbol{z}}}{\sqrt{N}}\sum_{\boldsymbol{R}} d_{\boldsymbol{R},z}\sin R_x k_y \cos R_y k_y, \tag{4.69b}$$

for the two basis-functions of Γ_5.[10] As in the spin-singlet case, we get different versions of the Γ_5 basis vectors depending on the order of our expansion in $\boldsymbol{R}$. Expanding to nearest neighbor sites and normalizing such that the states are orthonormal, produces the basis-functions

$$\boldsymbol{d}^{(\Gamma_5),1}_{\boldsymbol{k}} = -\frac{\hat{\boldsymbol{z}}}{2\pi}\sin k_y, \tag{4.70a}$$

$$\boldsymbol{d}^{(\Gamma_5),2}_{\boldsymbol{k}} = \frac{\hat{\boldsymbol{z}}}{2\pi}\sin k_x, \tag{4.70b}$$

of the two-dimensional IR Γ_5.

4.8 Decomposition of the Potential

Let at first $\hat{V}$be a general two-body operator that acts on an N-particle state which is a vector in $\mathcal{H}_N = \otimes_{i=1}^{N}\mathcal{H}$. The single particle Hilbert space $\mathcal{H}$ in question, is quantified by momentum and spin, such that $\mathcal{H} = \text{span}\{|\boldsymbol{k}, s\rangle\}$. Denoting for the moment the specific combinations of $\boldsymbol{k}$ and s as α as a shorthand, then $\hat{V}$ acts on basis vectors in $\mathcal{H}_N$ such that

$$\hat{V}|\alpha_1\rangle ... |\alpha_N\rangle = \sum_{1\leq i<j\leq N}\hat{V}_{ij}|\alpha_1\rangle ... |\alpha_N\rangle, \tag{4.71}$$

by definition of being a two-body operator [75]. Here, $\hat{V}_{ij}$ is an operator that only acts on the ith and jth ket. Even though $\hat{V}$acts on $\mathcal{H}_N$, because of how it can be written in terms of $\hat{V}_{ij}$, and this only acts on two states at a time, it follows that $\hat{V}$is completely determined by its action on the reduced two-particle Hilbert space $\mathcal{H}_2$. This implies that $\hat{V}$is fully described by its matrix elements

$$\langle\alpha|\langle\alpha'|\hat{V}|\beta\rangle|\beta'\rangle. \tag{4.72}$$

10. Since Γ_5 is two-dimensional as opposed to the other IRs in C_{4v}, any complete basis for Γ_5 requires two basis functions that can be related through transformation by a group element.

Inserting back the $|\boldsymbol{k}, s\rangle$ notation, these matrix elements are referred to as

$$V_{\boldsymbol{k}_1\boldsymbol{k}_2\boldsymbol{k}_3\boldsymbol{k}_4;\, s_1s_2s_3s_4} = \langle \boldsymbol{k}_1 s_1 | \langle \boldsymbol{k}_2 s_2 | \hat{V} | \boldsymbol{k}_4 s_4 \rangle | \boldsymbol{k}_3 s_3 \rangle. \tag{4.73}$$

When $\hat{V}$ is a BCS operator acting on the BCS Hilbert space described in Section 4.2, these matrix elements are denoted

$$V_{\boldsymbol{k}\boldsymbol{k}';\, s_1s_2s_3s_4} = \langle \boldsymbol{k} s_1 | \langle -\boldsymbol{k} s_2 | \hat{V} | \boldsymbol{k}' s_4 \rangle | -\boldsymbol{k}' s_3 \rangle. \tag{4.74}$$

Since $\hat{V}$ is Hermitian, it must be diagonalizable in some basis of eigenfunctions. Barring accidental degeneracy, a basis for a d-degenerate eigenvalue is also a basis for an IR of the symmetry group G of the Hamiltonian [76]. In the case of accidental degeneracy, then this d-dimensional vector space consists of several non-intersecting subspaces, where each subspace is a basis for a (possibly different) IR. Note that this does not mean that (barring accidental degeneracy) there exists one separate eigenvalue for each IR of G, since there might be several different eigenvalues with different eigenspace bases but where all of them are bases for the same IR. Regardless of these details, the connection between IRs and the eigenvalues of $\hat{V}$ is a great help in finding the bases for which it is diagonal.

Let the basis for a d_Γ-dimensional IR Γ be denoted $\{|\Gamma, q_\Gamma, m\rangle\}_{m=1}^{d_\Gamma}$, where $\hat{V}$ has an eigenvalue V_{Γ,q_Γ} for the vectors in this basis, and q_Γ is an index enumerating the different versions of bases of Γ that $\hat{V}$ might have in its set of eigenspace bases. Since $\hat{V}$ is diagonal in this set of bases, then

$$\hat{V} = \sum_{\Gamma q_\Gamma} V_{\Gamma,q_\Gamma} \sum_{m=1}^{d_\Gamma} |\Gamma, q_\Gamma, m\rangle\langle \Gamma, q_\Gamma, m|. \tag{4.75}$$

Because of the potential for accidental degeneracy,[11] we cannot guarantee that $V_{\Gamma,q_\Gamma} \neq V_{\Gamma',q_{\Gamma'}}$ for different Γ and Γ'. Inserting this expression for $\hat{V}$ into the matrix elements in Eq. (4.74) lets us write them in

11. A degeneracy of an eigenvalue is *accidental* if two degenerate eigenvectors belong to different IR vector spaces, while a non-accidental degeneracy of an eigenvalue happens when the eigenvectors in the eigen-space belong to a several-dimensional IR.

terms of IR basis vectors in the momentum spin function representation:

$$V_{\boldsymbol{k}\boldsymbol{k}';\,s_1s_2s_3s_4} = \sum_{\Gamma} V_{\Gamma,q_\Gamma} \sum_{m=1}^{d_\Gamma} \Psi^{\Gamma,q_\Gamma}_{s_1s_2}(\boldsymbol{k})\Psi^{\Gamma,q_\Gamma}_{s_3s_4}(-\boldsymbol{k}')^\dagger, \tag{4.76}$$

where

$$\Psi^{\Gamma,q_\Gamma}_{s_1s_2}(\boldsymbol{k}) = \langle \boldsymbol{k}, s_1 | \langle -\boldsymbol{k}, s_2 \mid \Gamma, q_\Gamma, m\rangle. \tag{4.77}$$

We can separate the set of different IR bases into bases that have vectors that transform either symmetrically or anti-symmetrically with respect to the group element of space inversion P. We call the representations of such bases even or odd representations. Even representations are those that map P to the identity operator $\mathbb{1}$ and as a consequence have functions with the symmetry $\Psi^{\Gamma,q_\Gamma,m}_{s_1s_2}(-\boldsymbol{k}) = \Psi^{\Gamma,q_\Gamma,m}_{s_1s_2}(\boldsymbol{k})$. Writing the spin-indices of these functions in terms of Pauli matrices by using the expansion in Eq. (4.8), and using the fermionic symmetry following the same logic as Section 4.2, then functions of even representations a can be written

$$\Psi^{a,q_a,m}_{s_1s_2}(\boldsymbol{k}) = \psi^{a,q_a,m}_{\boldsymbol{k}} i\sigma^y_{s_1s_2}. \tag{4.78}$$

Odd representations b map P to the inversion operator I such that $\Psi^{b,q_b,m}_{s_1s_2}(-\boldsymbol{k}) = -\Psi^{b,q_b,m}_{s_1s_2}(\boldsymbol{k})$. Expanding in Pauli matrices, then yields

$$\Psi^{b,q_b,m}_{s_1s_2}(\boldsymbol{k}) = \boldsymbol{d}^{b,q_b,m}_{\boldsymbol{k}} \cdot (\boldsymbol{\sigma} i\sigma^y)_{s_1s_2}. \tag{4.79}$$

Separating the sum over IRs Γ into sums over even (a) and odd (b) representations in the potential operator matrix elements in Eq. (4.76), we arrive at the fully expanded expression

$$\begin{aligned} V_{\boldsymbol{k}\boldsymbol{k}';\,s_1s_2s_3s_4} = &\sum_{aq_a} V_{a,q_a} \sum_{m=1}^{d_a} \psi^{a,q_a,m}_{\boldsymbol{k}} i\sigma^y_{s_1s_2} (\psi^{a,q_a,m}_{-\boldsymbol{k}'} i\sigma^y_{s_3s_4})^\dagger \\ &+ \sum_{bq_b} V_{b,q_b} \sum_{m=1}^{d_b} (\boldsymbol{d}^{b,q_b,m}_{\boldsymbol{k}} \cdot \boldsymbol{\sigma} i\sigma^y)_{s_1s_2} \left[(\boldsymbol{d}^{b,q_b,m}_{-\boldsymbol{k}'} \cdot \boldsymbol{\sigma} i\sigma^y)_{s_3s_4} \right]^\dagger. \end{aligned} \tag{4.80}$$

In this use of the dagger notation, the adjoint acts on both the spin- and momentum matrix indices, such that $\boldsymbol{d}^\dagger_{-\boldsymbol{k}} = \boldsymbol{d}^*_{\boldsymbol{k}}$ and $\sigma^\dagger_{s_1s_2} = \sigma^*_{s_2s_1}$.

On a square lattice, the functions $\psi_{\boldsymbol{k}}^{a,q_a,m}$ and $\boldsymbol{d}_{\boldsymbol{k}}^{b,q_b,m}$ of the eigenspace basis vectors $|\Gamma, q_\Gamma, m\rangle$ are given by the square lattice harmonics. Given an interaction potential $\hat{V}$ with a known form of $V_{\boldsymbol{k}\boldsymbol{k}';s_1s_2s_3s_4}$, to decompose it into the form of Eq. (4.80), we can first find the eigenvalues by calculating the matrix elements

$$\langle \Gamma, q_\Gamma, m|\hat{V}|\Gamma, q_\Gamma, m\rangle = V_{\Gamma,q_\Gamma}. \tag{4.81}$$

Then we can simply insert these eigenvalues and the known form of $\psi_{\boldsymbol{k}}^{a,q_a,m}$ and $\boldsymbol{d}_{\boldsymbol{k}}^{b,q_b,m}$ into Eq. (4.80), and we have a symmetry-decomposed potential!

Writing the potential on this form, easily lets us see if there are any attractive symmetric channels in the potential, which could lead to an instability and thus a phase-transition by pairing of the electrons according to the specified symmetry. A low energy effective theory can then be found in the unstable symmetry-channel by using the channel's square-lattice harmonics in determining the $\boldsymbol{J}$s in the Hubbard-Stratonovich transformation in Eq. (3.26), and then performing a saddle-point approximation.

Chapter 5

Lattice Models

When we have a model for the free energy of a statistical mechanical system that is too complicated to calculate analytically, one approach is to utilize computers and Monte-Carlo (MC) techniques to gain quantitative answers to questions about the system's behaviour. Such techniques often require the discretization of a continuous model down on a numerical lattice. The lattice can in principle be of any form as long as the continuum limit reproduces the original theory, however in this thesis we will exclusively focus on a square (cubic) numerical lattice due to its simplicity.

In this chapter we will introduce different aspects of discretizing a continuous free-energy model down on a square numerical lattice. If starting with a continuous model with a spatially dependent field $f(\boldsymbol{r})$, then the discretized model will have a corresponding field $f_{\boldsymbol{r}}$ only defined on the numerical lattice sites at

$$\boldsymbol{r} = \sum_{\mu} r_{\mu}\hat{\mu} = \sum_{\mu} a_{\mu} n_{\mu}\hat{\mu} \tag{5.1}$$

where a_{μ} is the distance between lattice sites, $n_{\mu} \in [0, 1, \dots, N_{\mu} - 1]$ and N_{μ} is the total number of sites in the μ-direction. The length of the numerical lattice in this direction is $L_{\mu} = a_{\mu} N_{\mu}$. The cubic numerical lattice is specified by $a_{\mu} = a \ \forall \mu$ and $\mu \in \{x, y, z\}$. Any integrals $\int \mathrm{d}^3 r \ F[f(\boldsymbol{r})]$ will in such a discretization have to be replaced with

sums such that

$$\int \mathrm{d}^3 r \mapsto a^3 \sum_{r_\mu = a}^{Na} . \tag{5.2}$$

If we are interested in bulk properties of the model in the thermodynamic limit, then specifying realistic boundary conditions of the numerical lattice are of less importance. In this case, periodic boundary conditions are from a computational- and theoretical perspective a convenient choice. We define periodic boundary conditions by the requirement that $f_{\boldsymbol{r}+L_\mu \hat{\mu}} = f_{\boldsymbol{r}}$ for any direction $\hat{\mu}$.

5.1 Discretizing derivatives

In a model where fields only are defined at discrete points in space, any spatial gradient of the fields must take the form of discrete differences of the field values at these points. In a cubic grid of points with defined field-values, such differences can be denoted by the forward-difference operator Δ_μ. This operator acts on a spatially discrete function $f_{\boldsymbol{r}}$ as a forward-difference in the direction of $\hat{\mu}$ such that

$$\Delta_\mu f_{\boldsymbol{r}} = f_{\boldsymbol{r}+a\hat{\mu}} - f_{\boldsymbol{r}}, \tag{5.3}$$

where a is the distance between lattice points. In a Euclidean geometry, the natural discretization of a derivative ∂_μ is $\partial_\mu \mapsto \Delta_\mu / a$, which reproduces the continuum derivative in the limit $a \to 0$ with a fixed grid-size. Using an appropriate set of units, we in most cases can set $a = 1$.

5.1.1 Covariant derivatives

When discretizing continuous gauge theories, some extra care must be taken when discretizing a covariant derivative. Because of the gauge field, the geometry is no longer naively Euclidean. Then we need to rotate a field-value at one point by a gauge group element to parallel-transport it to another point, such that the field values at these spatially separate points can be compared. Given a $U(1)$ gauge symmetry with gauge field components $A_\mu(\boldsymbol{r})$, the appropriate way of discretizing a covariant derivative is the identification [80]

$$D_\mu f(\boldsymbol{r}) = [\partial_\mu + igA_\mu(\boldsymbol{r})] f(\boldsymbol{r}) \mapsto \frac{1}{a}(f_{\boldsymbol{r}+a\hat{\mu}} U_{\boldsymbol{r},\mu} - f_{\boldsymbol{r}}). \tag{5.4}$$

The value of f at $\boldsymbol{r} + a\hat{\mu}$ is parallel transported back to $\boldsymbol{r}$ by the $U(1)$ group element [81]

$$U_{\boldsymbol{r},\mu} = e^{igA_{\boldsymbol{r},\mu}}, \tag{5.5}$$

where g is the coupling constant between f and the gauge field A, and

$$A_{\boldsymbol{r},\mu} \equiv \int_{\boldsymbol{r}}^{\boldsymbol{r}+a\hat{\mu}} \mathrm{d}\boldsymbol{r} \cdot \boldsymbol{A}(\boldsymbol{r}), \tag{5.6}$$

is a link-variable, linking $\boldsymbol{r}$ to its nearest neighbors.

In the limit of $a \to 0$, this identification reproduces the covariant derivative.[1] Furthermore, it produces terms that transform in an analogous way to the continuum version under gauge transformations, such that gauge invariant terms remain invariant after discretization. In the continuous fields, a gauge transformation is defined by

$$\begin{aligned} f(\boldsymbol{r}) &\to f(\boldsymbol{r}) e^{i\phi(\boldsymbol{r})}, \\ A_\mu(\boldsymbol{r}) &\to A_\mu(\boldsymbol{r}) - \frac{1}{g}\partial_\mu \phi(\boldsymbol{r}). \end{aligned} \tag{5.7}$$

Then the covariant derivative transforms as $D_\mu f(\boldsymbol{r}) \to e^{i\phi(\boldsymbol{r})} D_\mu f(\boldsymbol{r})$, such that terms such as $|D_\mu f(\boldsymbol{r})|^2$ are invariant under gauge-transformations. Inserting the gauge transformation into the discretized field $f_{\boldsymbol{r}}$ and the definition of the link-variables $A_{\boldsymbol{r},\mu}$, we see that these discretized fields transform as

$$\begin{aligned} f_{\boldsymbol{r}} &\to f_{\boldsymbol{r}}\, e^{i\phi_{\boldsymbol{r}}}, \\ A_{\boldsymbol{r},\mu} &\to A_{\boldsymbol{r},\mu} - \frac{1}{g}\Delta_\mu \phi_{\boldsymbol{r}}, \end{aligned} \tag{5.8}$$

where the field $\phi_{\boldsymbol{r}}$ is discretely defined on the same lattice points as $f_{\boldsymbol{r}}$. Inserting this into the discretization of the covariant derivative on the right-hand side of Eq. (5.4), we see that indeed the right-hand side transforms in the same way as the left, i.e. by picking up an overall factor $e^{i\phi_{\boldsymbol{r}}}$. This means that the discretized version of terms such as $|D_\mu f(\boldsymbol{r})|^2$, which were originally gauge-invariant, will be invariant under the gauge-transformation in Eq. (5.8) after discretization.

1. To show this, we see from Eq. (5.6) that $A_{\boldsymbol{r},\mu} \to a A_\mu(\boldsymbol{r})$. Then we expand the exponential in $U_{\boldsymbol{r},\mu}$ to first order and insert on the right-hand side of Eq. (5.4).

5.1.2 Discretized symmetry

One word of caution when discretizing continuous expressions is that discretized gradient terms will not in general have all the same spatial symmetries as the originating continuous terms. This is because the bias of the forward direction in the forward-difference operator and the cubic structure of the numerical lattice will in general break such symmetries.

The effects of the cubic symmetry of the numerical lattice can be thought of as caused by implicit lattice potentials that increases in influence towards lower temperatures and higher field strengths when the model contains an external field [82]. Such lattice potentials can e.g., cause topological defects to have preferred positions in discretizations of theories with translational symmetry.[2] As an example, consider again the discretization of the term $\int \mathrm{d}^3 r \ |\boldsymbol{D} f(\boldsymbol{r})|^2$ with discretized scalar field $f_{\boldsymbol{r}} = \rho_{\boldsymbol{r}} e^{i\theta_{\boldsymbol{r}}}$. The density term is rotationally symmetric[3] in 3D, however the discretized version can be written

$$2 \sum_{\boldsymbol{r}} \sum_{\mu} \rho_{\boldsymbol{r}}^2 [1 - \cos(\Delta_\mu \theta_{\boldsymbol{r}} + g A_{\boldsymbol{r},\mu})]. \tag{5.9}$$

From this form, we can see that the term is only symmetric by rotation by 90° in the planes normal to the x, y and z directions. The discretized term contains cubic distortions when rotating in directions in-between these, hence the $SO(3)$ rotational symmetry is broken down to the octahedral point group O.

The forward bias of the forward-difference discretization scheme can also lead to breaking of symmetries that both the continuous model and the numerical lattice have in common when the scalar field consists of multiple components. Consider a density term of the form

$$\Re\Big[D_x \eta_x D_y \eta_y \Big], \tag{5.10}$$

where η_x and η_y are two scalar fields that transform as components of spin and $\Re$ extracts the real part of the complex number. Under an active 90° $\hat{z}$-rotation (which is called a C_4 transformation), then

2. More on this in Section 7.
3. By rotationally symmetric we mean that if we were to rotate the field configurations of $f(\boldsymbol{r})$ and $\boldsymbol{A}(\boldsymbol{r})$ in any direction, by any amount, the term would still yield the same value.

$D_x \to D_y$, $D_y \to -D_x$, $\eta_x \to \eta_y$ and $\eta_y \to -\eta_x$. Inserting this into the continuous density term in Eq. (5.10), we see that it remains precisely the same, i.e. invariant. Now consider the discretization of this term by the discretization procedure detailed above. This would read

$$\begin{aligned}
&\rho^x_{\boldsymbol{r}+\hat{x}}\rho^y_{\boldsymbol{r}+\hat{y}}\cos\left[\theta^x_{\boldsymbol{r}+\hat{x}} - \theta^y_{\boldsymbol{r}+\hat{y}} + g(A_{\boldsymbol{r},x} - A_{\boldsymbol{r},y})\right] \\
-&\rho^x_{\boldsymbol{r}+\hat{x}}\rho^y_{\boldsymbol{r}}\cos(\theta^x_{\boldsymbol{r}+\hat{x}} - \theta^y_{\boldsymbol{r}} + gA_{\boldsymbol{r},x}) \\
-&\rho^x_{\boldsymbol{r}}\rho^y_{\boldsymbol{r}+\hat{y}}\cos(\theta^x_{\boldsymbol{r}} - \theta^y_{\boldsymbol{r}+\hat{y}} - gA_{\boldsymbol{r},y}) \\
+&\rho^x_{\boldsymbol{r}}\rho^y_{\boldsymbol{r}}\cos(\theta^x_{\boldsymbol{r}} - \theta^y_{\boldsymbol{r}}),
\end{aligned} \tag{5.11}$$

where we have used the notation $\eta^a_{\boldsymbol{r}} = \rho^a_{\boldsymbol{r}} e^{i\theta^a_{\boldsymbol{r}}}$ for the discrete scalar fields. In terms of these scalar fields and link-variables, a C_4 transformation consists of the mappings $\eta^x_{\boldsymbol{r}} \to \eta^y_{C_4\boldsymbol{r}}$ and $\eta^y_{\boldsymbol{r}} \to -\eta^x_{C_4\boldsymbol{r}'}$, such that e.g., $\rho^x_{\boldsymbol{r}+\hat{x}} \to \rho^y_{\boldsymbol{r}'+\hat{y}}$. The link-variables transform as $A_{\boldsymbol{r},\mu} \to A_{C_4\boldsymbol{r},C_4\mu}$, such that e.g., $A_{\boldsymbol{r},y} \to A_{\boldsymbol{r}',-x} = -A_{\boldsymbol{r}'-\hat{x},x}$. Using these transformations, and shifting the summation index of the external $\boldsymbol{r}$-sum, then the rotated discrete terms take the form

$$\begin{aligned}
&-\rho^x_{\boldsymbol{r}-\hat{x}}\rho^y_{\boldsymbol{r}+\hat{y}}\cos\left[\theta^x_{\boldsymbol{r}-\hat{x}} - \theta^y_{\boldsymbol{r}+\hat{y}} - g(A_{\boldsymbol{r},y} + A_{\boldsymbol{r}-\hat{x},x})\right] \\
+&\rho^x_{\boldsymbol{r}}\rho^y_{\boldsymbol{r}+\hat{y}}\cos(\theta^x_{\boldsymbol{r}} - \theta^y_{\boldsymbol{r}+\hat{y}} - gA_{\boldsymbol{r},y}) \\
+&\rho^x_{\boldsymbol{r}-\hat{x}}\rho^y_{\boldsymbol{r}}\cos(\theta^x_{\boldsymbol{r}-\hat{x}} - \theta^y_{\boldsymbol{r}} - gA_{\boldsymbol{r}-\hat{x},x}) \\
-&\rho^x_{\boldsymbol{r}}\rho^y_{\boldsymbol{r}}\cos(\theta^x_{\boldsymbol{r}} - \theta^y_{\boldsymbol{r}}),
\end{aligned} \tag{5.12}$$

which certainly is not the same as Eq. (5.11), i.e. the discretization of Eq. (5.10) is not invariant under a C_4 rotation. A more immediate way of seeing the problem is to recognize that the first term in Eq. (5.11) is a next-nearest neighbor coupling on the numeric lattice that only couples sites along one diagonal, but not the other as illustrated in Figure 5.1, thus rotational symmetry is broken by the discretization.

One remedy for this kind of problem is to re-establish the broken symmetry by an average over symmetry-transformed terms. In the case of the discretization of $\Re[D_x\eta_x D_y\eta_y]$ in Eq. (5.11), the C_4 symmetry can thus be re-established by taking the average of Eq. (5.11), Eq. (5.12), as well as the terms obtained by transforming the discretization in Eq. (5.11) by the rotations C_4^2 and C_4^3. Let $\mathcal{F}_{\boldsymbol{r}}$ denote the density terms in Eq. (5.11) and let $\mathcal{TF}_{\boldsymbol{r}}$ be the terms that result when

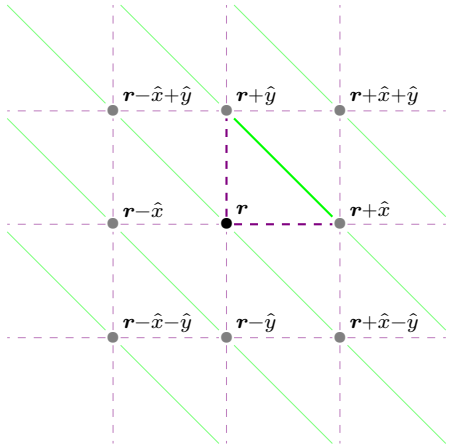

Figure 5.1: Couplings between sites on a single z-layer of the numerical lattice from the discretization in Eq. (5.11) of the term $\Re[D_x\eta_x D_y\eta_y]$. On-site terms are illustrated by a point ($\bullet$), while nearest neighbor and next-nearest neighbor couplings are illustrated by dashed and solid lines, respectively. The couplings obtained by evaluating Eq. (5.11) at a point $\boldsymbol{r}$ are slightly emphasized compared to the other lines.

transforming $\mathcal{F}$ by a symmetry transformation $\mathcal{T}$. The average of symmetry-transformed terms, which re-establishes the C_4 rotational symmetry, can then be written

$$\begin{aligned}\mathcal{F}^{\text{sym}}_{\boldsymbol{r}} &= \frac{1}{4}\sum_{\mathcal{T}\in\{\mathbb{1},C_4,C_4^2,C_4^3\}} \mathcal{T}\mathcal{F}_{\boldsymbol{r}} \\ &= \frac{1}{4}\sum_{hh'=\pm 1} hh'\rho^x_{\boldsymbol{r}+h\hat{x}}\rho^y_{\boldsymbol{r}+h'\hat{y}}\cos\left[\theta^x_{\boldsymbol{r}+h\hat{x}} - \theta^y_{\boldsymbol{r}+h'\hat{y}} + g(A_{\boldsymbol{r},hx} - A_{\boldsymbol{r},h'y})\right].\end{aligned} \tag{5.13}$$

In this expression, the next-nearest neighbour couplings are along all diagonals around the point $\boldsymbol{r}$ such that it is rotationally symmetric under C_4 and thus does not explicitly break symmetries that both the original theory and the numerical lattice have in common. Such breaking of symmetries can, as we have shown above, result from the naive application of a forward-difference discretization scheme[4] when discretizing terms with multiple gradient-directions and components. In

4. The symmetric expression in Eq. (5.13) can be more easily obtained by the use of a different discretization procedure than the discretization of the covariant

models with such terms, the symmetry averaged expression can then be useful in diminishing the effect of meta-stable states and faster convergence when investigating such models by means of numerical computation. Finally, we would like to stress that both versions yield the same theory in the continuum limit.

5.2 Including an external field

The interaction between superconductors and magnetic fields is an essential aspect in the study of superconductors and thus we will need to be able to add external magnetic fields to our models to study this interaction. An external field is usually included as a constant homogeneous magnetic field in a certain direction and is a parameter of the problem rather than a variable. In other words, we assume the magnetic flux to be the same everywhere and unchanging, and rather than ask what consequence the existence of a superconductor has on this field, we are interested in the effects the field has on the superconducting state. Physically this situation is relevant, e.g., if a relatively small and thin sheet of superconducting material is placed in between two strong electromagnets as illustrated in Figure 5.2.

One way to introduce a constant magnetic field in a lattice model, is simply to figure out what kind of vector potential $\boldsymbol{A}(\boldsymbol{r})$ would give a constant magnetic field $\boldsymbol{B}(\boldsymbol{r})$ through $\boldsymbol{B} = \nabla \times \boldsymbol{A}$, and then set the link-variables $A_{\boldsymbol{r},\mu}$ of Eq. (5.6) accordingly, with the only caveat being that for a lattice-model with periodic boundary conditions, the factor $e^{igA_{\boldsymbol{r},\mu}}$ has to satisfy periodic boundary conditions as well. This implies the condition

$$\forall \nu \quad A_{\boldsymbol{r},\mu} = A_{\boldsymbol{r}+L_\nu \hat{\nu},\mu} + 2\pi m_\nu / g, \tag{5.14}$$

where $m_\nu \in \mathbb{Z}$ and ν gives a direction on the lattice. For $m_\nu \neq 0$ this condition is called a twisted boundary-condition.

derivative in Eq. (5.4). Taking the average of a forward and backward difference that respects gauge-transformations we get the discretization mapping

$$D_\mu f(\boldsymbol{r}) \mapsto (e^{igA_{\boldsymbol{r},\mu}} f_{\boldsymbol{r}+\hat{\mu}} - e^{igA_{\boldsymbol{r},-\mu}} f_{\boldsymbol{r}-\hat{\mu}})/2.$$

Applying this symmetrized covariant discretization mapping to the density term in Eq. (5.10), yields Eq. (5.13).

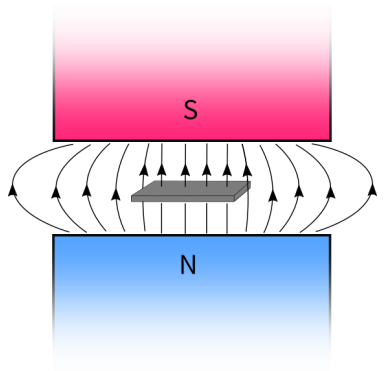

Figure 5.2: A thin sheet of superconducting material in the magnetic field produced by two magnets pointing in the same direction above and below the superconductor.

5.2.1 Landau Gauge

As an example, let's say we are interested in having an external field in the $\hat{z}$-direction with magnitude B. The vector-potential components A_x and A_y then have to satisfy the equation

$$\partial_x A_y - \partial_y A_x = B. \tag{5.15}$$

One configuration of the vector potential, which is called the *Landau gauge*, that satisfies this condition is $A_y = Bx$, with the other vector potential components set to zero. Inserting this into the definition of the link-variables in Eq. (5.6) yields $A_{\boldsymbol{r},\mu} = ar_x B\delta_{\mu,y}$. Here x is a continuous variable while r_x is the x-component of a lattice vector. Periodic boundary conditions on the lattice implies the condition $A_{\boldsymbol{r},y} = A_{\boldsymbol{r}+L_x\hat{x},y} - 2\pi m/g$, which finally restricts the value of the field B such that the link-variables in the Landau gauge must take the form

$$A_{\boldsymbol{r},\mu} = \delta_{\mu,y} r_x \frac{2\pi m}{gL_x}, \quad m \in \mathbb{Z}, \tag{5.16}$$

where $L_x = N_x a$ and N_x is the number of lattice sites in the x-direction. With this link-variable configuration, the field strength becomes $B = 2\pi f/ga^2$, where we have defined the filling fraction $f = m/N_x$, which in terms of vortices gives the number of magnetic single-quanta vortices pr. plaquette of the numerical lattice.

5.2.2 Symmetric Landau gauge

The Landau gauge has the disadvantage that it singles out a direction in the xy-plane, since the vector potential is set to $\boldsymbol{A}(\boldsymbol{r}) = Bx\hat{y}$, and thus is only spatially dependent in the x-direction. It could, because of this, be argued to break a rotational symmetry of the model in the xy-plane given that Aharenov-Bohm-like effects are significant to the results. To mitigate any such concern, one can consider a symmetric gauge given by the choice $\boldsymbol{A}(\boldsymbol{r}) = -\boldsymbol{r} \times B\hat{z}/2$, which is rotationally symmetric in the xy-plane, and like the Landau gauge, produces the field $\boldsymbol{B} = B\hat{z}$. Inserting this choice of vector potential into the link-variables, yields, using implicit summation over repeated indices, $A_{\boldsymbol{r},\mu} = \epsilon_{\mu z\nu} r_\nu aB/2$. Periodic boundary conditions in this case implies two restrictions on the field value B because the vector potential varies in both the x- and y-direction. Implementing these conditions, we can write the link-variables as

$$A_{\boldsymbol{r},\mu} = \epsilon_{\mu z\nu} r_\nu \frac{2\pi m}{gL_x}, \tag{5.17}$$

where m is a number $m \in \mathbb{Z}$ chosen such that there exists some $n \in \mathbb{Z}$ such that $mN_y = nN_x$, i.e. m is some multiple of N_x/N_y. Then the field value is given by $B = 2\pi f/ga^2$ for filling fraction $f = 2m/N_x$.

This gauge is a specification of the more general extended Landau gauge [68, 83], which is borne purely out of the assumptions of a field $\boldsymbol{B} \| \hat{z}$, $\boldsymbol{A}(\boldsymbol{r})$ linear in $\boldsymbol{r}$, and twisted periodic boundary conditions.

5.2.3 Fluctuating field

For a normal strongly type-II superconductor, the London penetration depth λ is much larger than the superconducting coherence length ξ. In this regime, it is valid to neglect spatial fluctuations in the gauge field since any deviation around the extremal field configuration is strongly suppressed. This is called the frozen gauge approximation and makes the vector potential act only as a constraint on the value of the uniform magnetic induction given by one of the gauges presented in the above sections [68]. When the superconducting state consists of multiple components, on the other hand, it becomes difficult to classify it simply in terms of type-I or type-II based solely on λ and ξ [84]. With multiple components, it becomes essential to fluctuate the gauge

field, because it mediates a significant indirect interaction between the components [70, 85].

Fluctuations of the gauge field imparts an energy cost on the system given in SI-units by the free energy[5]

$$F_A = \frac{1}{2\mu_0}(\nabla \times \boldsymbol{A})^2. \tag{5.18}$$

There are a couple of different ways of discretizing this energy for inclusion in a lattice model depending on whether one defines the link-variables compactly, i.e. $gA_{\boldsymbol{r},\mu} \in (-\pi, \pi)$, or non-compactly, i.e. $gA_{\boldsymbol{r},\mu} \in (-\infty, \infty)$. Both versions belong to the same universality class and thus produce the same results in a renormalization group sense, provided that the fluctuations are sufficiently small [80]. For noncompact link-variables, we simply replace the gradient with the lattice difference operator from Eq. (5.3) divided by the lattice spacing a, and the gauge-field components by their corresponding link-variables such that

$$\begin{aligned} \partial_\mu &\mapsto \Delta_\mu / a_\mu, \\ A_\mu(\boldsymbol{r}) &\mapsto A_{\boldsymbol{r},\mu}/a_\mu. \end{aligned} \tag{5.19}$$

The discretized free energy pr. lattice site then becomes

$$F_{A,\boldsymbol{r}} = \frac{(\boldsymbol{\Delta} \times \boldsymbol{A}_{\boldsymbol{r}})^2}{2\mu_0 a^4} = \frac{1}{2\mu_0 a^4} \sum_\mu (A^{\boxdot}_{\boldsymbol{r},\mu})^2, \tag{5.20}$$

where we have defined the link-variable plaquette-sum vector, with components given by

$$A^{\boxdot}_{\boldsymbol{r},\mu} = \epsilon_{\mu\alpha\beta}\Delta_\alpha A_{\boldsymbol{r},\beta} = \oint_{\boxdot_\mu} \mathrm{d}\boldsymbol{r}' \cdot \boldsymbol{A}(\boldsymbol{r}'). \tag{5.21}$$

In the line-integral on the right-hand side, the curve $\boxdot_\mu$ is given by a plaquette[6] normal to the vector $\widehat{\mu}$, starting at the lattice point at $\boldsymbol{r}$, and

5. One way of deriving said energy is to start with the sourceless Maxwell Lagrangian for a massless vector field $\mathcal{L}_M = -F^{\mu\nu}F_{\mu\nu}/4\mu_0$. In this relativistic notation $F^{\mu\nu} = \partial^\mu A^\nu - \partial^\nu A^\mu$, $A^0 = V$, $\partial_0 = \partial_t/c$ and we use the metric $g^{\mu\nu} = \mathrm{diag}(1, -1, -1, -1)$. Assuming time-independence and neglecting terms consisting only of Vsince they do not couple to the Higgs fields (e.g.the superconducting components) in minimal coupling, then the Lagrangian reduces to $\mathcal{L}_M \to -(\nabla \times \boldsymbol{A})^2/2\mu_0$ and the free energy in Eq. (5.18) results.
6. In this context, a plaquette is a square given by 4 neighboring lattice points contained in some plane.

moving along the square following the right-hand rule. The integration curve given by the plaquette $\boxdot_z$ is shown in Figure 5.3.

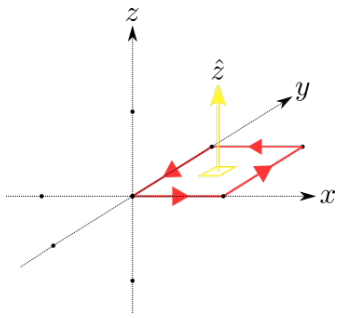

Figure 5.3: Integration path defined as $\boxdot_z$ along a plaquette of the numerical lattice in the xy-plane.

To impose an external field on a system with a fluctuating field, we divide the link-variables into a fluctuating part $A^f_{\boldsymbol{r},\mu}$ with periodic boundary conditions, and a constant part $A^0_{\boldsymbol{r},\mu}$, such that $A_{\boldsymbol{r},\mu} = A^f_{\boldsymbol{r},\mu} + A^0_{\boldsymbol{r},\mu}$. The field is then imposed by setting the constant part such that there is a net field induction through the system, e.g.by setting it to one of the gauges in Section 5.2.1 or 5.2.2.

Chapter 6

Monte-Carlo Techniques

In this chapter, we discuss some techniques useful in MC simulations of systems in statistical physics. In such systems, these techniques will be used to calculate thermal averages using random numbers. Let Z denote the partition function and $\mathcal{H}$ the Hamiltonian of the system. Then the thermal average of an observable $\mathcal{O}$ is defined as

$$\langle \mathcal{O} \rangle = \frac{1}{Z} \sum_{\psi} \mathcal{O}(\psi) e^{-\beta \mathcal{H}(\psi)}, \tag{6.1}$$

where ψ denotes states of the system, and we thus sum over all possible states. In the case of a quantum many-particle system, this sum turns into a multi-dimensional integral over quantum coherent states. Now, any attempt at estimating these integrals through an interpolation scheme is destined to fail because if we divide a 1-dimensional integral into M pieces and the error of the interpolation scheme scales as $\sim M^{-\kappa}$, then applied to a d-dimensional integral, its error will scale as $M^{-\kappa/d}$. What MC techniques then provides is a way of using random numbers in calculating Eq. (6.1) without actually summing over all the states. We do this by drawing random states ψ_i from a carefully selected probability distribution and using statistics to estimate how close the resulting thermal average is likely to be to the true thermal average. Letting M be the number of samples, then the error scales as $M^{-1/2}$ and is independent of the number of dimensions of the integral.

As in the case of the stationary phase approximation, the calculation of the sum in Eq. (6.1) can be made much more effective by considering which terms give large contributions. If we have a probability distribution $\pi(\psi)$ of sampled states ψ that is peaked around states that give large contributions to $\langle\mathcal{O}\rangle$, then our estimate will converge much quicker towards the true value than if we were to sample states uniformly. In a sense, we are interested in sampling only the important states, and hence this is called importance sampling. Let $\{\tilde{\psi}_i\}$ be a set of states that are uniformly sampled, while $\{\psi_i\}$ are sampled with probability distribution $\pi(\psi_i)$. The statistical estimator $\langle\bar{\mathcal{O}}\rangle$ of the thermal average of the observable $\mathcal{O}$ is then

$$\langle\bar{\mathcal{O}}\rangle = \sum_i \mathcal{O}(\tilde{\psi}_i)\frac{e^{-\beta\mathcal{H}(\tilde{\psi}_i)}}{Z(\{\tilde{\psi}_i\})} = \sum_i \mathcal{O}(\psi_i)\frac{e^{-\beta\mathcal{H}(\psi_i)}}{\pi(\psi_i)Z(\{\psi_i\})}. \tag{6.2}$$

Now, assuming that the state-dependence of the observable is less important than the exponential, then the largest contributions to the sum will come from states that are such that $e^{-\beta\mathcal{H}}/Z$ is large. We thus want to pick states such that

$$\pi(\psi_i) = e^{-\beta\mathcal{H}(\psi_i)}/Z. \tag{6.3}$$

Then, given M states sampled according to this probability distribution, the statistical estimator reduces to the arithmetic average

$$\langle\bar{\mathcal{O}}\rangle = \frac{1}{M}\sum_i \mathcal{O}(\psi_i). \tag{6.4}$$

6.1 Markov-Chain Monte-Carlo method

The Markov-Chain Monte-Carlo (MCMC) method is a strategy of obtaining a sample of random states ψ_k, where the states are drawn sequentially in such a way that the probability $P_k(\psi)$ of drawing a new state $\psi_k = \psi$ is only dependent on what the last state ψ_{k-1} was. The chain developed by drawing states in this way, thus has no memory of the rest of the content of the chain, except for its last link ψ_{k-1}. A chain with this property is called a Markov-Chain, hence the name.

We want the sampled states to be drawn according to the probability distribution $\pi(\psi_k)$ discussed above. This is assured with the criteria of ergodicity and detailed balance. Ergodicity means in this context that

the states are drawn in such a way that if we were to draw infinitely many states, then we would have drawn all possible states ψ in the original sum in Eq. (6.1).

The criterion of detailed balance comes from the idea that we want the probability that a certain state is drawn at any given point, to be independent of when/where that point is located in the chain. Let $P_k(\psi)$ be the probability that ψ is drawn at the kth point in the chain. Because of the Markov-chain property, this probability is fully determined by the probability that the previous state in the chain transitions into the state ψ. Let $\mathcal{T}(\psi' \to \psi)$ denote the probability that state ψ' transitions into state ψ, i.e. that the state ψ is drawn given a previously drawn state ψ'. Then the probability that the state drawn at the point $k+1$ in the chain is ψ, is given by

$$\begin{aligned} P_{k+1}(\psi) &= \sum_{\psi'} P(\psi_k = \psi' \ \wedge \ \psi' \text{ transitions to } \psi) \\ &= \sum_{\psi'} P_k(\psi')\mathcal{T}(\psi' \to \psi) \\ &= P_k(\psi) + \sum_{\psi'} \Big[P_k(\psi')\mathcal{T}(\psi' \to \psi) - P_k(\psi)\mathcal{T}(\psi \to \psi') \Big], \end{aligned} \tag{6.5}$$

where we have used that $\sum_{\psi'} \mathcal{T}(\psi \to \psi') = 1$ since the state must transition to some state. Now since we want the probability $P_k(\psi)$ to be invariant of the point's position in the chain k and be given by our desired probability density $\pi(\psi)$, we demand that $P_{k+1}(\psi) = P_k(\psi) = \pi(\psi)$. This implies that the last sum in Eq. (6.5) vanishes. Because the probability density $\mathcal{T}$ is arbitrary, the sum needs to vanish term-wise, yielding the condition of detailed balance:

$$\pi(\psi')\mathcal{T}(\psi' \to \psi) = \pi(\psi)\mathcal{T}(\psi \to \psi'). \tag{6.6}$$

This states that for the selection process of choosing states for points in the Markov-chain to be invariant of the relative locations of the points in the chain, the process must be reversible.

6.2 Metropolis-Hastings method

The Metropolis-Hastings (MH) method is an algorithm for drawing states in a Markov-Chain that specifies a transition probability $\mathcal{T}(\psi \to$

ψ') between states ψ and ψ' that satisfies the detailed balance criterion. The algorithm proceeds as follows:

1. Given a state ψ_k, generate a new state ψ_p where the process of generating this state has an, as of now, arbitrary probability distribution denoted $q(\psi_p \,|\, \psi_k)$ with the only requirement being that it leads to ergodic selection.

2. Accept this new proposed state ψ_p, with the probability $\alpha(\psi_p \,|\, \psi_k)$, defined as

$$\alpha(\psi_p \,|\, \psi_k) = \min\left\{1,\ \frac{\pi(\psi_p)q(\psi_k \,|\, \psi_p)}{\pi(\psi_k)q(\psi_p \,|\, \psi_k)}\right\}. \tag{6.7}$$

3. If ψ_p is accepted, we set $\psi_{k+1} = \psi_p$. If not, then $\psi_{k+1} = \psi_k$. Finally return to 1. to pick the next state in the chain.

By this procedure, then the probability of transitioning between a state ψ at point k to a state ψ' at point $k+1$ is given by the probability that the state ψ' is picked and that ψ' is accepted, such that

$$\mathcal{T}(\psi \to \psi') = \alpha(\psi' \,|\, \psi)\, q(\psi' \,|\, \psi). \tag{6.8}$$

This transition probability satisfies detailed balance since inserting Eq. (6.8) and (6.7) yields

$$\begin{aligned} \pi(\psi')\mathcal{T}(\psi' \to \psi) &= \min\{\pi(\psi)q(\psi' \,|\, \psi),\ \pi(\psi')q(\psi \,|\, \psi')\} \\ &= \pi(\psi)\mathcal{T}(\psi \to \psi'). \end{aligned} \tag{6.9}$$

6.2.1 Practical considerations

Usually, the above is a bit too general for practical implementation since we would have to calculate or know the probability distribution $q(\psi' \,|\, \psi)$ used in picking new proposed states. If we assume q to be symmetric, such that

$$q(\psi' \,|\, \psi) = q(\psi \,|\, \psi'), \tag{6.10}$$

then we do not need to calculate it explicitly since it cancels out of the equation for α in Eq. (6.7).

A further simplification can be achieved by inserting the expression for $\pi(\psi)$ in Eq. (6.3) into the q symmetric version of α, which in this case reduces to

$$\alpha(\psi' \,|\, \psi) = \min\left\{1,\ e^{-\beta\left[\mathcal{H}(\psi')-\mathcal{H}(\psi)\right]}\right\}. \tag{6.11}$$

This form has the merit that the acceptance probability is only dependent on the difference between the energy of the updated and original state. If the state of the system ψ is a collection of site-dependent sub-states $\phi(\boldsymbol{r}_j)$, e.g., how the state of an Ising-chain is given by a collection of site-dependent spins, then the calculation of $\mathcal{H}(\psi)$ must include all the sites. If we update only a single site $\boldsymbol{r}_j$ of ψ to get ψ', which we call a local MC update, then all the sites that do not have an interaction with $\boldsymbol{r}_j$ cancels out in the difference $\mathcal{H}(\psi') - \mathcal{H}(\psi)$. Then we only need to calculate the difference in the sub-states that are affected by $\boldsymbol{r}_j$ to calculate the energy-difference. This is an essential property to have when creating a parallelized version of this algorithm, since different parts of the lattice of sites then can be updated in an asynchronous manner without affecting each other. In other words: by simplifying to the energy difference, the update scheme becomes local, which makes local MC updates grid-parallelizable.

To use pseudo-random numbers to accept a new state ψ' with probability α, we pick a uniformly distributed number $r \in (0, 1]$. Then we use the fact that

$$P[r \leq \alpha(\psi' \,|\, \psi)] = \alpha(\psi' \,|\, \psi), \tag{6.12}$$

which implies that updating the state if $r \leq \alpha$, is equivalent to updating the state with probability α. Given the form of α in Eq. (6.11), then

$$r \leq \alpha(\psi' \,|\, \psi) \ \Leftrightarrow\ \ln r \leq -\beta[\mathcal{H}(\psi') - \mathcal{H}(\psi)]. \tag{6.13}$$

To update the state with probability α, we thus simply take the natural logarithm of r, and update the state if the right-hand side of Eq. (6.13) is true.

To obtain good statistics, we want, as a rule of thumb, the acceptance rate to be about $30 - 60\%$ for high temperature states.[1] The

1. High temperature states refers to states that are well above any transition temperature of the system.

acceptance rate is defined as the number of proposed states ψ' that are accepted, divided by the total number of proposed states, within some finite time-interval, and will in general be proportional to the acceptance probability $\alpha(\psi' \mid \alpha)$. The acceptance rate can be adjusted by changing the way new states ψ' are proposed. Let ψ be composed of site-specific sub-states $\phi(\boldsymbol{r}_j)$ and let a state ψ' be proposed by changing the values of the sub-state $\phi(\boldsymbol{r}_0)$. Choosing values closer to the original sub-state $\phi(\boldsymbol{r}_o)$, the difference $\mathcal{H}(\psi') - \mathcal{H}(\psi)$ decreases such that $\alpha(\psi' \mid \psi)$ in Eq. (6.11) approaches 1 and thus the acceptance rate increases.

Proposing states such that the acceptance rate is very high by using this technique, can lead to new states not changing very much with each MC update. This can lead to freezing of the simulation, where the measurements do not change even after a significant number of MC, updates because a large number of updates in the same direction is needed to significantly change the measurements. On the other hand, too low of an acceptance rate will also freeze the simulation since then obviously states are very unlikely to change, leading to the same measurements repeatedly. Ultimately, whether the acceptance rate should be considered too high or too low, should be guided by the physics of the system since in the case that the system has reached a global minimum in the energy-landscape and has low temperature, the proper statistics is obtained by an update scheme that gives a low acceptance rate. It is not advisable to change the acceptance rate during a measurement-run over decreasing temperatures, as this has tended to freeze the measurements at varying temperatures leading to confusion when trying to find a transition point.

6.3 Thermalization procedures

Thermalization in a MCMC simulation, refers to the process of discarding a set number of MC updates before starting to measure the states in the Markov-chain. The reason for doing this is because the first states in the chain will usually be very unlikely in the ensemble of states, and thus including them will give these states an artificially high statistical weight, unless we measure long enough. That time could be very long indeed if the starting states are very unlikely, thus, to get

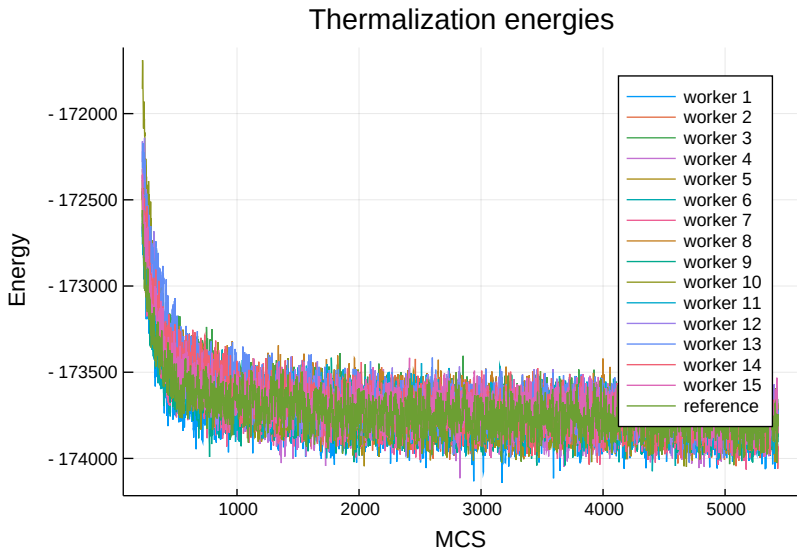

Figure 6.1: Thermalization of a 64^3 single-component XY-system from random initial states to a numerical temperature $T = 0.5$. The different curves represent the energy of different realizations of the same system initialized at different random states over several MCSs. The random initial states have a relatively high energy that stabilizes to the same value for all realizations in an exponential fashion.

measurements in a reasonable time, these unlikely starting states are discarded.

How many states to discard, is usually estimated with the help of an energy vs. Monte-Carlo sweep (MCS)[2] plot as shown in Figure 6.1. Since the initial state usually has a different energy than the average energy in the Markov-chain, the energy can be seen to rapidly stabilize to the average value in such a plot.

Whether the energy stabilizes from above or below will depend on what the initial state is, and what the temperature of the simulation has been set to. An ab-initio state in which the values of the sub-states are set to uniformly distributed random values within their validity range, normally corresponds to a high temperature and high energy

2. A Monte-Carlo sweep is a term used for attempting to update all the different sites of a system once.

state, hence thermalizing from such a state will have the energy stabilize from above. Another possibility for an ab-initio state, is some kind of mean-field minimal solution of the Hamiltonian, where sub-states at different sites are correlated. In this case, the energy will usually be low, and the thermalization energy will thus stabilize from below. This option has the disadvantage that if the mean field solution lies inside some local energy minimum, then simulations that start in this state might not be able to get out and find the global minimum. In contrast, simulations that are thermalized from random high energy states will have the possibility of finding the global minimum, even if some simulations also fall down in the local minimum of the mean-field solution. In general, it is recommended to thermalize several independent systems from different initial conditions and check that they yield quantitatively similar results to make it less likely that the results come from a local minimum or meta-stable state.

A last suggestion for an initial state of the system is the last state of a previous simulation. In this case, the thermalization will stabilize depending on the relative temperature of the two simulations. To be sure that the measurements are not correlated with the measurements of the last simulation, one should discard a number of states equal to the *auto-correlation time* of the system. The continuation from a previous simulation is a useful practice if gathering results over an extended temperature range where the systems need a large thermalization time in order to stabilize. One would then typically start measuring at a high temperature, and then decrease the temperature successively in steps with a separate thermalization- and measure-period for each step.

For systems prone to fall into local minima, it was found that a more careful thermalization process analogous to the measurement procedure described above, decreased the probability of freezing into such minima. Instead of thermalizing from a high energy / high temperature state directly down to the desired temperature, which we call quenching, a cooldown period was added. During the cooldown period, the temperature was lowered stepwise from a high temperature T_0 to a target temperature T, with intermediate temperatures

$$T_k = \left(\frac{T}{T_0}\right)^{\frac{k}{N}} T_0. \tag{6.14}$$

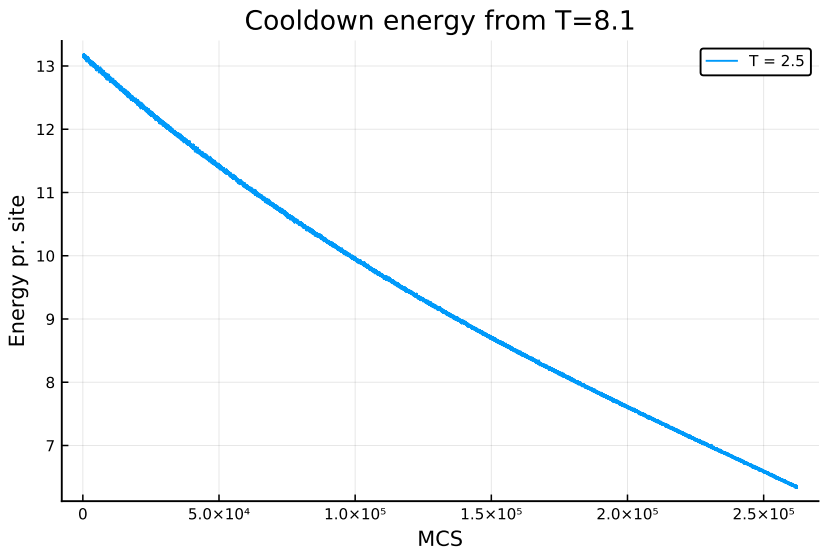

Figure 6.2: Energy pr. site of a 64^3 site model system of a $p + ip$ chiral superconductor during the cooldown stage. The temperature is lowered as a geometric sequence and a fixed number of MCSs are done at each temperature step. Comparing with the thermalization in Figure 6.1, we see that the cooldown period gives a significantly more gradual thermalization.

The intermediate temperatures were geometrically distributed over the cooldown region to ensure a higher density of intermediate steps towards lower temperatures. At each temperature step, a fixed number of MCSs were performed such that more MCSs were done towards the lower temperature than higher. This was done because the simulations in general took longer to thermalize when the temperature decreased. An example of how the energy changed during such a thermalization period is shown in Figure 6.2.

The cooldown period was then followed by a conventional thermalization stage where the temperature was held constant at T. In most cases, the energy had already stabilized at this point, such that the energy measurements during this extra thermalization stage typically only showed fluctuations around the mean.

6.4 Parallel tempering

Parallel tempering is a method of simulating multiple systems over a range of different temperatures where the systems can exchange positions with their neighbors in this temperature range according to a MH-like update step. Since the different systems all have the same parameters except for temperature, when viewed from the perspective of a single temperature, this leads to a normal Metropolis-Hastings MCMC simulation with an occasional global update of all sites of the system, whenever the system at that temperature exchanges with the system at a neighboring temperature. From the dual perspective of a single system, parallel tempering (PT) allows the system to make a random walk in temperature space.

This global updating, or movement in temperature space, has the advantage that it can prevent systems from getting stuck in local minima, by allowing them to move to a higher temperature where it is easier to fluctuate to a more favorable configuration. In systems that have a jagged energy-landscape with lots of local minima, this can be of great benefit and can reduce the required time it takes to measure observables with a certain accuracy by several orders of magnitude [86].

To implement parallel tempering MCMC in a temperature-centric perspective, let $\{T_i\}_{i=1}^{M}$ be a sorted list of M ascending temperatures, and let $\{\lambda_i\}_{i=1}^{M}$ be a list of indices λ, that identify replica states $\{\psi_\lambda\}_{\lambda=1}^{M}$ of the system such that the replica with temperature T_i is given by ψ_{λ_i} and its energy is given by E_{λ_i}. The simulation then proceeds according to the algorithm

1. Perform Δt normal MC updates on all replica states, e.g., using the MH method.

2. For each replica state ψ_λ, calculate the corresponding energy E_λ.

3. For each pair of neighboring temperatures T_i and T_{i+1} where $T_i < T_{i+1}$:

   a) Calculate the quantity

$$\Delta = (E_{\lambda_{i+1}} - E_{\lambda_i})\Big(\frac{1}{T_{i+1}} - \frac{1}{T_i}\Big). \tag{6.15}$$

b) Then swap the indices $\lambda_i \leftrightarrow \lambda_{i+1}$ with probability $\min\{1, e^{\Delta}\}$. This can as in the MH method be done by generating a random number $r \in [0, 1)$ and then swapping indices if $\ln r \leq \Delta$.

4. If the replicas ψ_λ have internal knowledge of their temperatures, then distribute T_i to ψ_{λ_i}, for all temperatures T_i.

5. Sample observables and return to 1.

This algorithm is easily parallelizable since the bulk of computing time will be going to doing the Δt MC-updates, which can be performed in parallel by having each replica state ψ_λ be assigned to a separate thread / processor. If each thread in addition keeps track of the replica's energy at the end of the MC updates, the only information that needs to be transferred between worker processes and the process doing the PT update step, is the values of the energies to the PT process, and afterwards: the set of new temperatures back to the worker processes. The PT process itself only needs to calculate $M - 1$ simple expressions and move around the indices in an array.

For the PT method to generate good statistics efficiently, some care should be taken in the distribution of the temperatures T_i. A rule of thumb is to distribute them geometrically, i.e. according to

$$T_i = \left(\frac{T_M}{T_1}\right)^{\frac{k-1}{M-1}} T_1, \tag{6.16}$$

with the argument that lower temperatures generally have a lower relaxation rate. With geometric distribution, the temperatures are denser towards the low end such that the acceptance rate of swaps of replicas at neighboring temperatures would in general become flatter and more independent of temperature. Should the specific heat diverge at some point T_c in the temperature range, as in the case of a phase transition, then this distribution would no longer be optimal since the acceptance probability of temperature swaps is inversely proportional to C_v, and thus the acceptance rate would no longer be flat. In this case, more temperatures should be distributed around T_c in order for systems to be able to random walk from one side of T_c to the other.

From the perspective of an individual replica, the overall goal with the distribution of temperatures is to maximize the number of times

the replica moves from the lowest temperature T_1, up to the highest temperature T_M, and back to the lowest temperature again. This will then maximize the number of statistically independent visits of the system to each temperature. The hope is that a flat acceptance rate with respect to the distributed temperatures will facilitate a good number of such roundtrips. The number of roundtrips can be optimized with more advanced methods such as the *feedback-optimized parallel-tempering MC method*, which models the movement of replicas by parallel tempering as a diffusion process [87].

6.5 Grid parallelization

A simple way of utilizing multiple processor cores (or cpus) on a multiprocessor system, is to run independent MC simulation on each processor. This is usually very efficient if a parameter of the system such as temperature is to be varied over some interval. Then, each simulation could have a different value of this parameter. In this case, it is recommended to also implement PT since the extra overhead is minimal and the speedup of the simulations can be significant.

Alternatively, all the simulations can run with the same value on different processes, and the samples from the individual simulations can then be combined to a super-sample. This is often referred to as "dummy-parallelization". It has the advantages that the individual sampling-runs can be shortened, and the implementation of the parallelization is straight-forward. A drawback with this method is however that separate simulations have to be thermalized individually, such that the more the super-sample is split on different processes, the more processor time is wasted on thermalization. Additionally, if the individual simulation-runs depend on some sort of freezing, like how vortices freeze to the numeric lattice, then individual simulations could freeze at different angles such that they cannot be combined to form good statistics.

A solution to the above issues with this simple parallelization, is provided by grid-parallelization. This parallelization method is suited for simulations that consist of interacting sites either in 2D or 3D where local MC updates are to be performed. We will focus on the case of a 3D simulation where the sub-sites are organized in a numerical cubic lattice. The idea is to split the cube into different sub-cuboids as illus-

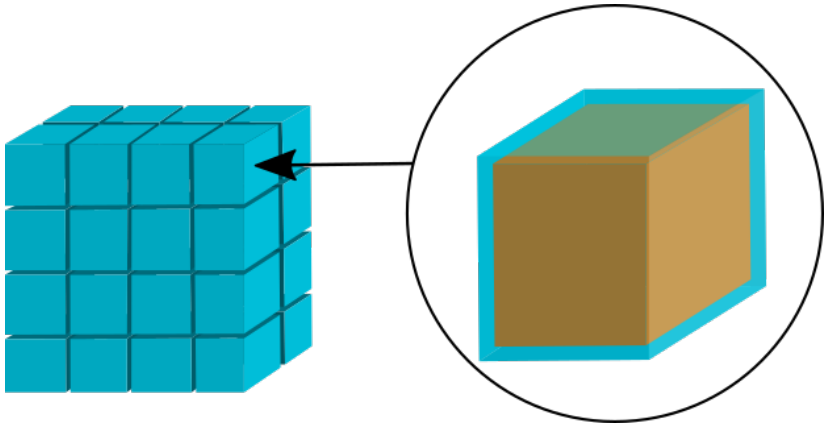

Figure 6.3: Illustration of the subdivision of the numerical grid into sub-cuboids. The right side illustrates that the sites in each sub-cuboid can be categorized as either internal sites, which can be updated asynchronously on different sub-cuboids and is illustrated in the figure by the internal orange cube, or sites in a border region.

trated on the left side of Figure 6.3. Each sub-cuboid's internal sites can then be updated in the normal MC fashion, in parallel with the internal sites of other sub-cuboids. If the individual sites of the original system interacts with neighboring sites,[3] then it will be necessary for each sub-cuboid to have a border whose thickness depends on the range of the interaction. The sites in this border-region will then have an interaction with sites in the border-region of other sub-cuboids, such that care must be taken not to update a site based on the value of a neighboring site that is no longer valid. One solution to this is simply updating all the sites in the border-regions serially, i.e. update the border sites in a single sub-cuboid, communicate the updated values to the affected neighboring sub-cuboids, then move to the next sub-cuboid, etc. Or it could be even more effective to parallelize the updates of the border sites as well by further subdividing the border-sites into different categories. As an example, one could define *internal* border-sites on the face of a sub-cuboid to be the border-sites that only depend on sites in

3. In the case of a local MH update this can take the form of an energy-difference of the system at a proposed update-site that depends on the value of fields at neighboring sites.

the single neighboring sub-cuboid that is in the direction of the face-plane normal vector. Then all the right-facing internal border-sites can be done in parallel on all sub-cuboids, followed by all the top-facing internal border-sites, etc. The specifics of how the border-categories should be defined in order to achieve full parallelization, will in general depend on the specifics of the interaction between the sites.

6.6 Reweighting

Reweighting techniques are methods for finding estimates of parameter-dependent observables based on previously obtained samples of these observables from MC-simulations that have been done at parameter values independent of the ones we are interested in. Given a set of samples of some observable $\{o_i\}_{i=1}^{M}$ from previous MC simulation(s), these techniques provide a set of weights $\{w(\beta')_i\}_{i=1}^{M}$ that can be used to estimate the observable at a parameter value β' by the reweighting

$$\hat{o}(\beta') = \sum_i w(\beta')_i o_i. \tag{6.17}$$

This is very useful when estimating some observable over a temperature-range, since then a single simulation can yield results not only for a single temperature, but for an extended region. If this region is close to a phase-transition, then this can be used as a way of avoiding the critical slowing down of simulations at phase transitions by instead simulating at temperatures *close* to the critical temperature T_c, and then using reweighting techniques to estimate results *at* T_c. All this is possible because a simulation at a given temperature[4] produces an extended statistical distribution of energy values for the sampled states. This energy distribution will in general overlap with the energy-distribution produced when simulating at a temperature that is sufficiently close to the original. Because of this overlap, it is possible to statistically extrapolate the value of observables at the neighboring temperature.

Reweighting techniques are categorized as single-histogram and multi-histogram reweighting-techniques depending on whether they use statistical information from a single histogram or can combine histograms generated at multiple parameter values. The single-histogram techniques are used to estimate values of the observables at neighboring

4. It is possible to use reweighting techniques on other parameters of the simulation as well, as long as they are, like inverse-temperature, linear in the action.

temperature-values and has the virtue of being comparatively simple to implement and understand. The multi-histogram techniques, on the other hand, have the advantage that the additional statistical information in general gives better estimates, and can even give better estimates at the original temperatures that the simulations were performed at, but have a more involved implementation.

In our simulations we used a Julia implementation[5] of the multi-histogram technique originally developed by Bojesen, a technique which they used in [88], and which was updated for the current Julia release and modified by us.

6.6.1 Ferrenberg-Swendsen single-histogram method

To derive the Ferrenberg-Swendsen single-histogram reweighting technique, let o_i be samples of an observable $\mathcal{O}$ from sample states ψ_i sampled at parameter value β of a system with a Hamiltonian $\mathcal{H}$, such that $\mathcal{O}(\psi_i) = o_i$. Then, from out discussion of importance sampling, the estimate of the average of the observable when the states are sampled according to a probability distribution $\pi(\psi_i)$, is given by

$$\langle \hat{\mathcal{O}} \rangle_\beta = \frac{\sum_i o_i e^{-\beta \mathcal{H}(\psi_i)} / \pi(\psi_i)}{\sum_i e^{-\beta \mathcal{H}(\psi_i)} / \pi(\psi_i)}. \tag{6.18}$$

Using a simulation with importance sampling at parameter-value β to generate the sampled states, the probability distribution was

$$\pi(\psi_i) = \frac{e^{-\beta \mathcal{H}(\psi_i)}}{Z_\beta} = \frac{e^{-\beta \mathcal{H}(\psi_i)}}{\sum_\psi e^{-\beta \mathcal{H}(\psi)}}, \tag{6.19}$$

where the sum in the denominator is over all possible states ψ and not only sampled states. Inserting $\pi(\psi_i)$ into $\langle \mathcal{O} \rangle_\beta$ in Eq. (6.18), this equation reduces to the arithmetic average, however if we now imagine wanting an estimate of $\langle \mathcal{O} \rangle_{\beta'}$ at an arbitrary parameter value β', then insertion yields

$$\langle \hat{\mathcal{O}} \rangle_{\beta'} = \frac{\sum_i o_i e^{-(\beta' - \beta)\mathcal{H}(\psi_i)}}{\sum_i e^{-(\beta' - \beta)\mathcal{H}(\psi_i)}}. \tag{6.20}$$

5. This implementation is available at https://github.com/Sleort/FerrenbergSwendsenReweighting.jl/tree/1.0.3_update

This expression then gives an estimate of the average of the observable $\mathcal{O}$ at an arbitrary parameter value β' using states ψ_i that were sampled at a specific parameter value β. This is called the Ferrenberg-Swendsen single-histogram reweighting technique [89], and in terms of the reweighting expression in Eq. (6.17) we can read off that the weights of this technique are given by

$$w(\beta')_i = \exp\Big[-\ln\Big(\sum_j e^{-(\beta'-\beta)[\mathcal{H}(\psi_j)-\mathcal{H}(\psi_i)]} \Big) \Big]. \tag{6.21}$$

Although simple, this technique's ability to extract information about observables around the simulated parameter-value, makes it extremely valuable in for instance the study of scaling relations, and to accurately calculate the peak of thermodynamic variables at phase-transitions where the MC-simulations themselves take a significant amount of computing time.

6.6.2 Numeric evaluation of exponential sums

The reason for introducing the extra exponential in the form of $w(\beta')_i$ in Eq. (6.21) is because sums of exponential numbers generally are hard to do numerically using finite-precision floating point numbers, however the logarithm of such a sum can be found using an iterative scheme. Let $S^{(k)}$ be a sum of k exponential numbers decreasing in magnitude that presumably are too large to be stored individually, such that

$$S^{(k)} = e^{a_1} + e^{a_2} + ... + e^{a_k}, \tag{6.22}$$

with $a_{i+1} \leq a_i$, is numerically hard to do. Assuming however that fractions of the numbers can be stored, then we can numerically calculate

$$\ln S^{(2)} = a_1 + \ln\Big(1 + e^{a_2 - a_1}\Big). \tag{6.23}$$

Following the iteration

$$\ln S^{(k)} = \ln S^{(k-1)} + \ln\Big(1 + e^{a_k - \ln S^{(k-1)}}\Big), \tag{6.24}$$

then $\ln S^{(k)}$ can be found for arbitrary k without ever storing a single exponential number, only fractions of such numbers that are close to each other.

6.6.3 Multi-histogram Ferrenberg-Swendsen method

Let $\{\psi_i^k\}_{i=1}^{N_k}$ be sets of states sampled at the N_0 inverse temperatures $\{\beta_k\}_{k=1}^{N_0}$ of a system with Hamiltonian $\mathcal{H}$. The energy of these states is then given by E_i^k, and samples of an observable $\mathcal{O}$ at these states are given by $\mathcal{O}(\psi_i^k) = o_i^k$. The energy-samples can then be used to construct N_0 histograms

$$h_k(E) = \sum_{i=1}^{N_k} \delta_{E,E_i^k}, \tag{6.25}$$

giving the number of sampled states at a certain energy in the simulation with parameter value β_k. The goal is to use these histograms to estimate the density of states of the system which we for the purpose of the derivation of this method will define $n(E) = \sum_\psi \delta_{E,\mathcal{H}(\psi)}$. The essential steps in this derivation can be found in the original paper in Ref. [90], as well as Ref. [91] and [92]. With these definitions, the energetic probability distribution of the system at an inverse temperature β is given by

$$W(\beta, E) = n(E)e^{-\beta E}/Z_\beta, \tag{6.26}$$

where $Z_\beta = \sum_\psi e^{-\beta\mathcal{H}(\psi)}$ is the partition function. Based on the sampled histograms, $W(\beta_k, E)$ at temperature β_k can be estimated by $\hat{p}_k(E) = h_k(E)/N_k$, i.e. $\langle\ \hat{p}_k(E)\ \rangle = W(\beta_k, E)$. This implies that $\langle\ h_k(E)\ \rangle = N_k W(\beta_k, E)$, and assuming for now that the samples of states ψ_i^k and ψ_j^k are statistically independent, it can be shown by, among other things, insertion of the definition of $h_k(E)$ in Eq. (6.25), that

$$\langle\ h_k(E)^2\ \rangle = N_k W(\beta_k, E)[1 + (N_k - 1)W(\beta_k, E)]. \tag{6.27}$$

Inserting these cumulants of the histograms into the variance, we get

$$\delta^2 h_k(E) = \langle\ h_k(E)^2\ \rangle - \langle\ h_k(E)\ \rangle^2 \approx g_k N_k W(\beta_k, E), \tag{6.28}$$

by assuming $W(\beta_k, E) \ll 1$. The factor $g_k = 1 + 2\tau_k$, where τ_k is the autocorrelation time of the samples at β_k, is included to generalize the result to samples where ψ_i^k and ψ_j^k are not statistically independent.

By solving Eq. (6.26) w.r.t. $n(E)$ and inserting the estimator of $W(\beta_k, E)$, an estimator of the density of states is given by

$$\hat{n}_k(E) = \hat{p}_k(E) Z_{\beta_k} e^{\beta_k E}, \tag{6.29}$$

where Z_{β_k} is assumed known, an assumption we will have to reconcile later. By the error propagation formula, then the variance of this estimator is given by

$$\delta^2 \hat{n}_k(E) = (Z_{\beta_k} e^{\beta_k E}/N_k)^2 \delta^2 h_k(E). \tag{6.30}$$

The estimator $\hat{n}_k(E)$ is an estimator of $n(E)$ using only a single histogram. We combine the estimators of single histograms using a weighted sum

$$\hat{n}(E) = \sum_k r_k \hat{n}_k(E), \tag{6.31}$$

where the coefficients r_k must satisfy the condition $\sum_k r_k = 1$ for the expectation value of $\hat{n}(E)$ to give the density of states. The coefficients r_k are determined by minimizing the variance $\delta^2 \hat{n}_k(E)$ subject to the constraint $\sum_k r_k = 1$ using a Lagrange multiplier, which yields the estimator

$$\hat{n}(E) = \frac{\sum_{k=1}^{N_0} g_k^{-1} h_k(E)}{\sum_{l=1}^{N_0} N_l g_l^{-1} e^{-\beta_l E} Z_{\beta_l}^{-1}}. \tag{6.32}$$

The assumption that Z_{β_k} is known is now reconciled. Since we can write the partition function using the density of states through

$$Z_\beta = \sum_\psi e^{-\beta \mathcal{H}(\psi)} = \sum_E n(E) e^{-\beta E}, \tag{6.33}$$

then we use the density of states estimator to estimate the partition function and use this estimate of the partition function $\hat{Z}_{\beta_k}$ in the density of states estimator. This then creates an implicit equation for $\hat{Z}_{\beta_k}$ that must be solved self-consistently. Inserting the definition of $h_k(E)$ and exchanging sums to remove the histograms, this equation takes the form

$$\hat{Z}_\beta = \sum_{k=1}^{N_0} \sum_{i=1}^{N_k} \frac{g_k^{-1} e^{-\beta E_i^k}}{\sum_{l=1}^{N_0} N_l g_l^{-1} e^{-\beta_l E_i^k} \hat{Z}_{\beta_l}^{-1}}, \tag{6.34}$$

which gives N_0 equations for N_0 unknowns $\hat{Z}_{\beta_k}$ when evaluated at the different $\beta = \beta_m$.

Solving Eq. (6.34) is usually done with the help of an iterative solution method for non-linear equations such as the Newton-Raphson method. To numerically calculate a solution, it is inconvenient to work

with the full quantities $\hat{Z}_{\beta_m}$ since these are usually extremely large. Instead, it is sufficient to calculate the variables

$$L_m \equiv \ln \hat{Z}_{\beta_m} - \ln \hat{Z}_{\beta_1}, \tag{6.35}$$

since the weights in the reweighting of observables can be written in terms of them. Dividing Eq. (6.34) by Z_{β_1}, we get that the $N_0 - 1$ equations we need to solve self consistently for the $N_0 - 1$ variables L_m, are given by

$$L_m = \ln \left\{ \sum_{k=1}^{N_0} \sum_{i=1}^{N_k} \frac{g_k^{-1} e^{-\beta_m E_i^k}}{\sum_{l=1}^{N_0} g_l^{-1} e^{-\beta_l E_i^k - L_l}} \right\}. \tag{6.36}$$

This form has the big advantage that the overall logarithm allows us to not have to calculate the exponential sums directly, but instead only calculate logarithms of these sums. For each sum $\sum_i e^{a_i}$ containing exponentials, which are potentially too large to be stored numerically, we simply re-exponentiate the entire sum to $\exp \ln \sum_i e^{a_i}$ and then use the method outlined in Section 6.6.2 to calculate $\ln \sum_i e^{a_i}$. Because of the overall logarithm, the exponential drops out in the last re-exponentiation such that we never have to store a single exponential number.

After finding self-consistent values for the $N_0 - 1$ variables L_m, the weights w_i^k for reweighting the observable $\mathcal{O}$ can be found. In terms of the density of states $n(E)$, the thermal average of the observable is written

$$\langle \mathcal{O} \rangle_\beta = \frac{\sum_E \mathcal{O}(E) n(E) e^{-\beta E}}{\sum_E n(E) e^{-\beta E}}. \tag{6.37}$$

Inserting the reweighting estimate of $\hat{n}(E)$ in Eq. (6.32) for $n(E)$, we get the reweighting estimate

$$\langle \hat{\mathcal{O}} \rangle_\beta = \frac{\hat{Z}_{\beta_1}}{\hat{Z}_\beta} \sum_{k=1}^{N_0} \sum_{i=1}^{N_k} \frac{o_i^k g_k^{-1} e^{-\beta E_i^k}}{\sum_{l=1}^{N_0} N_l g_l^{-1} e^{-\beta_l E_i^k - L_l}}, \tag{6.38}$$

where $\hat{Z}_{\beta_1} / \hat{Z}_\beta$ is given by

$$\frac{\hat{Z}_\beta}{\hat{Z}_{\beta_1}} = \sum_{k=1}^{N_0} \sum_{i=1}^{N_k} \frac{g_k^{-1} e^{-\beta E_i^k}}{\sum_{l=1}^{N_0} N_l g_l^{-1} e^{-\beta_l E_i^k - L_l}}, \tag{6.39}$$

through Eq. (6.34). The two equations for $\langle\hat{\mathcal{O}}\rangle_\beta$ in Eqs. (6.38) and (6.39) together with the self-consistency equation in Eq. (6.36), is sufficient to describe the multi-histogram method. Notice that in these equations the histograms on which the method was derived do not figure but have been replaced by the more fundamental energy samples. This form makes the method more convenient to implement for systems with continuous energy distributions since it removes the need for a sum over all possible energies.

When calculating the exponential sums in the weights implied by Eqs. (6.38) and (6.39), numerical overflow can be avoided by first using logarithms to calculate the logarithm of a set of related un-normalized weights as before, then subtracting the maximum logarithmic value for each weight such that each weight is $\lesssim 1$ and then using the sum of these weights to properly normalize in the end.

6.6.4 Initial guess

An iterative non-linear solver usually needs an initial guess at the solution. In the case of the multi-histogram method equations, a good initial guess can be provided by the single-histogram Ferrenberg-Swendsen method. Since only fractions of partition function values are needed, we may set that $\hat{Z}_{\beta_1} = 1$ and use the Ferrenberg-Swendsen method based on the β_1 energies to estimate the value $\hat{Z}^0_{\beta_2}$ of $\hat{Z}_{\beta_2}$ at neighboring inverse-temperature β_2 by the formula

$$\hat{Z}^0_{\beta_2} = \sum_{i=1}^{N_1} e^{-(\beta_2-\beta_1)E^1_i}. \tag{6.40}$$

In terms of the numerically convenient variables L_m, then this first guess L^0_2 takes the form

$$L^0_2 = \ln\Big[\frac{1}{N_1}\sum_{i=1}^{N_1} e^{-(\beta_2-\beta_1)E^1_i}\Big]. \tag{6.41}$$

Continuing to estimate the partition function $\hat{Z}_{\beta_m}$ through the single-histogram Ferrenberg-Swendsen method based on the data at β_{m-1}, then we may find all subsequent L^0_m by applying the iteration scheme

$$L^0_m = L^0_{m-1} + \ln\Big[\frac{1}{N_{m-1}}\sum_{i=1}^{N_{m-1}} e^{-(\beta_m-\beta_{m-1})E^{m-1}_i}\Big]. \tag{6.42}$$

Chapter 7

Vortices in superconductors

In conventional type-I superconductors, the Meissner effect prevents any magnetic field from penetrating the superconductor when it is in the superconducting state. In a type-II superconductor, the transition between the normal- and superconducting state is more gradual than in the type-I case due to an intermediate transitional state where topological defects in the superconducting field becomes stable, allowing quanta of magnetic field to pass through the material. The transitional value of the external field strength below which no magnetic field penetrates the superconductor is called B_{c1}. The upper transitional field strength above which the material stops being superconducting altogether is called B_{c2}. The state with regions of topological defects through which magnetic field quanta can penetrate, which are interspersed in a sea of superconducting state, exists between these values. It is important to note that the Meissner effect is still present in this transitional state — preventing magnetic field lines from penetrating the superconducting state. However, at topological defects, the material switches to the normal state and thus allows magnetic field-lines to penetrate at these points. The final continuous transition to the normal state at B_{c2} is then caused by the proliferation of vortex-loops, sending the whole material to the normal state.

The regions of normal state containing a topological defect of the superconducting state and through which magnetic field quanta can penetrate are known as superconducting vortices because they are sur-

rounded by a circulating superconducting current. This current is set up by the presence of the magnetic field and shields the rest of the superconducting condensate from its influence.

Whether a superconductor is type-I or type-II can conventionally be predicted by examination of the relative value of the magnetic field penetration depth λ and the superconducting coherence length ξ, which together form the GL parameter $\kappa = \lambda/\xi$. These parameters come out of the description of the superconducting state given by the GL theory of a single-component complex field minimally coupled to a gauge field. If $\kappa \gg 1$, then we say we have a strongly type-II superconductor, while is $\kappa \ll 1$, the superconductor is strongly type-I. The transitional value between type-I and type-II has a theoretical mean-field value of $\kappa = 1/\sqrt{2}$, however numerical calculations have given it the value $\kappa = (0.76 \pm 0.04)/\sqrt{2}$ all within the conventional GL formalism.

In a type-II conventional superconductor without any structural defects, as we increase the field strength, we introduce more vortices into the material in order to carry the required number of magnetic field quanta. At first these vortices behave like a liquid where they mutually repel each other if they get close. As more vortices are introduced to the system, the inter-vortex repulsion leads to them forming a two-dimensional lattice with equidistant lattice spacing. Since the triangular lattice is the lattice with the highest packing fraction, i.e. the lattice that has the highest density of sites at a given lattice spacing, the lattice formed will be triangular. Such a triangular (hexagonal) lattice of single quanta vortices is known as the Abrikosov lattice since it consists of single quanta vortices which are known as Abrikosov vortices.

7.1 Vorticity observables

A condensate described by a complex field ψ with phase θ can have topological defects given by discontinuities in the field θ due to its compact nature ($\theta \in [0, 2\pi)$). Such topological defects can be quantified by a non-zero winding-number N_v, which measures how the phase $\theta(\boldsymbol{r})$ moves around the unit circle as we change the position $\boldsymbol{r}$ in a closed loop around the defect. These topological defects then lead to singularities in the field $\nabla\theta$ which allows a nonzero value of $\nabla \times \nabla\theta$ at

these points.[1] Integrating over a surface S with surface normal vector $\hat{s}$ of the system and using Stokes' theorem then yields

$$\int_S \mathrm{d}^2 r(\nabla \times \nabla\theta) \cdot \hat{s} = \oint_{\partial S} \nabla\theta \cdot \mathrm{d}\boldsymbol{r} = 2\pi N_v, \quad N_v \in \mathbb{Z}, \tag{7.1}$$

where ∂S is a path around the boundary of S traversed counterclockwise. The last equality comes from the observation that ∂S is far away from the singularity such that $\nabla\theta$ is continuous along the path and N_v thus counts the number of times the vector θ rotates counterclockwise back to its initial position. If there is no topological defect inside the boundary ∂S then θ will increase as much as it decreases along the path, such that $N_v = 0$. If a topological defect in the form of a vortex is present, then $N_v \neq 0$ [93]. N_v can then be interpreted as the total vorticity of the field θ over the surface S. Since N_v is the total vorticity, which can consist of several individual defects, then from Eq. (7.1) we see that

$$\boldsymbol{n}_v = \frac{\nabla \times \nabla\theta}{2\pi} \tag{7.2}$$

must be interpreted as a vector of the local density of vorticity.

If the system described above contains a gauge field that is coupled to ψ, then any meaningful observable needs to be gauge-invariant. We clearly see that the expression in Eq. (7.2) is gauge-dependent by sending $\theta \to \theta + \phi$. To make a gauge-invariant observable under the gauge-transformation in Eq. (5.7), we see that we need to modify the definition to

$$\boldsymbol{n}_v = \frac{\nabla \times (\nabla\theta + g\boldsymbol{A})}{2\pi}. \tag{7.3}$$

This expression then defines $\boldsymbol{n}_v$ as a gauge invariant vector of local vorticity density of the compact field θ.

In lattice models we want to discretize the vorticity density in Eq. (7.3) in order to effectively calculate it in MC simulations of the lattice model. In such a discrete model we have to take care to re-compactify the quantity $\nabla\theta + g\boldsymbol{A}$ to only be defined on some interval of length 2π. Using the discretization mapping of ∂_μ and $A_\mu(\boldsymbol{r})$ from Eq. (5.19), we want $\Delta_\mu\theta + gA_{\boldsymbol{r},\mu} \in [-\pi, \pi)$. Defining the operator

$$\hat{C}_\pi\, x = \mathrm{mod}(x + \pi, 2\pi) - \pi, \tag{7.4}$$

1. From vector calculus we know that for a continuously differentiable field $f(\boldsymbol{r})$, it is the case that $\nabla \times \nabla f = 0\ \forall \boldsymbol{r}$.

the discretized vorticity density can be written

$$\begin{aligned} \boldsymbol{n}_{v,\boldsymbol{r}} &= \frac{\hat{e}_\mu \epsilon_{\mu\nu\lambda} \Delta_\nu \hat{C}_\pi(\Delta_\lambda \theta_{\boldsymbol{r}} + g A_{\boldsymbol{r},\lambda})}{2\pi a^2} \\ &= \frac{1}{2\pi a^2} \sum_\mu \hat{e}_\mu \sum_{\boxdot_\mu} \hat{C}_\pi(\Delta_\lambda \theta_{\boldsymbol{r}} + g A_{\boldsymbol{r},\lambda}). \end{aligned} \tag{7.5}$$

Implicit summation over repeated indices is used on the first line, while on the second, the components of the vector $\boldsymbol{n}_{v,\boldsymbol{r}}$ are written as plaquette-sums. Plaquette sums are sums of direction dependent quantities along a path $\boxdot_\mu$, which is described below Eq. (5.21) and illustrated in Figure 5.3. In the plaquette-sum, the directional quantity is always chosen along the path, and the path is traversed according to the right-hand rule with normal vector $\hat{e}_\mu$ [80, 94].

If the lattice system has an external field that yields a filling fraction f, e.g.produced by one of the gauges in Section 5.2, then each plaquette-sum in Eq. (7.5) will have a contribution f/a^2. To motivate this assume, e.g., that $\theta_{\boldsymbol{r}}$ is the same everywhere such that $\Delta_\lambda \theta_{\boldsymbol{r}} = 0$ and insert the Landau gauge from Eq. (5.16) into the z-component of $\boldsymbol{n}_{v,\boldsymbol{r}}$. This yields f/a^2. Hence, to assure that the vortex observable yields the actual vortex quanta integer values when evaluated on a lattice with a uniform external field in the z direction with filling fraction f, we have to use the lattice function

$$n^z_{\boldsymbol{r}} = (\boldsymbol{n}_{v,\boldsymbol{r}})_z - \frac{f}{a^2}. \tag{7.6}$$

If the system consists of multiple condensate components $\psi^h = \rho^h e^{i\theta^h}$, then we can define a separate vorticity flux density $n^{z,h}_{\boldsymbol{r}}$ for each component h by letting $\theta \mapsto \theta^h$ in the definitions of $n^z_{\boldsymbol{r}}$ in Eqs. (7.5) - (7.6).

7.2 Unconventional vortices

In a conventional superconductor, the isotropic (i.e. s-wave) nature of the superconducting state implies that stable vortices can only contain a single quanta of magnetic flux. In other words, if through some random thermal fluctuation, a defect appears that contains n quanta of magnetic flux, this will soon decay into n individual vortices that each contains a single magnetic flux quantum. We call these n individual

vortices: single-quanta vortices. For the individual stable topological defects to contain multiple quanta of magnetic flux, the superconducting state has to be unconventional in some way. One way in which a superconductor can host stable vortices with multiple quanta is if the superconducting state for some reason has an unconventional symmetry. This could, e.g., be caused by unconventional (i.e. non-phononic) mechanisms of Cooper-pair formation such as Van der Waals or spin-mediated interaction [65]. In this case, multiple components might be needed in order to describe the symmetry, which can result in the stabilization of vortices with double as well as fractionalized quanta [95].

A more specific example is that this can happen when a magnetic field penetrates a sample of material that is in a $p+ip$ superconducting state, i.e. a state where the pairing function is described by two components that each have a $k_x \pm ik_y$ dependence on the crystal momentum $\boldsymbol{k}$ in the continuum limit. The linear k-dependence implies a finite angular momentum of the Cooper pairs with $l = 1$, and that the phases of the components are locked by an angular momentum difference $\Delta l = 2$ in the ground state. This has the consequence $n_+ = n_- + 2$ on any non-trivial winding numbers n_+ and n_- of the two different components, which implies that if a vortex exists some place where the sub-dominant component has winding number $n_- = 0$, then the dominant component must have $n_+ = 2$ and thus the vortex must be a double quantum vortex.[2]

In the type of superconductor described above, the winding numbers n_+ and n_- fully determine the structure of possible vortices. In the following we will use the notation (n_+, n_-) to specify these types of vortices, and assume that '$+$' is the dominant component. The possibilities for single-quanta vortices in this notation are thus the vortices $(1, -1)$ and $(-1, -3)$. The latter type has a higher winding number in the sub-dominant component, which implies a more complex core structure and has a higher energy cost pr. vortex [96]. This means that

2. It is the winding number of the dominant component that determines the number of magnetic flux quanta that the vortex is allowed to contain because the sub-dominant component is zero in locations far away from the vortex core by the nature of being sub-dominant. Thus, it doesn't contribute to the closed loop integral in Eq. (7.1) when integrating the supercurrent in a circle around the vortex.

of the two, it is the $(1, -1)$ variety that will be expected to be stable in experiments.

It is also possible to have double quanta vortices, which are either of the $(2, 0)$ or $(-2, -4)$ variety. Again, the type of vortex with the higher winding number in the sub-dominant component exhibits a more complex core structure. For the choices of various internal parameters of such systems that we have studied, it is the $(2, 0)$ type of vortex that is associated with the lowest energy cost and thus the one that is stable [96–98].

As we have mentioned, the different types of vortices will in general have different types of core-structures even though they may permit the same number of magnetic flux quanta to penetrate. One diagnostic tool to separate different kinds of vortices, is thus to observe the structure of the vortex core. Aside from plotting the actual vorticity $n_{\pm}$ of the component through Eq. (7.6), this can be done by e.g., plotting the amplitudes of the dominant and sub-dominant component, plotting the phase-difference $\theta_+ - \theta_-$ of the different components, or plotting the magnetic field in the region of the vortex core. A rendition of the essential features of plots of dominant component vorticity density n_+ and phase-difference is shown in Figure 7.1 for the two vortex types $(1, -1)$ and $(2, 0)$. We see from the figure that the double quanta vortex type $(2, 0)$ can be distinguished from the single quanta vortex by having an extended ring of vorticity density, as well as having a core region in the phase difference plot that is rotated by $\pi/2$ radians from the asymptotic value of this phase difference. These features were used in our work to identify double and single quanta vortices in MC simulations.

7.3 Ensembles of vortices

With increasing field strength, more quanta of magnetic flux will penetrate the mixed phase and thus it will contain an increasing number of vortices that form flux-lines through the system. If any structural defects are present in the system, then this leads to local suppression of the superconducting condensate such that vortices are less energetically costly, and vortices will thus be predominantly located in such regions. This is called pinning of vortices because these regions attract vortices and since their location is determined by external factors and

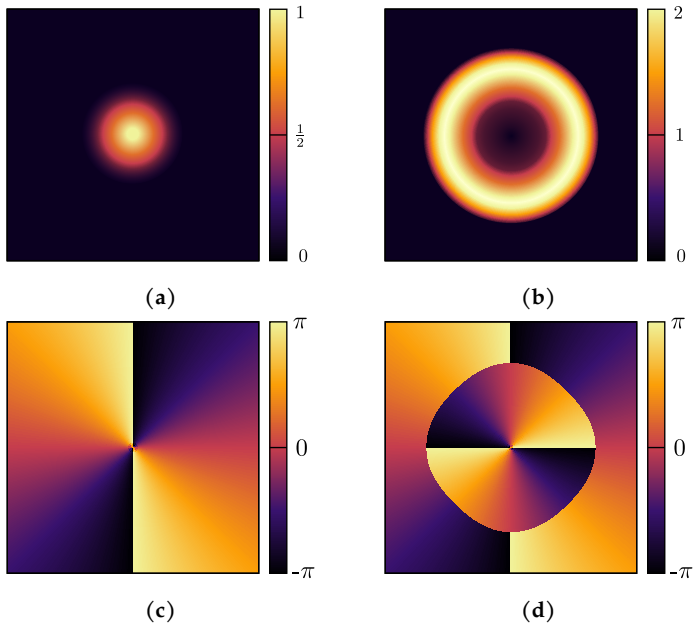

Figure 7.1: Schematic of vorticities and corresponding phase difference signature $\theta_+ - \theta_-$ of vortices in a system with external magnetic field $\boldsymbol{B} = B\hat{z}$. a and c shows vorticity and phase-difference respectively for a singly-quantized vortex with winding number $n_+ = 1$ and $n_- = -1$. b and d shows vorticity and phase difference respectively for a doubly-quantized vortex with winding number $n_+ = 2$ and $n_- = 0$. The figures are directly based on the ones presented in Ref. [97].

not by the inter-vortex interactions themselves. Free vortices are mobile in response to an electric current and this leads to energy-loss and resistance in the mixed phase. Pinning regions have the effect of resisting such movement and thus can contribute to increasing the amount of resistance-free current [99].

In the absence of such pinning, vortex tubes that run through the material in the direction of an external magnetic field can be ordered in a lattice according to their mutual interaction. Such a lattice is called an Abrikosov lattice or a flux line lattice since the vortex lines/tubes carry quanta of flux of the external magnetic field. The Abrikosov lattice then exists in the mixed phase of type-II superconductors and is destroyed when either the temperature or magnetic field strength is

increased beyond a certain level $B_{c2}(T)$ where the material enters the normal non-superconducting phase. This transition can be characterized in terms of a proliferations of unbound vortex loops which destroys the phase-coherence of the superconducting state [100].

If the interaction between the flux lines is weak compared to entropic forces such as thermal fluctuations, then fluctuations of the vortex flux lines can cause melting of the vortex lattice. In this molten state, the vortex flux lines still interact repulsively which yields an average preferred inter-vortex distance given by the balance between inter-vortex repulsion and the inclusion of the necessary number of vortices in order to carry the external magnetic field, however any directionally dependent long range correlation is lost. This corresponds to the behavior of particles in a liquid, and the molten state is thus called a vortex liquid. Such states are commonly found in high-T_c superconductors such as $YBa_2Cu_3O_{7-\delta}$. The transition between an ordered lattice of vortices and a vortex liquid is known as a vortex lattice melting transition. This transition can also be achieved by tuning the strength of the magnetic field. This implies a magnetic field strength B_{c1}, below which the Meissner effect completely excludes all magnetic fields, and a strength $B_M > B_{c1}$ above which the vortices behave as a liquid, i.e. without any long range correlations except that of an average distance. Finally superconductivity is destroyed at $B_{c2} > B_M$ when a proliferation of vortex loops destroy all vortex correlations and the material enters the normal state. These different states of the vortex lattice map out a region in the $B - T$ parameter space such as the one shown in Figure 7.2. There can also exist intermediate glassy phases of vortex matter between the extremes of a completely ordered lattice and a liquid when pinning of vortices is combined with low temperature in an external magnetic field [101, 102].

The structure and behavior of a flux-line lattice in the mixed phase of a type-II superconductor is dependent on the symmetry and nature of the superconducting phase. In conventional single-component superconductors with s-wave symmetry, the vortices interact asymptotically[3] through isotropic repulsion that can be modeled by a modified Bessel function of the second kid [27, 104, 105]. In a clean ma-

3. In this context "asymptotically" means in the asymptotic limit of large separation between vortices.

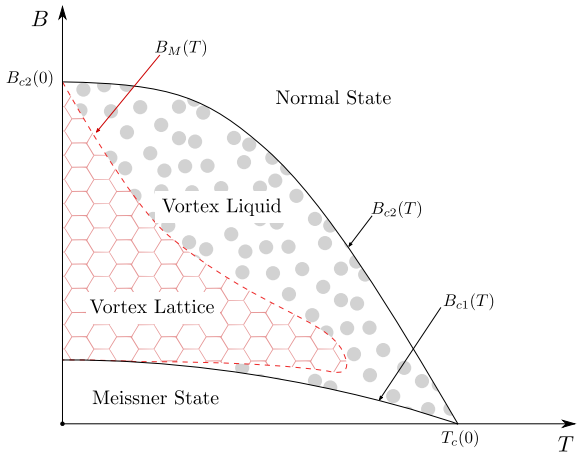

Figure 7.2: Simplified phase diagram of the states of vortex matter in a type-II superconductor in the B — T phase space. This is based on the Lindemann criterion [103].

terial, this interaction leads experimentally to a triangular (hexagonal) lattice of vortices due to this lattice symmetry having the largest packing-fraction of any two-dimensional lattice, i.e. it is the lattice that gives the highest density of vortices given a set inter-vortex distance and thus gives the lowest energy configuration [106, 107]. Theory predicts that also a square lattice of single quanta vortices should be possible at higher fields for $\kappa \gtrsim 1/\sqrt{2}$ [104], however in the London-approximation, which is valid at $\kappa \gg 1$, the triangular symmetry is the most stable for all fields [108]. Interestingly, the vortex lattice symmetry can be incommensurate to the underlying crystal lattice structure.

In theoretical models of unconventional superconductors, such as superconductors with multiple components and non-isotropic symmetry, even more complex behavior of the mixed phase is predicted. We have already mentioned the appearance of a vortex-liquid state separate from the vortex lattice state in high-T_c superconductors, which are overwhelmingly of the extreme type-II category and described by a single component unconventional d-wave symmetry. In superconductors with multiple components where each component can be modeled by a conventional London-approximation, a phase transition from the superconducting state to a superfluid state is possible in the mixed

phase by melting of a composite Abrikosov vortex lattice into a state with a remaining ordered neutral mode [69].

7.3.1 Vortex matter in $p_x + ip_y$-superconductors

In our work we have been specifically interested in the vortex matter of superconductors with p-wave symmetry. These types of superconductors are described by two components that are intrinsically coupled and give rise to unconventional composite vortices as described in Section 7.2. The stable single-quanta composite vortices, which are denoted as vortex type $(1, -1)$ in the notation of Section 7.2, are theoretically predicted to form lattices with square symmetry [109–111]. Such symmetry has been observed in the vortex lattice of the unconventional superconductor Sr_2RuO_4 [112–115] and is thus part of the body of evidence supporting a p-wave symmetry of the superconducting state of this material. The theoretical predictions are supported by numerical calculations that also show that at lower fields, a triangular vortex lattice consisting of double-quanta $(2, 0)$-vortexes is the preferred configuration [97]. Since these calculations did not account for thermal fluctuations in a convincing way, we used large-scale MC simulations to consider this effect on the vortex matter. Our results support the transition of a triangular vortex lattice consisting of double-quanta vortices to a square vortex lattice consisting of single quanta vortices at higher fields and temperatures. These results are presented in Paper II.

7.4 Observables of lattice symmetry

In this section we discuss two tools usable in lattice theories for considering the symmetry of vortex line lattices. These tools are based on the observables of vortex flux density discussed in Section 7.1, but in this case we are interested in measuring the structural correlations of a collection of vortex lines.

7.4.1 Structure function

The structure function of a discrete cuboid system of N_μ lattice sites along the $\hat{\mu}$ direction and with local vorticity $n^z_{\boldsymbol{r}}$ as defined in Eq. (7.6),

is defined as

$$S(\boldsymbol{k}_\perp) = \frac{1}{(fN_xN_yN_z)^2}\left\langle \left| \sum_{\boldsymbol{r}} a^2 n^z_{\boldsymbol{r}} e^{i\boldsymbol{k}_\perp\cdot\boldsymbol{r}_\perp}\right|^2\right\rangle, \tag{7.7}$$

where a is the lattice spacing, $\boldsymbol{r}_\perp$ is the projected lattice vector $\boldsymbol{r}_\perp = \boldsymbol{r} - (\boldsymbol{r}\cdot\hat{z})\hat{z}$ down on the xy-plane, and f is the filling fraction, i.e. the number of vortex quanta pr. plaquette in the xy-plane. The filling fraction f relates to the inclusion of an external magnetic field in the z-direction as described in Section 7.1. This function takes a reciprocal 2D momentum vector as an argument and measures the structural correlation of the vortex lattice at this Bragg-point with normalization such that $S(0) = 1$.

To motivate this expression, consider a continuous cuboid system with a uniform field in the z-direction with average flux density of numer of magnetic flux quanta $\tilde{f}$ that gives rise to a lattice of vortex lines along the z-direction. Let $n^z(\boldsymbol{r})$ be a flux density distribution of local vorticity in the z-direction such that if a vortex line with winding number $n \in \mathbb{Z}$ goes through the point $\boldsymbol{r}_0$, then $\int_A \mathrm{d}^2r\ n^z(\boldsymbol{r}_0) = n$, where A is an area that contains the vortex line. Taking the average over the z-direction keeps the value n of any vortex flux lines since they will be coherent over this dimension of the system. In contrast, any contributions from vortex loops, which could result from random thermal fluctuations, will vanish in the limit of a large system size, hence

$$w(\boldsymbol{r}_\perp) = \int_0^{L_z} \mathrm{d}r_z\ n^z(\boldsymbol{r})/L_z, \tag{7.8}$$

contributes to filtering out the vortex lines from the thermal noise. This w produces a distribution of vortex lines over the extent of the system in the xy plane. Since we are interested in structural correlations in this system we perform the 2D Fourier transform and look at its amplitude through

$$\tilde{S}(\boldsymbol{k}_\perp) = \left| \int \mathrm{d}^2r\ w(\boldsymbol{r}_\perp) e^{i\boldsymbol{k}_\perp\cdot\boldsymbol{r}_\perp}\right|^2. \tag{7.9}$$

This function then produces a reciprocal lattice of the 2D lattice of vortex lines where Bragg-points that correspond to structural correlations have increased value. To arrive at the structure-function we need only now to take the thermal average to average over thermal fluctuations

of the vortex lattice lines and normalize such that $S(0) = 1$. To find this normalization constant, we have to calculate the integral

$$\int \mathrm{d}^2 r \; n^z(\boldsymbol{r}) = ?, \tag{7.10}$$

over the systems extent in the xy plane. However, from the definition of $n^z(\boldsymbol{r})$, the answer is given to us. Since $n^z(\boldsymbol{r})$ measures the flux density of vorticity in the xy-plane, then the integral is simply the total vorticity, which can be written as $\tilde{f} L_x L_y$, by the definition of $\tilde{f}$. Finally then, we arrive at the normalized dimensionless quantity

$$S(\boldsymbol{k}_\perp) = \frac{1}{(\tilde{f} L_x L_y L_z)^2} \left\langle \left| \int \mathrm{d}^3 r \; n^z(\boldsymbol{r}) e^{i \boldsymbol{k}_\perp \cdot \boldsymbol{r}_\perp} \right|^2 \right\rangle. \tag{7.11}$$

Discretizing this expression through the method in Section 5, i.e. by letting $\int \mathrm{d}r \mapsto a \sum_{\boldsymbol{r}}$, $n^z(\boldsymbol{r}) \mapsto n^z_{\boldsymbol{r}}$ and $L_\mu = a N_\nu$ then we find that the filling fraction f which is the number of vortex quanta pr. plaquette of the lattice[4] is related to $\tilde{f}$ through $f = a^2 \tilde{f}$ and we reproduce the expression in Eq. (7.7).

As an example of how the structure function singles out specific structural correlations, consider Figure 7.3. Figure 7.3b shows a plot of the structure function for all crystal momenta $\boldsymbol{k}_\perp$ in the 1st Brillouin zone. The 6 yellow points surrounding the origin corresponds to correlations in the structure of the vortex lattice in these 6 directions, which implies a hexagonal lattice. The hexagonal lattice is shown directly in Fig. 7.3a, which in this case is a hexagonal lattice of double-quanta vortices. Choosing specific points in the plot of Fig. 7.3b and plotting the structure functions value at different values of a parameters of the system, e.g. temperature, is a common method for evaluating different phases of the structure of the vortex lattice for example for measuring when the vortex lattice melts into a vortex liquid (see e.g. [69, 70, 116–118]).

7.4.2 Angular histogram

Building on the idea of measuring a specific point in the structure function to signify a structural transition, we developed an angular

4. We note that by the definitions here, f is a dimensionless quantity, while $\tilde{f}$ has dimension inverse length square.

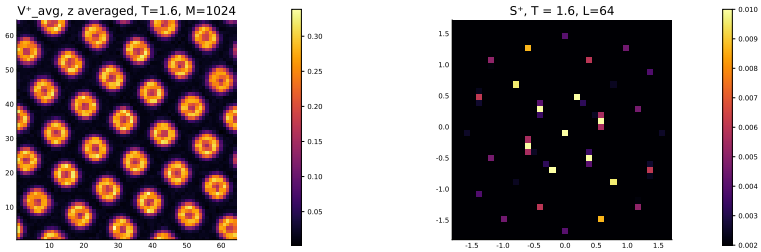

(a) (b)

Figure 7.3: Plots of vorticity of the $+$-component of a $p+ip$ superconductor system. Figure a shows a plot of the real space vorticity which corresponds to a thermal average of a discretized version of $w(\boldsymbol{r}_\perp)$ from Eq. (7.9). Fig. b shows the corresponding structure function which shows a creat hexagonal structure of the vortex line lattice.

histogram approach that is robust towards rotations of the vortex lattice. We found this to be important in measuring the transition from a hexagonal to a square vortex lattice since the angular symmetry of the model allowed the hexagonal vortex lattice to freeze in various directions. To combat this rotation, we built a histogram of the angular distance between peaks in the structure function over several MC steps. For a hexagonal lattice, such a histogram is peaked at the bin containing the angular distance $\pi/3$, while a square lattice would be peaked at $\pi/2$. Plotting these bins of angular distance over various temperatures, we were able to measure the transition from the square to the hexagonal lattice as seen in Figure 7.4.

The histogram was constructed algorithmically by creating a set of angular distances between peaks of the structure function for each MC step. We first found the radius where the peaks were located by searching the average structure function over the entire MC series, within a specified radius interval for the radius ρ_m, that produced the largest value of the discretization of the integral

$$\int_0^{2\pi} \mathrm{d}\theta \; S(\rho, \theta), \tag{7.12}$$

where $S(\rho, \theta)$ is the structure function given in polar coordinates about the Bragg-point $\boldsymbol{k}_\perp = 0$. The entire series of MC data was then blocked

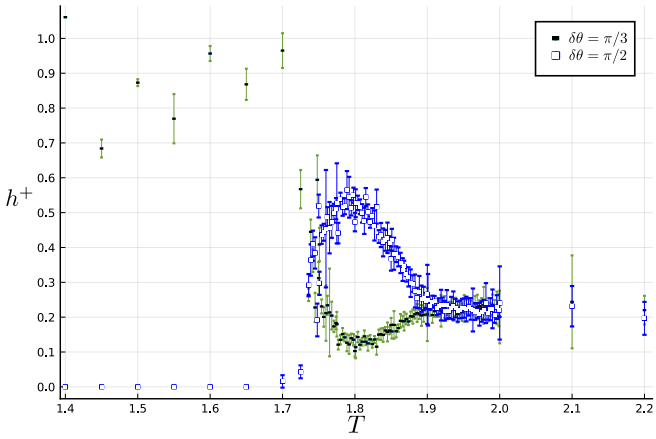

Figure 7.4: Plot of the bins of angular distance $\delta\theta = \pi/3$ and $\delta\theta = \pi/2$, as a function of simulation temperature.

into sections containing $\Delta\tau$ numbers of individual MC measurements of the structure function. Each such interval of structure function measurements were then averaged over to yields separate averaged measurements of the structure function. The averaging over sufficient number of measurements $\Delta\tau$ is absolutely necessary in order to reveal the hidden vortex lattice from the noise. From each block t, a structure function ring $S^t(\theta)$ was then created by selecting the highest value of the blocked structure function over a ribbon centered at radius ρ_m such that

$$S^t(\theta) = \max_{\rho_m - \delta\rho \leq \rho \leq \rho_m + \delta\rho} \{S^t(\rho, \theta)\}. \tag{7.13}$$

A collection of n peak positions $P^t = \{\theta^p\}$ was then found for each block by finding the highest possible S_m such that $S^t(\theta)$ crossed the line at S_m a number of $2n$ times. From this set of peaks, then all possible distances between these peak positions were constructed by

$$\Theta^t = \{\delta\theta_{ij} = |\theta_i^p - \theta_j^p| \quad | \quad i \neq j,\ \theta_i^p, \theta_j^p \in P^t\}. \tag{7.14}$$

Let $\Theta = \bigcup_t \Theta^t$ be the union of all block sets of mutual angular peak distances. The final histogram h was then constructed based on all of the distances in Θ. Let the bin in this histogram of the interval $[0, 2\pi)$ that contains the angular distance $\delta\theta$ be denoted $\Delta\delta\theta$ such that

$$\Delta\delta\theta = [\delta\theta - \delta\theta_-, \delta\theta + \delta\theta_+), \tag{7.15}$$

for some non-negative $\delta\theta_-$ and $\delta\theta_+$. The value of the histogram $h(\Delta\delta\theta)$ at this bin was then calculated by

$$h(\Delta\delta\theta) = \frac{1}{|\Delta\delta\theta||\Theta|} \sum_{\delta\theta' \in \Theta} \delta_{\delta\theta' \in \Delta\delta\theta}, \tag{7.16}$$

where $|\Delta\delta\theta|$ is the size of bin $\Delta\delta\theta$, $|\Theta|$ is the number of mutual distances $\delta\theta'$ in Θ and $\delta_{\delta\theta' \in \Delta\delta\theta}$ is the Kronecker delta function defined as

$$\delta_{\delta\theta' \in \Delta\delta\theta} = \begin{cases} 1 & : \delta\theta' \in \Delta\delta\theta \\ 0 & : \delta\theta' \notin \Delta\delta\theta \end{cases}. \tag{7.17}$$

An example of the resulting histogram from calculating $h(\Delta\delta\theta)$, given equal size of the $\Delta\delta\theta$ intervals is shown in Figure 7.5. In this figure we observe a large peak at $\delta\theta = \pi/2 \approx 1.6$. This correlation comes from the fact that there are 4 peaks in the structure function that are equidistant to eachother in angular distance from the origin. From this we draw the conclusion that the histogram represents a signature of a square vortex lattice. The even larger peak at $\delta\theta = \pi$ comes from a mathematical symmetry of the 2D Fourier transform that says that $\mathcal{F}(\boldsymbol{k}) = \mathcal{F}(-\boldsymbol{k})^*$. The small peak at $\delta\theta = 3\pi/2$ is a remnant of the peak at $\pi/2$, while the peak at low $\delta\theta$ is a artifact coming from noise in the data.

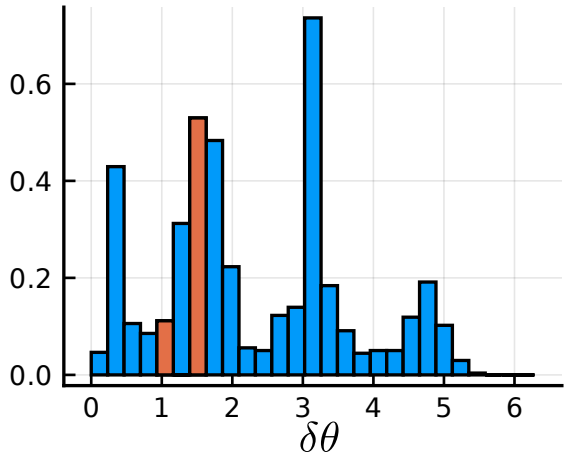

Figure 7.5: Plot of the bins of h in Eq. (7.16) for a simulation of a square vortex lattice. The bins corresponding to $\delta\theta = \pi/3$ and $\delta\theta = \pi/2$ are colored orange to mark the main contributions from a triangular- and square lattice respectivly.

Chapter 8

Outlook

In this thesis we have given an introduction to some of the fundamental techniques we employed in our theoretical investigations into the nature of unconventional superconductivity with p-wave pairing symmetry. These investigations have resulted in three papers.

In Paper I we used a group-theoretical approach to motivate the form of the effective interaction potential between electrons whose low energy excitations could be described in terms of Cooper-pairs with p-wave symmetry. This potential was then used as a basis for deriving the effective free energy for such a superconductor when it was influenced by explicite spin-orbit interaction. We found that the effective free energy had the expected form given by its group-theoretical constraints, but that previous assumptions about its coefficients needed revision because of the effect of spin-orbit coupling.

In Paper II we used large-scale Monte-Carlo simulations to investigate the vortex matter of a p-wave superconductor with a free energy similar to the one derived in Paper I. We found a transition between a square vortex-lattice of single-quanta vortices to an hexagonal vortex lattice consisting of double quanta vortices as the temperature was lowered in a finite field parallel to the crystallographic c-axis.

In Paper III we investigated this same superconductor when exposed to zero external magnetic field and found an Ising phase transition in the neutral sector of the theory. This transition did not separate from the phase-transition of the charged sector in contrast to other models

of two-component superconductors. The reason for the connection between the charged and neutral modes seemed to be because of their group-theoretical nature as components of a single irreducible representation. This identification implies equal stiffness for both components and an explicit coupling through mixed gradient and mixed-component terms in the effective free energy.

Looking towards the future, it now seems less likely that the unconventional superconductor Sr_2RuO_4 should be theoretically modeled as a $p + ip$ superconductor in spite of the strong evidence for its spontaneous time-reversal-symmetry breaking nature [119–121] and the good agreement between theory and experiment for the qualitative nature of its vortex lattices [97, 114]. Rather, the prevailing view based on the current evidence has shifted to suggesting a degeneracy between a $d_{x^2-y^2}$ and a $g_{xy(x^2-y^2)}$ superconducting state [122, 123]. It might in this regard be interesting to use Monte-Carlo simulations to investigate the vortex lattice behavior of such a superconductor and see how it matches with experiments on Sr_2RuO_4.

In the exploration of such a novel symmetry state it might be beneficial to utilize more modern forms of Monte-Carlo analysis such as those offered by the advances in machine-learning to yield convincing results in an efficient manner [124–126].

Building on the results of Paper I, it would be of interest to investigate numerically how the kinetic dimensionless phenomenological parameters in the Ginzburg-Landau model depend on the microscopic parameters, especially spin-orbit coupling strength and spin-orbit coupling spin z-component.

Bibliography

1. **F.N. Krohg, A. Sudbø.**
   Derivation of a Ginzburg-Landau free energy density of a $p + ip$ superconductor from spin-orbit coupling with mixed gradient terms.
   Phys. Rev. B 98, 014510 (1 July 2018).
   DOI: 10.1103/physrevb.98.014510

2. **F.N. Krohg, E. Babaev, H.H. Haugen, A. Sudbø.**
   Thermal fluctuations and vortex lattice structures in chiral p-wave superconductors: robustness of double-quanta vortices.
   arXiv: Superconductivity (Apr. 2021).
   arXiv: 2007.09161 [cond-mat.supr-con].

3. **M. Allen *et al.***
   IPCC, 2018 Summary for Policymakers.
   in
   Global Warming of $1.5^{\circ}C$. An IPCC Special Report on the impacts of global warming of $1.5^{\circ}C$ above pre-industrial levels and related global greenhouse gas emission pathways, in the context of strengthening the global response to the threat of climate change, sustainable development, and efforts to eradicate poverty
   (eds **V. Masson-Delmotte *et al.***)
   (World Meteorological Organization, Geneva, Switzerland, 2018).

4. **UNFCCC Secretariat.**
Nationally determined contributions under the Paris Agreement: Synthesis report.
Tech. rep.
(United Nations Framework Conventions on Climate Change, Glasgow, 2021).

5. **M. Corduan *et al.***
Topology Comparison of Superconducting AC Machines for Hybrid Electric Aircraft.
IEEE Transactions on Applied Superconductivity 30, 1–10 (2020).
DOI: 10.1109/tasc.2019.2963396

6. **Y. Cheng *et al.***
Design and Analysis of 10 MW HTS Double-Stator Flux-Modulation Generators for Wind Turbines.
IEEE Transactions on Applied Superconductivity, 1–1 (2021).
DOI: 10.1109/tasc.2021.3061928

7. **Y. Liu *et al.***
Measurement of Magnetic Materials at Room and Cryogenic Temperature for Their Application to Superconducting Wind Generators.
IEEE Transactions on Applied Superconductivity 28, 1–6 (2018).
DOI: 10.1109/tasc.2018.2799163

8. **P. Tixador *et al.***
Status of the European Union Project FASTGRID.
IEEE Transactions on Applied Superconductivity 29, 1–5 (2019).
DOI: 10.1109/tasc.2019.2908586

9. **M. Stemmle, F. Merschel, M. Noe, A. Hobl.**
AmpaCity — Advanced superconducting medium voltage system for urban area power supply.
in *2014 IEEE PES T D Conference and Exposition*
(2014),
1–5.
DOI: 10.1109/tdc.2014.6863566

10. **Z.S. Hartwig *et al.***
VIPER: an industrially scalable high-current high-temperature superconductor cable.
Superconductor Science and Technology 33, 11LT01 (Oct. 2020).
DOI: 10.1088/1361-6668/abb8c0

11. **D. Whyte.**
Small, modular and economically attractive fusion enabled by high temperature superconductors.
Philosophical Transactions of the Royal Society A: Mathematical, Physical and Engineering Sciences 377, 20180354 (2019).
DOI: 10.1098/rsta.2018.0354
eprint: https://royalsocietypublishing.org/doi/pdf/10.1098/rsta.2018.0354.

12. **M. Mentink *et al.***
Evolution of the Conceptual FCC-hh Baseline Detector Magnet Design.
IEEE Transactions on Applied Superconductivity 28, 1–10 (2018).
DOI: 10.1109/tasc.2017.2782708

13. **J.D.S. Bommer *et al.***
Spin-Orbit Protection of Induced Superconductivity in Majorana Nanowires.
Phys. Rev. Lett. 122, 187702 (18 May 2019).
DOI: 10.1103/physrevlett.122.187702

14. **P. Bernstein, J. Noudem.**
Superconducting magnetic levitation: principle, materials, physics and models.
Superconductor Science and Technology 33, 033001 (Jan. 2020).
DOI: 10.1088/1361-6668/ab63bd

15. **J.R. Alonso, T.A. Antaya.**
Superconductivity in Medicine.
Reviews of Accelerator Science and Technology 05, 227–263 (2012).
DOI: 10.1142/s1793626812300095
eprint: https://doi.org/10.1142/S1793626812300095.

16. **H.K. Onnes.**
The disappearance of the resistivity of mercury.
Commun. Phys. Lab. Univ. Leiden (May 1911).

17. **W. Meissner, R. Ochsenfeld.**
Ein neuer Effekt bei Eintritt der Supraleitfähigkeit.
Naturwissenschaften 21, 787–788 (Nov. 1933).
DOI: 10.1007/bf01504252

18. **F. London, H. London, F.A. Lindemann.**
The electromagnetic equations of the supraconductor.
Proceedings of the Royal Society of London. Series A - Mathematical and Physical Sciences 149, 71–88 (1935).
DOI: 10.1098/rspa.1935.0048
eprint: https://royalsocietypublishing.org/doi/pdf/10.1098/rspa.1935.0048.

19. **V.L. Ginzburg, L.D. Landau.**
On the theory of superconductivity.
Zh. Eksper. Teor. Fiz. 20, 1064–82 (1950).

20. **L.D. Landau.**
On the theory of phase transitions. II.
Phys. Z. der Sowjet Union 11, 545 (1937).

21. **A.A. Abrikosov.**
Doklady Akademii Nauk SSSR 86 (1952).

22. **H. Fröhlich.**
Theory of the Superconducting State. I. The Ground State at the Absolute Zero of Temperature.
Phys. Rev. 79, 845–856 (5 Sept. 1950).
DOI: 10.1103/physrev.79.845

23. **A.B. Pippard, W.L. Bragg.**
An experimental and theoretical study of the relation between magnetic field and current in a superconductor.
Proceedings of the Royal Society of London. Series A. Mathematical and Physical Sciences 216, 547–568 (1953).
DOI: 10.1098/rspa.1953.0040
eprint: https://royalsocietypublishing.org/doi/pdf/10.1098/rspa.1953.0040.

24. **L.D. Landau.**
The Theory of a Fermi Liquid.
JETP 3, 920 (Mar. 1956).

25. **J. Bardeen, L.N. Cooper, J.R. Schrieffer.**
Microscopic Theory of Superconductivity.
Phys. Rev. 106, 162–164 (1 Apr. 1957).
DOI: 10.1103/physrev.106.162

26. **J. Bardeen, L.N. Cooper, J.R. Schrieffer.**
Theory of Superconductivity.
Phys. Rev. 108, 1175–1204 (5 Dec. 1957).
DOI: 10.1103/physrev.108.1175

27. **A.A. Abrikosov.**
On the Magnetic properties of superconductors of the second group.
Sov. Phys. JETP 5, 1174–1182 (Dec. 1957).

28. **N.N. Bogoliubov.**
A new method in the theory of superconductivity I.
Soviet Phys. JETP 7, 41 (July 1958).

29. **N.N. Bogoliubov.**
A new method in the theory of superconductivity III.
Soviet Phys. JETP 7, 51 (July 1958).

30. **N.N. Bogolyubov, V.V. Tolmachev, D.V. Shirkov.**
A New method in the theory of superconductivity.
Fortsch. Phys. 6, 605–682 (1958).
DOI: 10.1002/prop.19580061102

31. **P.G. de Gennes, P.A. Pincus.**
Superconductivity of metals and alloys (ed **D. Pines**) (1966).
ISBN: 0-7382-0101-4

32. **L.P. Gor'kov.**
On the energy spectrum of superconductors.
Soviet Physics JETP 7, 505 (Sept. 1958).

33. **L.P. Gor'kov.**
Microscopic derivation of the Ginzburg-Landau equations in the theory of superconductivity.
Soviet Physics JETP 9, 1364 (Dec. 1959).

34. G.M. Éliashberg.
Interaction between electrons and lattice vibrations in a superconductor.
Soviet Phys. JETP 11, 696 (Sept. 1960).

35. P.W. Anderson.
Knight Shift in Superconductors.
Phys. Rev. Lett. 3, 325–326 (7 Oct. 1959).
DOI: 10.1103/physrevlett.3.325

36. A.V. Balatsky, I. Vekhter, J.-X. Zhu.
Impurity-induced states in conventional and unconventional superconductors.
Rev. Mod. Phys. 78, 373–433 (2 May 2006).
DOI: 10.1103/revmodphys.78.373

37. I. Giaever.
Energy Gap in Superconductors Measured by Electron Tunneling.
Phys. Rev. Lett. 5, 147–148 (4 Aug. 1960).
DOI: 10.1103/physrevlett.5.147

38. B. Josephson.
Possible new effects in superconductive tunnelling.
Physics Letters 1, 251–253 (1962).
DOI: 10.1016/0031-9163(62)91369-0

39. G. Eilenberger.
Transformation of Gorkov's equation for type II superconductors into transport-like equations.
Zeitschrift für Physik A Hadrons and nuclei 214, 195–213 (Apr. 1968).
DOI: 10.1007/bf01379803

40. K.D. Usadel.
Generalized Diffusion Equation for Superconducting Alloys.
Phys. Rev. Lett. 25, 507–509 (8 Aug. 1970).
DOI: 10.1103/physrevlett.25.507

41. A.J. Leggett.
A theoretical description of the new phases of liquid ^{3}He.
Rev. Mod. Phys. 47, 331–414 (2 Apr. 1975).
DOI: 10.1103/revmodphys.47.331

42. F. Steglich *et al.*
Superconductivity in the Presence of Strong Pauli Paramagnetism: $CeCu_2Si_2$.
Phys. Rev. Lett. 43, 1892–1896 (25 Dec. 1979).
DOI: 10.1103/physrevlett.43.1892

43. B. White, J. Thompson, M. Maple.
Unconventional superconductivity in heavy-fermion compounds.
Physica C: Superconductivity and its Applications 514. Superconducting Materials: Conventional, Unconventional and Undetermined, 246–278 (2015).
DOI: 10.1016/j.physc.2015.02.044

44. J.G. Bednorz, K.A. Müller.
Possible highTc superconductivity in the Ba−La−Cu−O system.
Zeitschrift für Physik B Condensed Matter 64, 189–193 (June 1986).
DOI: 10.1007/bf01303701

45. M.K. Wu *et al.*
Superconductivity at 93 K in a new mixed-phase Y-Ba-Cu-O compound system at ambient pressure.
Phys. Rev. Lett. 58, 908–910 (9 Mar. 1987).
DOI: 10.1103/physrevlett.58.908

46. V.J. Emery.
Theory of high-T_c superconductivity in oxides.
Phys. Rev. Lett. 58, 2794–2797 (26 June 1987).
DOI: 10.1103/physrevlett.58.2794

47. P. Monthoux, A.V. Balatsky, D. Pines.
Toward a theory of high-temperature superconductivity in the antiferromagnetically correlated cuprate oxides.
Phys. Rev. Lett. 67, 3448–3451 (24 Dec. 1991).
DOI: 10.1103/physrevlett.67.3448

48. P. Monthoux, D. Pines.
Spin-fluctuation-induced superconductivity in the copper oxides: A strong coupling calculation.
Phys. Rev. Lett. 69, 961–964 (6 Aug. 1992).
DOI: 10.1103/physrevlett.69.961

49. P. Monthoux, D.J. Scalapino.
Self-consistent d_x^2-y^2 pairing in a two-dimensional Hubbard model.
Phys. Rev. Lett. 72, 1874–1877 (12 Mar. 1994).
DOI: 10.1103/physrevlett.72.1874

50. B. Keimer, S.A. Kivelson, M.R. Norman, S. Uchida, J. Zaanen.
From quantum matter to high-temperature superconductivity in copper oxides.
Nature 518, 179–186 (Feb. 2015).
DOI: 10.1038/nature14165

51. M. Sigrist, K. Ueda.
Phenomenological theory of unconventional superconductivity.
Rev. Mod. Phys. 63, 239–311 (2 Apr. 1991).
DOI: 10.1103/revmodphys.63.239

52. D.A. Wollman, D.J. Van Harlingen, W.C. Lee, D.M. Ginsberg, A.J. Leggett.
Experimental determination of the superconducting pairing state in YBCO from the phase coherence of YBCO-Pb dc SQUIDs.
Phys. Rev. Lett. 71, 2134–2137 (13 Sept. 1993).
DOI: 10.1103/physrevlett.71.2134

53. C.C. Tsuei, J.R. Kirtley.
Pairing symmetry in cuprate superconductors.
Rev. Mod. Phys. 72, 969–1016 (4 Oct. 2000).
DOI: 10.1103/revmodphys.72.969

54. Y. Maeno *et al.*
Superconductivity in a layered perovskite without copper.
Nature 372, 532–534 (Dec. 1994).
DOI: 10.1038/372532a0

55. H. Ding *et al.*
Spectroscopic evidence for a pseudogap in the normal state of underdoped high-Tc superconductors.
Nature 382, 51–54 (July 1996).
DOI: 10.1038/382051a0

56. Y. Kamihara, T. Watanabe, M. Hirano, H. Hosono.
Iron-Based Layered Superconductor La$[O_{1-x}F_x]$FeAs ($x = 0.05-0.12$) with Tc = 26K.
Journal of the American Chemical Society 130, 3296–3297 (Mar. 2008).
DOI: 10.1021/ja800073m

57. R.M. Fernandes, A.V. Chubukov, J. Schmalian.
What drives nematic order in iron-based superconductors?
Nature Physics 10, 97–104 (Feb. 2014).
DOI: 10.1038/nphys2877

58. J. Paglione, R.L. Greene.
High-temperature superconductivity in iron-based materials.
Nature Physics 6, 645–658 (Sept. 2010).
DOI: 10.1038/nphys1759

59. D.V. Semenok *et al.*
Superconductivity at 161 K in thorium hydride ThH10: Synthesis and properties.
Materials Today 33, 36–44 (2020).
DOI: 10.1016/j.mattod.2019.10.005

60. E. Snider *et al.*
Room-temperature superconductivity in a carbonaceous sulfur hydride.
Nature 586, 373–377 (Oct. 2020).
DOI: 10.1038/s41586-020-2801-z

61. W. Wang *et al.*
Evidence for an edge supercurrent in the Weyl superconductor MoTe2.
Science 368, 534–537 (2020).
DOI: 10.1126/science.aaw9270
eprint: https://science.sciencemag.org/content/368/6490/534.full.pdf.

62. J.M. Park, Y. Cao, K. Watanabe, T. Taniguchi, P. Jarillo-Herrero.
Tunable strongly coupled superconductivity in magic-angle twisted trilayer graphene.
Nature 590, 249–255 (Feb. 2021).
DOI: 10.1038/s41586-021-03192-0

63. P.W. Anderson, P. Morel.
Generalized Bardeen-Cooper-Schrieffer States and the Proposed Low-Temperature Phase of Liquid He^3.
Phys. Rev. 123, 1911–1934 (6 Sept. 1961).
DOI: 10.1103/physrev.123.1911

64. P.W. Anderson, W.F. Brinkman.
Anisotropic Superfluidity in ^3He*: A Possible Interpretation of Its Stability as a Spin-Fluctuation Effect.*
Phys. Rev. Lett. 30, 1108–1111 (22 May 1973).
DOI: 10.1103/physrevlett.30.1108

65. M. Sigrist.
Introduction to Unconventional Superconductivity.
AIP Conference Proceedings 789, 165–243 (2005).
DOI: 10.1063/1.2080350
eprint: http://aip.scitation.org/doi/pdf/10.1063/1.2080350.

66. M. Sigrist.
Introduction to unconventional superconductivity in non-centrosymmetric metals.
AIP Conference Proceedings 1162, 55–96 (2009).
DOI: 10.1063/1.3225489
eprint: http://aip.scitation.org/doi/pdf/10.1063/1.3225489.

67. A.J. Leggett.
Superfluid 3-He: The early days as seen by a theorist.
Nobel Lecture, December 8, 2003.
eprint: https://www.nobelprize.org/uploads/2018/06/leggett-lecture.pdf.

68. A.K. Nguyen, A. Sudbø.
Topological phase fluctuations, amplitude fluctuations, and criticality in extreme type-II superconductors.
Phys. Rev. B 60, 15307–15331 (22 Dec. 1999).
DOI: 10.1103/physrevb.60.15307

69. J. Smiseth, E. Smørgrav, E. Babaev, A. Sudbø.
Field- and temperature-induced topological phase transitions in the three-dimensional N*-component London superconductor.*
Phys. Rev. B 71, 214509 (21 June 2005).
DOI: 10.1103/physrevb.71.214509

70. **E. Smørgrav, J. Smiseth, E. Babaev, A. Sudbø.**
Vortex Sublattice Melting in a Two-Component Superconductor.
Phys. Rev. Lett. 94, 096401 (9 Mar. 2005).
DOI: 10.1103/physrevlett.94.096401

71. **T.A. Bojesen, E. Babaev, A. Sudbø.**
Phase transitions and anomalous normal state in superconductors with broken time-reversal symmetry.
Phys. Rev. B 89, 104509 (10 Mar. 2014).
DOI: 10.1103/physrevb.89.104509

72. **P.N. Galteland, E. Babaev, A. Sudbø.**
Fluctuation effects in rotating Bose-Einstein condensates with broken $SU(2)$ and $\mathrm{U}(1) \times \mathrm{U}(1)$ symmetries in the presence of intercomponent density-density interactions.
Phys. Rev. A 91, 013605 (1 Jan. 2015).
DOI: 10.1103/physreva.91.013605

73. **N. Metropolis.**
The beginning of the Monte Carlo method.
Los Alamos Science 15, 125 (Jan. 1987).
DOI: 10.2172/1054744

74. **H. Nishimori, G. Ortiz.**
Elements of Phase Transitions and Critical Phenomena (2015).
ISBN: 9780198754084

75. **J.W. Negele, H. Orland.**
Quantum Many-Particle Systems 1st ed. (ed **D. Pines**) (1998).
ISBN: 0-7382-0052-2
DOI: https://doi.org/10.1201/9780429497926

76. **T. Inui, Y. Tanabe, Y. Onodera.**
Group Theory and Its Applications in Physics (1990).
DOI: 10.1007/978-3-642-80021-4

77. **A. Pal, J.A. Ouassou, M. Eschrig, J. Linder, M.G. Blamire.**
Spectroscopic evidence of odd frequency superconducting order.
Scientific Reports 7, 40604 (Jan. 2017).
DOI: 10.1038/srep40604

78. I.A. Sergienko, S.H. Curnoe.
Order parameter in superconductors with nondegenerate bands.
Phys. Rev. B 70, 214510 (21 Dec. 2004).
DOI: 10.1103/physrevb.70.214510

79. E. Merzbacher.
Quantum Mechanics 3rd (1999).
ISBN: 9788126533176

80. A. Shimizu, H. Ozawa, I. Ichinose, T. Matsui.
Lattice Ginzburg-Landau model of a ferromagnetic p-wave pairing phase in superconducting materials and an inhomogeneous coexisting state.
Phys. Rev. B 85, 144524 (14 Apr. 2012).
DOI: 10.1103/physrevb.85.144524

81. G. Münster, M. Walzl.
Lattice Gauge Theory - A short Primer.
arXiv: High Energy Physics (Dec. 2000).
arXiv: hep-lat/0012005 [hep-lat].

82. Y.-H. Li, S. Teitel.
Vortex-line fluctuations in model high-temperature superconductors.
Phys. Rev. B 47, 359–372 (1 Jan. 1993).
DOI: 10.1103/physrevb.47.359

83. A.K. Nguyen, A. Sudbø.
A new broken $U(1)$-symmetry in extreme type-II superconductors.
Eur. Phys. Lett. 46, 780–786 (6 June 1999).
DOI: 10.1209/epl/i1999-00332-7

84. E. Babaev, M. Speight.
Semi-Meissner state and neither type-I nor type-II superconductivity in multicomponent superconductors.
Phys. Rev. B 72, 180502 (18 Nov. 2005).
DOI: 10.1103/physrevb.72.180502

85. J. Smiseth, E. Smørgrav, A. Sudbø.
Critical Properties of the N-Color London Model.
Phys. Rev. Lett. 93, 077002 (7 Aug. 2004).
DOI: 10.1103/physrevlett.93.077002

86. H.G. Katzgraber.
Introduction to Monte Carlo Methods.
arXiv: Statistical Mechanics (May 2011).
arXiv: 0905.1629v3 [cond-mat.stat-mech].

87. H.G. Katzgraber, S. Trebst, D.A. Huse, M. Troyer.
Feedback-optimized parallel tempering Monte Carlo.
Journal of Statistical Mechanics: Theory and Experiment 2006, P03018–P03018 (Mar. 2006).
DOI: 10.1088/1742-5468/2006/03/p03018

88. T.A. Bojesen.
Multihistogram reweighting for nonequilibrium Markov processes using sequential importance sampling methods.
Phys. Rev. E 87, 045302 (4 Apr. 2013).
DOI: 10.1103/physreve.87.045302

89. A.M. Ferrenberg, R.H. Swendsen.
New Monte Carlo technique for studying phase transitions.
Phys. Rev. Lett. 61, 2635–2638 (23 Dec. 1988).
DOI: 10.1103/physrevlett.61.2635

90. A.M. Ferrenberg, R.H. Swendsen.
Optimized Monte Carlo data analysis.
Phys. Rev. Lett. 63, 1195–1198 (12 Sept. 1989).
DOI: 10.1103/physrevlett.63.1195

91. M. Newman, G. Barkema.
Monte Carlo Methods in Statistical Physics (1999).
ISBN: 9780198517979

92. K. Rummukainen.
Monte Carlo simulation methods.
University of Helsinki lecture notes.
eprint: https://www.mv.helsinki.fi/home/rummukai/lectures/montecarlo_oulu/.

93. E. Smørgrav.
Critical properties of effective gauge theories for novel quantum fluids.
:179.
PhD thesis (NTNU, 2005).
eprint: https://ntnuopen.ntnu.no/ntnu-xmlui/handle/11250/246193.

94. **S. Kragset, E. Babaev, A. Sudbø.**
Effects of boundaries and density inhomogeneity on states of vortex matter in Bose-Einstein condensates at finite temperature.
Phys. Rev. A 77, 043605 (4 Apr. 2008).
DOI: 10.1103/physreva.77.043605

95. **E. Babaev.**
Vortices with Fractional Flux in Two-Gap Superconductors and in Extended Faddeev Model.
Phys. Rev. Lett. 89, 067001 (6 July 2002).
DOI: 10.1103/physrevlett.89.067001

96. **J. Garaud, E. Babaev.**
Properties of skyrmions and multi-quanta vortices in chiral p-wave superconductors.
Scientific Reports 5, 17540 (Dec. 2015).
DOI: 10.1038/srep17540

97. **J. Garaud, E. Babaev, T.A. Bojesen, A. Sudbø.**
Lattices of double-quanta vortices and chirality inversion in $p_x + ip_y$ superconductors.
Phys. Rev. B 94, 104509 (10 Oct. 2016).
DOI: 10.1103/physrevb.94.104509

98. **J.A. Sauls, M. Eschrig.**
Vortices in chiral, spin-triplet superconductors and superfluids.
New Journal of Physics 11, 075008 (July 2009).
DOI: 10.1088/1367-2630/11/7/075008

99. **S. Ishida *et al.***
Unique defect structure and advantageous vortex pinning properties in superconducting CaKFe4As4.
npj Quantum Materials 4, 27 (June 2019).
DOI: 10.1038/s41535-019-0165-0

100. **K. Fossheim, A. Sudbø.**
Superconductivity: physics and applications 1st ed. (June 2004).
ISBN: 0-470-84452-3

101. **J. Aragón Sánchez *et al.***
Unveiling the vortex glass phase in the surface and volume of a type-II superconductor.
Communications Physics 2, 143 (Nov. 2019).
DOI: 10.1038/s42005-019-0243-4

102. **R.H. Koch *et al.***
Experimental evidence for vortex-glass superconductivity in Y-Ba-Cu-O.
Phys. Rev. Lett. 63, 1511–1514 (14 Oct. 1989).
DOI: 10.1103/physrevlett.63.1511

103. **J.E. Sonier.**
The Magnetic Penetration Depth and the Vortex Core Radius in Type-II Superconductors.
PhD thesis (University of British Columbia, Apr. 1998).
DOI: 10.14288/1.0085673

104. **L. Kramer.**
Thermodynamic Behavior of Type-II Superconductors with Small κ near the Lower Critical Field.
Phys. Rev. B 3, 3821–3825 (11 June 1971).
DOI: 10.1103/physrevb.3.3821

105. **A. Chaves, F.M. Peeters, G.A. Farias, M.V. Milo ševi ć.**
Vortex-vortex interaction in bulk superconductors: Ginzburg-Landau theory.
Phys. Rev. B 83, 054516 (5 Feb. 2011).
DOI: 10.1103/physrevb.83.054516

106. **D. Cribier, B. Jacrot, B. Farnoux, L.M. Rao.**
Study of the Lattice of Vortex Lines in Superconducting Niobium by Neutron Diffraction.
Journal of Applied Physics 37, 952–952 (1966).
DOI: 10.1063/1.1708536

107. **U. Essmann, H. Träuble.**
The direct observation of individual flux lines in type II superconductors.
Physics Letters A 24, 526–527 (1967).
DOI: 10.1016/0375-9601(67)90819-5

108. **J. Matricon.**
Energy and elastic moduli of a lattice of vortex lines.
Physics Letters 9, 289–291 (1964).
DOI: 10.1016/0031-9163(64)90365-8

109. **D. Agterberg *et al.***
Vortex lattice structures and pairing symmetry in Sr2RuO4.
Physica C: Superconductivity 341-348, 1643–1646 (2000).
DOI: 10.1016/s0921-4534(00)01492-1

110. **R. Heeb, D.F. Agterberg.**
Ginzburg-Landau theory for a p-wave Sr_2RuO_4 *superconductor: Vortex core structure and extended London theory.*
Phys. Rev. B 59, 7076–7082 (10 Mar. 1999).
DOI: 10.1103/physrevb.59.7076

111. **D.F. Agterberg.**
Vortex Lattice Structures of Sr_2RuO_4.
Phys. Rev. Lett. 80, 5184–5187 (23 June 1998).
DOI: 10.1103/physrevlett.80.5184

112. **T.M. Riseman *et al.***
Observation of a square flux-line lattice in the unconventional superconductor Sr 2 RuO 4.
Nature 396, 242–245 (Nov. 1998).
DOI: 10.1038/24335

113. **C.M. Aegerter *et al.***
Evidence for a square vortex lattice in from muon-spin-rotation measurements.
Journal of Physics: Condensed Matter 10, 7445–7451 (Aug. 1998).
DOI: 10.1088/0953-8984/10/33/013

114. **S.J. Ray *et al.***
Muon-spin rotation measurements of the vortex state in Sr_2RuO_4*: Type-1.5 superconductivity, vortex clustering, and a crossover from a triangular to a square vortex lattice.*
Phys. Rev. B 89, 094504 (9 Mar. 2014).
DOI: 10.1103/physrevb.89.094504

115. **P.J. Curran *et al.***
Vortex imaging and vortex lattice transitions in superconducting Sr_2RuO_4 *single crystals.*
Phys. Rev. B 84, 104507 (10 Sept. 2011).
DOI: 10.1103/physrevb.84.104507

116. A.K. Nguyen, A. Sudbø.
Phase coherence and the boson analogy of vortex liquids.
Phys. Rev. B 58, 2802–2815 (5 Aug. 1998).
DOI: 10.1103/physrevb.58.2802

117. A.K. Nguyen, A. Sudbø, R.E. Hetzel.
Vortex-Loop Unbinding and Flux-Line Lattice Melting in Superconductors.
Phys. Rev. Lett. 77, 1592–1595 (8 Aug. 1996).
DOI: 10.1103/physrevlett.77.1592

118. A.K. Nguyen, A. Sudbø.
Onsager loop transition and first-order flux-line lattice melting in high-T_c superconductors.
Phys. Rev. B 57, 3123–3143 (5 Feb. 1998).
DOI: 10.1103/physrevb.57.3123

119. G.M. Luke *et al.*
Time-reversal symmetry-breaking superconductivity in Sr2RuO4.
Nature 394, 558–561 (Aug. 1998).
DOI: 10.1038/29038

120. J. Xia, Y. Maeno, P.T. Beyersdorf, M.M. Fejer, A. Kapitulnik.
High Resolution Polar Kerr Effect Measurements of Sr_2RuO_4: Evidence for Broken Time-Reversal Symmetry in the Superconducting State.
Phys. Rev. Lett. 97, 167002 (16 Oct. 2006).
DOI: 10.1103/physrevlett.97.167002

121. V. Grinenko *et al.*
Split superconducting and time-reversal symmetry-breaking transitions, and magnetic order in Sr_2RuO_4 under uniaxial stress.
arXiv: Superconductivity (Jan. 22, 2020).
arXiv: 2001.08152 [cond-mat.supr-con].

122. S.A. Kivelson, A.C. Yuan, B. Ramshaw, R. Thomale.
A proposal for reconciling diverse experiments on the superconducting state in Sr2RuO4.
npj Quantum Materials 5, 43 (June 2020).
DOI: 10.1038/s41535-020-0245-1

123. **S. Ghosh *et al.***
Thermodynamic evidence for a two-component superconducting order parameter in Sr2RuO4.
Nature Physics 17, 199–204 (Feb. 2021).
DOI: 10.1038/s41567-020-1032-4

124. **T.A. Bojesen.**
Policy-guided Monte Carlo: Reinforcement-learning Markov chain dynamics.
Phys. Rev. E 98, 063303 (6 Dec. 2018).
DOI: 10.1103/physreve.98.063303

125. **Y. Nagai, M. Okumura, A. Tanaka.**
Self-learning Monte Carlo method with Behler-Parrinello neural networks.
Phys. Rev. B 101, 115111 (11 Mar. 2020).
DOI: 10.1103/physrevb.101.115111

126. **E. Bedolla, L.C. Padierna, R. Castañeda-Priego.**
Machine learning for condensed matter physics.
Journal of Physics: Condensed Matter 33, 053001 (Nov. 2020).
DOI: 10.1088/1361-648x/abb895